MOLECULAR DYNAMICS STUDY OF SINGLE PARTICLE AND COLLECTIVE EFFECTS IN DUSTY PLASMAS

By

SRIMANTA MAITY

PHYS06201504005

Institute for Plasma Research, Gandhinagar

A thesis submitted to the
Board of Studies in Physical Sciences

In partial fulfillment of the requirements
for the Degree of

DOCTOR OF PHILOSOPHY

of

HOMI BHABHA NATIONAL INSTITUTE

November, 2019

Homi Bhabha National Institute

Recommendations of the Viva Voce Committee

As members of the Viva Voce Committee, we certify that we have read the dissertation prepared by **Srimanta Maity** entitled "Molecular dynamics study of single particle and collective effects in dusty plasmas" and recommend that it may be accepted as fulfilling the thesis requirement for the award of Degree of Doctor of Philosophy.

-- **Date :** 25/11/2019

Chairman : Prof. Sudip Sengupta

Amita Das -- **Date :** 25/11/2019

Convener : Prof. Amita Das

J.K. Bhattacharjee -- **Date :** 25/11/2019

Examiner: Prof. Jayanta Kumar Bhattacharjee

-- **Date :** 25/11/2019

Member : Prof. H. Bailung

Devendra Sharma -- **Date :** 25/11/2019

Member : Dr. Devendra Sharma

-- **Date :** 25/11/2019

Member : Dr. Sarveshwar Sharma

Final approval and acceptance of this thesis is contingent upon the candidate's submission of the final copies of the thesis to HBNI.

I hereby certify that I have read this thesis prepared under my direction and recommend that it may be accepted as fulfilling the thesis requirement.

Amita Das -- **Date :** 25/11/2019

Guide : Prof. Amita Das **Place:** IPR, Gandhinagar

STATEMENT BY AUTHOR

This dissertation has been submitted in partial fulfilment of requirements for an advanced degree at Homi Bhabha National Institute (HBNI) and is deposited in the Library to be made available to borrowers under rules of the HBNI.

Brief quotations from this dissertation are allowable without special permission, provided that accurate acknowledgement of source is made. Requests for permission for extended quotation from or reproduction of this manuscript in whole or in part may be granted by the Competent Authority of HBNI when in his or her judgement the proposed use of the material is in the interests of scholarship. In all other instances, however, permission must be obtained from the author.

Srimanta Maity

SRIMANTA MAITY

DECLARATION

I, hereby declare that the investigation presented in the thesis has been carried out by me. The work is original and the work has not been submitted earlier as a whole or in part for a degree/diploma at this or any other Institution or University.

Srimanta Maity

SRIMANTA MAITY

List of Publications arising from the thesis

Journals:

- **"Interplay of single particle and collective response in molecular dynamics simulation of dusty plasma system",**
  Srimanta Maity, Amita Das, Sandeep Kumar, and Sanat Kumar Tiwari,
  Physics of Plasmas (25), 043705 (2018)

- **"Molecular dynamics study of crystal formation and structural phase transition in Yukawa system for dusty plasma medium",**
  Srimanta Maity and Amita Das,
  Physics of Plasmas (26), 023703 (2019)

Conferences and Schools

International Participation:

- **Laser Plasma Accelerator Workshop,** *March 06-17, 2017, International Centre for Theoretical Sciences (ICTS-TIFR), Bangalore, India.*

- **"Molecular dynamics study of structural phase transition in a dusty plasma bilayer",**
  Srimanta Maity and Amita Das,
  46th European Physical Society Conference on Plasma Physics (EPS 2019), July 8-12, 2019, University of Milano-Bicocca, Milan, Italy.

- **"Molecular dynamics study of collective dynamics from a moving charged particle in dusty plasmas",**
  Srimanta Maity and Amita Das,
  12th International Conference on Plasma Science and Applications (ICPSA 2019), November 11-14, 2019, University of Lucknow, India.

National Participation:

- **DST-SERB School on Plasma Theory,** *November 09-29, 2016, IASST, Guwahati, India.*

- **"Single particle and collective features in dusty plasma medium by Molecular dynamics simulations",**
  Srimanta Maity, Sandeep Kumar, Amita Das, and Sanat Kumar Tiwari,
  32th National Symposium on Plasma Science and Technology, 07-10th November, 2017, IPR, Gandhinagar (Gujarat), India.

Srimanta Maity

SRIMANTA MAITY

Dedicated to

my family, girlfriend, and friends...

ACKNOWLEDGEMENTS

First and foremost, I would like to express my great gratitude to my thesis advisor Prof. Amita Das for guiding me all the way in my research. She is largely responsible for whatever scientific thoughts, attitudes, and ethics I have gained so far in my research career. I am very thankful to her for the freedom she gave me in choosing research topics for my Ph.D study. I have always received constant encouragement and motivation from her side to pursue my work with independent thoughts and ideas. Her deep insights into research problems, approaches to tackle the problems, and awesome writing skill have always been a great source of inspiration and knowledge to me. I could not have imagined having a better mentor for my Ph.D study.

I would like to express my sincere regards to my doctoral committee members late Prof. Predhiman Kaw, Prof. Sudip Sengupta, Prof. Subrata Pradhan, Dr. Devendra Sharma, and Dr. Sarveshwar Sharma for their careful monitoring of my progress during the Ph.D tenure. Helpful discussions along with their comments and remarks in the doctoral committee's reviews always keep me in the right track in this Ph.D journey. Their appreciations and suggestions have always encouraged me to give my best in the work.

I am also indebted to Dr. Subroto Mukherjee, Dr. Prabal Kumar Chattopadhya, Prof. Sudip Sengupta, Dr. Mrityunjay Kundu, Dr. R. Ganesh, Dr. Devendra Sharma, Dr. N. Ramasubramanian, Dr. G. Ravi, Dr. V. P. Anitha, Dr. S. K. Pathak, Dr. Mainak Bandyopadhyay, Dr. Shantanu Kumar Karkari, Dr. Asim Kumar Chattopadhyay, Dr. Nirmal K Bisai, and Dr. P V Subhash, for their excellent teaching and support during my first-year course-work at IPR.

I would also like to acknowledge the computer center staff, library staff, and the administration staff at the IPR for always being cooperative. I would also like to thank all my seniors Ujjwal, Rameshwar, Sayak, Soumen, Manjit, Gurudatt, Sanat, Aditya, Vikram, Akanksha, Vidhi, Vara, Neeraj, Roopendra, Bibhu, Mangilal, Harish, Megharaj, Sameer, Chandrasekhar, Bibhu, Deepa, Veda, Dushyant, Ratan, Umesh, Surabhi, Debraj, Arghya, Bhumika, Modhu, Sonu, Amit, Narayan, Sandeep, Atul, Sagar, Jervis, Alam, Prabhakar, Meenakshi, Pallavi, Harshita, Arun, Shivam, Rupak, Avnish, Gaurav, Subrata, and other IPR scholars and colleagues for making a wonderful friendly environment in the IPR hostel campus.

I would also like to convey my warm greetings to my friends Garima, Arun, Arnab, Avik, Saswata, Debolina, Bapi, Priti, Mayank, Neeraj, Piyush, Neha, Dipshikha, Sumit, Ayan, Prabir, Souvik, Subrata, Dipankar, Raju for their best wishes and care. Thanks for gifting me lots of memory and I wish never to forget you all. Special gratitude and love to my girlfriend Garima for being around me in all my good, bad, happy, and frustrating days and for her unconditional love and support.

I also thank my classmates Garima, Arnab, Priti, Dipshikha, Neeraj, Mayank, Jay, Yogesh, Mantu, Jal, Bhumi for their support and making Ph.D. life easier. My sincere thanks to Dr. Sandeep Kumar, Dr. Ratan Kumar Bera, and Dr. Sanat Kumar Tiwari for teaching numerical and computational knowledge to me. I also wish a special thank to Dr. Bhavesh Patel, Dr. Chandrasekhar Shukla, Dr. Deepa Verma, Dr. Atul Kumar, Devshree, Ayushi, Mr. Avadesh Maurya, and Prince Kumar for good memories with them while discussing, teaching, and debating on various research problems, numerical techniques, and even on different social issues. I am also thankful to Mr. Avadesh Maurya for his technical and official support being a wonderful office roommate throughout my Ph.D. tenure.

I would also like to acknowledge HBNI, IPR, DST-SERB, ICTS for proving me fund to participate and present my Research work in international schools and conferences.

My acknowledgement would be incomplete without thanking the biggest source of my strength, my family. I thank my mother Mrs. Anima Maity, father Mr. Arun Kumar Maity, grandfather Mr. Ananta Kumar Maity, grandmother Mrs. Basanti Maity. Right from the start, they are the one who nurtured me, prayed over me, worried about me, guided me and supported me in every pursuit. Thank you for being there every day with just the love I needed. I also want to thank my sister Miss Kakali Maity and other cousins for all the fun and fights we used to have together.

Contents

SYNOPSIS

Dusty plasma is a multicomponent plasma consisting of electrons, ions, neutrals, and dust grains. These dust particles may be solid or liquid droplets with the size in the range of nano [1,2] to micrometer [3,4] scale. They are not neutral but charged either negatively or positively depending upon the charging mechanism operating in the background plasma. There are several elementary processes that can lead to the charging of dust grains including interactions with plasma particles (electrons and ions), photoelectric emission, field emission, thermionic emission, etc. Typically in experiments, when dust grains are immersed in a plasma, the plasma ions and electrons get collected on the surface of the dust grains. Electrons with higher mobility compared to ions, bombard and stick to the dust surface. This causes the dust grains to acquire a high value of negative charge. A micron-size dust grain typically acquires a charge of the order of $10^4 - 10^5$ elementary charges. These dust grains behave like another charged species of the plasma. They interact with each other and display collective features. Such a system is termed as dusty plasma.

The dusty plasma is found naturally as well as it is specifically prepared in the laboratory to carry out controlled experiments of interest. The planetary rings, comet tails, interplanetary and interstellar clouds, international space stations, etc., [5–8] are all examples where dusty plasmas exist. The study of dusty plasma, thus, has a relevance in the context of many space and astrophysical phenomena. Furthermore, dust particles play a significant role in industries where plasma is utilized for the technological purpose (e.g. etching technologies in microelectronics, production of thin films and nanoparticles, etc. [9–11]). Fusion devices [12] are yet another example where dust in plasmas plays a significant role. In order to have a better control on these processes, it is essential to understand the effect of dusts on the plasma properties, as well as their dynamics in the plasma environment.

The presence of charged dust grains, as an extra component in plasma, not only changes the charge quasi-neutrality condition of the plasma medium but also introduces a rich variety of new physical processes in the system, including dust acoustic waves [13–15], dust lattice waves [16, 17], dust ion acoustic waves [18, 19], dust acoustic solitary waves [20–22], and so on. Due to large charges carried by the dusts, the average inter-grain potential energy often exceeds the value of average thermal energy of dust particles. The ratio of these two energies is defined as Coulomb coupling parameter, $\Gamma = Q^2/4\pi\epsilon_0 a k_B T$. Here, Q is the charge on dust grains, a is the average inter-grain distance, and T defines the grain temperature. Depending upon the value of Γ, dusty plasma can go through several phases from gaseous to liquid and to the crystalline state. They are also found to behave like complex visco-elastic fluids [23–25]. Thus, dusty plasma system offers itself as an interesting model for studying various natural phenomena in laboratory regarding collective modes [23], coherent structures [26–28], instabilities [29, 30], process of crystallization [31, 32], properties of complex fluids [24], etc.

The high value of the dust to ion mass ratio (m_d/m_i), as well as a considerably low value of charge to mass ratio of dust grains (Q/m_d) makes the response time scale associated with the dust dynamics to be much longer compared to that of both electron and ion species. Thus, for the dust response time scale of interest, the response of electrons and ions can comfortably be treated as inertialess. The number density of electron and ion species can be assumed to follow the Boltzmann distribution. They are assumed to instantaneously shield the charge of individual dust grains. Thus, instead of Coulomb interaction, dust grains interact with each other via screened Coulomb or Yukawa pair potential, $U(r) = (Q/4\pi\epsilon_0 r)\exp(-r/\lambda_D)$. Here, λ_D is the typical Debye length of the background electron-ion plasma and the screening parameter, defined as $\kappa = a/\lambda_D$ represents the interaction distance between the dust grains. Thus, the study of dusty plasma system also has a relevance to other Yukawa systems including colloidal medium [33].

The characteristic eigenmode frequency associated with dust dynamics being very low (typically, 1-100 Hz), individual particles can be traced by normal charge coupled devices. Their dynamics can often be observed by unaided eyes due to their large size. Hence, particle level dynamics leading to macroscopic correlated phenomena can be directly observed and analyzed, for example, dust crystal cracking induced by energetic particles, diffusion, viscous effects, etc., can be tracked as it happens. The phenomena of phase transition as it occurs can be tracked using the dusty plasma medium. This makes dusty plasma medium to be an ideal test bed to study many phenomena in fluid and condensed matter systems at the particle level. Dusty plasma crystal formations [31, 32], static and dynamical phase behavior [34, 35], possible lattice modes [36, 37] and their coupling [38], melting transitions [39, 40], etc., have been reported in both simulations and experimental studies.

In this thesis, we show the interplay between the single particle effects and collective phenomena in the context of dusty plasma depicted by Yukawa interaction through molecular dynamics (MD) simulations. Initially, we have created a two-dimensional dusty plasma crystal and characterized its equilibrium structural properties with the help of pair correlation function and Voronoi diagrams. We have also studied the response of this dusty plasma crystal to an external perturbation, by adding an extra charged particle to the medium. The addition of this particle can be considered as similar to inserting a probe with a biased voltage in the medium experimentally. It has been shown that disturbances induced in a dust crystal elicit both collective and single particle responses [41]. The effects of the perturbation strength and the neutral damping on both the single particle and collective features have also been studied in this work.

The thesis also contains the molecular dynamics (MD) studies on the formation of three-dimensional dusty plasma crystal. In experiments, dusty plasma crystal levitates by balancing two oppositely directed forces: (a) force due to the gravity, and (b) electrostatic force of cathode sheath experienced by each dust grains. Keeping this in mind, we have carried out three-dimensional molecular dynamics simulations, where pair interaction amidst the dust grains is taken to be Yukawa (screened Coulomb). Beside the Yukawa interaction, particles are also subjected to the external force due to gravity $-mg\hat{z}$ (i.e. acting vertically downward) and the force exerted by the electric field $Q\mathbf{E}_{ext}(z) = QA\exp(-\alpha z)\hat{z}$ (which acts vertically upward for negatively charged dust particles). It is shown that in thermal equilibrium, particles choose to levitate at different heights along $\hat{z}$ forming layered structures, instead of filling up the whole simulation box. The basic mechanism of forming these multiple layered structures has been studied. The width of the particle distribution along $\hat{z}$, as well as the number of layers, have been characterized with the changing values of system parameters. The internal structural properties of crystalline bilayers have also been studied in details [42].

The thesis comprises of six chapters. A brief summary of the content of these chapters has been provided below:

- **Chapter - I:** This chapter contains an introduction to the field of dusty plasma medium and different descriptions which have so far adopted for its study. A summary of the current status of the field of dusty plasma along with the motivation and outline of the work done in the thesis has also been presented.

- **Chapter - II:** This chapter contains the Molecular Dynamics (MD) simulation description and set up which has been used extensively for various studies in this thesis. An equilibrium two-dimensional dusty plasma crystal layer has been formed with the help of simulations for a high value of the Coulomb coupling parameter. With the objective of studying the response of this equilibrated state to external perturbations, the crystal structure is perturbed by adding an extra charged particle. The added particle is chosen to have a considerably higher charge than the dust particles. The potential due to this additional particle can be taken to mimic an applied voltage of an external probe inserted in the plasma. It is observed that the dusty plasma medium elicits both collective and single particle responses. Furthermore, it has also been shown that there is a strong interplay between these two responses subsequently. At the location of inserted additional charge, a collective disturbance is seen. In addition, a few highly energetic dust particles get generated. They rapidly shoot outwards and deform and crack the crystal structure in their path. They perturb even those locations of the medium where the collective response has not had the time to reach. Subsequently, the interaction with the dust lattice reduces the energy of these dust particles and they slow down. In this phase, they are observed to excite secondary centers of collective excitation. We have obtained the condition when the ballistic propagation of these energetic particles stops and they excite secondary collective responses in the medium. The effect of the strength of initial perturbations on both single particle and collective features has been studied by varying the charge of the externally inserted particle.

- **Chapter - III:** Often in experiments [43, 44], as well as simulation observations [45, 46] highly charged objects (projectile) are moved through the dusty plasma medium and/or the medium itself is in motion with respect to such an obstacle. In this chapter, we have used MD to simulate this situation. For this case too, we demonstrate that there is a strong interplay of single particle and collective effects. It is well known that when an object moves through a medium at speeds exceeding the speed of sound in the medium, it generates a shock wave ahead of it and a Mach cone wake structure behind it [43–45]. We have shown in our studies that in this case too a few dust particles acquire a very high energy and shoot in random directions. These particles have a ballistic propagation producing cracking and deformations in the crystal structure. Thus, these energetic particles disturb the medium in those locations, which otherwise should have remained undisturbed. As a consequence, the tail region of the shock is observed to be deformed and no proper Mach cone structure is observed in the downstream region of the perturbing projectile object. At times energetic dust particles have also been observed to move ahead of the shock, cracking and deforming the crystal and ultimately generating secondary centers of collective perturbations in the crystal much ahead of the shock region. The temperature of a localized region disturbed by one of these energetic particles has been evaluated and observed to be much higher. This triggers a phase transition from crystallized to the visco-elastic fluid. Later on, when the shock and the projectile catches up with this region, it encounters an altogether different phase of the medium. The changed characteristics of the medium effects the projectile and shock dynamics. We have also studied the role of neutral damping for both single particle and collective features displayed in these simulations. The frictional drag and random kicks to the dust grains by neutral atoms have been considered. As expected, it has been shown that with increasing damping both the cracking lengths and time taken to excite secondary centers of collective excitations by energetic particles get reduced.

- **Chapter - IV:** In this chapter, we focus on the formation of dust crystal in three-dimensions. Three-dimensional molecular dynamics simulations have been performed with Yukawa pair potential between dust grains for this purpose. Beside the pair interaction each dust particles are also subjected to forces (a) due to gravity, $m\mathbf{g}$ (acting vertically downward, i.e., along $-\hat{z}$), and (b) force due to externally applied sheath electric field, $Q\mathbf{E}_{ext}(z) = QA\exp(-\alpha z)\hat{z}$. The details of the simulation parameters chosen for these simulations have been discussed in the chapter. The 2-D dust layer formation has been illustrated through simulations. The single dust layer forms at the minima of external potential. However, when one varies the parameters α and κ (the screening distance of Yukawa potential) transformation to bi-layer and multiple layers are observed. The underlying physics of layer formation and its dependence on α and κ parameters have been elucidated.

- **Chapter - V:** It has been demonstrated in chapter IV that for certain range of α and κ values, particles chose to levitate in two different layers along $\hat{z}$, instead of filling up the whole simulation box, thereby forming a bi-layer crystal structure. In this chapter, the internal structures of these bilayers have been characterized. The radial distribution function and Voronoi diagrams are employed for the purpose. It is shown that for some values of α and κ, the dust particles settle on a lattice structure with hexagonal (triangular) symmetry. With increasing values of α and κ, however, the lattice structure changes to a square (rhombic) form. By calculating the lattice angle in each layer, we have been able to discern the values of α and κ for which these structural transitions happen. We, however, observe that the transition is not sudden from a bond angle of 60^o (representing hexagonal lattice) to 90^o (corresponding to square lattice). For an intermediate value of α and κ, the crystal phase seems to pass through a disordered phase with an average bond angle which is in between 60^o to 90^o.

- **Chapter - VI:** This chapter contains the summary of the thesis work along with future directions emphasizing the relevance of the work to other areas of physics.

List of Figures

1

Introduction

The dusty plasma medium has an interdisciplinary impact, as it connects suitably with many different frontier areas of research and also has important implications in a variety of applications. Moreover, a major attraction of this medium is the ease with which it can be prepared in the strongly coupled regime [47], without requiring any stringent criteria on temperature and density.

At very high values of coupling parameters (the ratio of inter-particle potential energy to thermal kinetic energy $\Gamma > 170$) the dusty plasma system goes into crystalline phase. Experimentally, formation of such a state was observed for the first time in 1994 [31, 32, 48] for this particular medium, thereby, paving a way for realising similarity between this state of medium to the condensed crystalline state of the matter. For values of Γ between unity and 170, the dusty plasma shows similarities with many other exotic phases of matter. Pierre-Gilles de Gennes was the first to introduce the concept of "soft matter". He defined it as a class of materials that are "supramolecular, exhibit macroscopic softness, and have metastable states and sensitivity of their equilibrium to external conditions." The dusty plasma medium seems to possess most of this criteria and can qualify as a medium having attributes similar to those of the soft matter state [49]. Thus, the study of dusty plasmas in the strong coupling phase may reveal new physics insights in the field of soft matter. The dusty plasma medium is also known to exhibit fluid characteristics right from the hydrodynamic to visco - elastic behavior.

A further interesting aspect of the dusty plasma medium is that no sophisticated diagnostic is required to track the response of individual particles in experiments. Thus, it is an ideal medium in which the emergence of collective phenomena from individual particle response can be observed.

In this thesis, we have explored the process of self-organization of charged dust micro-particles under the influence of external perturbations using molecular dynamics (MD) simulations. In particular we have focused on observing both the collective and single particle response and their interplay in response to external perturbations in two-dimensions (2-D). We have also explored and characterized the regime for the formation of a variety of 3-D layered structure in the combined field of gravitational and applied external Electric field.

In this introductory chapter, we provide a brief introduction to the field of dusty plasma medium, highlighting its unique characteristic features. Different descriptions, models and techniques which have so far been adopted for its study have been presented. A summary of the current status of the field of dusty plasma has also been provided. The motivation and the outline of the content of work carried out in the thesis has also been presented.

1.1 Background

Plasma is considered as a fourth fundamental state of matter. The other three well-known states of matter are solid, liquid, and gas. In a solid, the forces among the constituent particles (i.e., ions, atoms or molecules) are so strong that they can not move freely. Particles can only vibrate around their equilibrium positions. If we increase the temperature of a solid, after a threshold, they convert to the liquid. This threshold value of temperature depends upon the constituent particles and their bonding. At higher temperature, the atoms and molecules are free to move apart and form a gaseous state. When a medium is heated at even higher temperature or subjected to a strong electromagnetic field, the constituent particles itself get ionized and break into ions and electrons forming a new state of matter, termed as plasma. Unlike neutral gases, the dynamics of such an ionized medium with the constituent charged particles are strongly influenced by the long-range electromagnetic fields. It was Tonks and Langmuir [50], who used the word "plasma" for the first time in 1929 to designate the inner portion of an ionized gas produced by means of an arc-type discharge in a tube in which the densities of ions and electrons are high but substantially equal. This ionized state of matter (plasma) is the most abundant (e.g. 99%) form of matter in our visible universe [51]. Thus, plasma is an attractive research field not only from a fundamental point of view but has tremendous potential for technological revolutions including fusion.

In most cases, a regular electron-ion plasma coexists with some heavier mass species (much more heavier compared to electrons and ions), known as dust particulates. These heavier particulate of matter does not remain neutral but gets charged because of the constant impingement of plasma particles (electrons and ions) on their surfaces. Thus, these dust particulates become an additional charged component (other than electrons and ions) of the medium. Such a mixture of charged dust grains, electrons, and ions along with the neutrals forms a typical "dusty plasma" system.

The dusty plasmas are found naturally as well as it can be specifically prepared in the laboratory to carry out controlled experiments of interest. The planetary rings, comet tails, interplanetary and interstellar clouds, international space stations, etc., [5–8, 52, 53] are all examples where dusty plasmas exist. The study of dusty plasma, thus, has relevance in the context of many space and astrophysical phenomena. Furthermore, dust particles play a significant role in industries where plasma is utilized for the technological purpose (e.g. plasma vapor depositions, chip productions, etching technologies in microelectronics, production of thin films and nanoparticles, Rocket exhaust, plasma thrusters, plasma torches, etc. [9–11]). Fusion devices are yet another example where dust in plasmas plays a significant role [12]. In order to have a better control over these processes, it is essential to understand the effect of dusts on the plasma properties, as well as their dynamics in the plasma environment.

1.2 Objective and motivation

Dusty plasma medium is an ideal test bed to study many phenomena in fluid and condensed matter systems at the particle level. The individual particles of interest (charged dust grains) are large enough to be tracked by normal charge-coupled devices, which is impractical in most other liquids and solids. Hence, particle level dynamics leading to macroscopic correlated phenomena can be directly observed and analyzed. For instance, phenomena such as phase transitions as it occurs can be tracked using a dusty plasma medium.

The objective of this thesis work is related to the study of kinetic processes as well as the characterizations of the formation of a self-organized system under various external conditions using dusty plasma medium as a model system. In particular, The response of an equilibrated ordered system to external perturbations has been studied in details in the context of dusty plasma medium. The formation of dusty plasma crystal in three-dimensions and associated structural phase transitions have also been investigated in this thesis work.

Dusty plasmas in the strong coupling regime are often considered as a new state of matter. In order to make an analogy between the strongly coupled dusty plasmas and typical condensed matters, we have investigated the equilibrium structures and their sensitivity to the various external conditions in terms of both single particle and collective responses of the medium using molecular dynamics (MD) simulations. This thesis work is related to the stability, growth, and self-organization of charged microparticles, with the major focus on the physics of those processes. Thus, one of the goals of this study is to have better control and efficiently manipulate the structure and its basic properties.

1.3 Basic aspects of dusty plasmas

Dusty plasmas are multicomponent complex systems which consist of three charged species namely, electrons, ions, and nano to micrometer sized particles (dust grains), along with the neutrals. Depending upon the charging mechanism operating in the plasma environment, These dust particles can get either positively or negatively charged. In typical dusty plasma experiments, electrons with higher mobility compared to ions get attached to the dust surface, causing them to acquire high negative charges. However, in some special circumstances, like photoelectric emission, field emission, secondary electron emission, etc., dust grains may get positively charged.

The presence of these charged dust grains as an extra component, not only alters the charged neutrality condition but also introduces a rich variety of low frequency dynamics in the plasma medium. In this section, we will briefly discuss some basic characteristics features of a dusty plasma medium such as its characteristics length and time scales, and also the parameters such as the Coulomb coupling, screening parameter, etc., which define the medium.

1.3.1 Charge neutrality condition

In typical laboratory conditions, when dust grains are embedded in the plasma environment, background electrons and ions stick to the dust grain surface during the charging process and as a result, the typical quasi-neutrality condition of the plasma gets altered. But in equilibrium, in the absence of any external disturbance, the net resulting electric charge of the medium is still zero, i.e., plasma along with these charged grains (dusty plasma) is also macroscopically neutral. The charge neutrality condition for a dusty plasma medium can be expressed as,

$$Z_i e n_{i0} = e n_{e0} \pm Z_d e n_{d0} \tag{1.1}$$

where n_{i0}, n_{e0}, and n_{d0} are the unperturbed number density of plasma electrons, ions, and charged dust grains, respectively. Here, e is the magnitude of an electronic charge, Z_i is the charge state of ions, i.e., for the singly ionized case $Z_i = 1$, and Z_d is the number of net charges residing on the surface of each dust grain in equilibrium. The $\pm$ signs stand for negatively and positively charged dust grains, respectively.

1.3.2 Characteristics length and time scales

Like a typical electron-ion plasma, dusty plasmas also have some unique scales of response, which directly depend upon the characteristics properties (like temperature, density, etc.) of the medium (both the background plasma and dust grains). In this part of the section, we will discuss some of the associated scales responsible for introducing several additional new dynamics in the medium.

There are three different length scales of a dusty plasma system, namely dust grain diameter (d), inter-grain distance (a_d), and plasma Debye length (λ_D) deciding the nature of the dynamics of charged dust grains in a plasma environment. One of the unique features of a plasma medium is screening out the external electrostatic potential introduced into the medium. This screening is typically characterized by the plasma Debye length λ_D, defined as

$$\lambda_D = \frac{\lambda_{Di}\lambda_{De}}{\sqrt{{\lambda_{Di}}^2 + {\lambda_{De}}^2}} \tag{1.2}$$

where $\lambda_{Di(e)} = \sqrt{\epsilon_0 k_B T_{i(e)}/n_{i(e)}Q^2_{i(e)}}$ is the ion (electron) Debye length. In a typical dusty plasma experiment with negatively charged dust grains, $n_e << n_i$ and $T_e >> T_i$, i.e., $\lambda_{De} >> \lambda_{Di}$. Consequently, $\lambda_D \approx \lambda_{Di}$, i.e., screening length mainly depends on the ion temperature and ion density. When a neutral dust particle is placed in the plasma medium, it immediately gets charged by the constant bombardment of electrons and ions of the plasma on its surface. This charging process comes to an equilibrium when electron flux to the dust surface is balanced by that of ions. The final amount of charge resides on the dust surface as well as dust surface potential is determined by the size of the dust grains. In a typical experimental condition, a micron-size dust grain acquires a charge of the order of $10^4 - 10^5$ elementary charges. In a situation $d << \lambda_D < a_d$, the charge of the individual dust grain gets shielded by the opposite charge species of the plasma. These charged dust particles can be considered as the isolated charged species and will not participate in the collective dynamics of the medium, known as "Dust in plasma". On the other hand, when $d << \lambda_D > a_d$, the potential of one charged grain will affect the dynamics of others. Consequently, they will response collectively and should be considered as a new charged species in the medium, called as "a dusty plasma".

A considerable low value of charge to mass ratio of dust grains Q/m_d makes the response time scales associated with the dust dynamics to be much longer compared to that of electrons and ions. Thus, with the inclusion of charged dust grains, plasma medium becomes even richer with several new low-frequency modes such as dust acoustic wave, dust acoustic solitons, dust ion acoustic wave, dust ion acoustic solitons, dust acoustic shocks, and so on. The characteristic frequency of collective electrostatic oscillations associated with the dust dynamics can be defined as $\omega_{pd} = \sqrt{n_d Q^2/\epsilon_0 m_d}$, where n_d, Q, and m_d are the density, charge, and mass of the dust grains, respectively. Dust grains with diameters above 1 micron respond on the scale of $10 - 100$ milliseconds, while the response time scale of electrons and ions in a typical discharge plasma lies in the nanosecond to microsecond regime. In some dusty plasma experiments, besides the collective response, the time scales associated with dust-neutral collisions, dust-ion collisions may also play significant roles in their dynamics.

1.3.3 Coulomb coupling parameter

The high charge on dust often renders the average inter-grain potential energy to exceed the value of average thermal energy of the dust particles. The ratio of these two energies are defined as Coulomb coupling parameter,

$$\Gamma = \frac{Q^2}{4\pi\epsilon_0 a_d k_B T} \tag{1.3}$$

where T is the temperature of the dust grains. As the charge of the individual grain is shielded by the background electron-ion plasma, the ratio of inter-grain interaction energy to the average thermal energy of dust grains is often defined by an effective coupling parameter,

$$\Gamma_{eff} = \Gamma \exp\{(-a_d/\lambda_D)\} \tag{1.4}$$

where the ratio a_d/λ_D is known as the screening parameter κ which takes care of the shielding of grain potential due to background plasma.

Depending upon the value of Γ and κ, dusty plasma can go through several phases from gaseous to liquid and to the crystalline state. They are also found to behave like complex visco-elastic fluids.

1.3.4 Forces on charged dust particles

One of the interesting features of a dusty plasma medium is that there are many forces such as gravitational forces, drag forces, etc., which are mostly irrelevant in a usual electron-ion plasma which become very important here and govern the dynamics of the medium. Therefore, here we introduce some of these important forces acting on a charged dust grain in a plasma environment, briefly.

(a) Electromagnetic force

One of the main forces acting on a moving charged dust grain is the electromagnetic force (Lorentz force)

$$\mathbf{F}_L = Q\mathbf{E} + Q(\mathbf{v} \times \mathbf{B}) \tag{1.5}$$

where Q, $\mathbf{v}$, $\mathbf{E}$, and $\mathbf{B}$ are the charge and velocity of the dust grains, electric field, and magnetic field.

The first term of equation 1.5 represents the force due to the electric field which may comes from electrostatic potential of individual charged grains (responsible for pair interaction between the particles), externally applied electric field, electric field associated with the polarization of screening cloud around each charged particle, sheath electric field at the walls of an experimental chamber, etc. In a typical ground-based dusty plasma experiment, the sheath electric field is the one which is responsible for the levitation of charged dust grains.

Forces associated with the magnetic fields (second term of equation 1.5) on dust particles are generally ignored as the self consistent magnetic field in the dusty plasma laboratory experiments are weak. Moreover, the dust mass being considerably high the requirement on magnetic field to influence the dust dynamics in laboratory experiments significant is quite high (of the order of $2-4$ T for micron sized dust particles). This value being high laboratory experiments with magnetized dust on micron sized particles have not been carried out so far. In astrophysical plasmas the existence of high magnetic field can influence the dust dynamics significantly and their effect needs to be retained. However, lately there have been laboratory experiments in the presence of very magnetic fields. New dynamical effects are being observed in such experiments which are of significant interest [54–57].

(b) Gravitational force

The dust particles have a significantly higher mass then electrons and ions and the gravitational field on them cannot be ignored compared to other forces. The gravitational force acting on a dust grain can be expressed as:

$$\mathbf{F}_G = m_d\boldsymbol{g} = (4/3)\pi(r_d)^3\rho_d\boldsymbol{g} \tag{1.6}$$

where r_d, ρ_d are the radius, mass density of dust grains, respectively and $\boldsymbol{g}$ is the acceleration due to gravity. It is clearly seen that this force becomes dominant for the particle with size in the range micrometer or above and is negligible for the nano-meter size particles. In space, dust grains are typically huge in size. In that case, besides the gravitational attraction of the nearby planet, dust particles can also interact with each other (grain-grain interactions) through the gravitational fields produced by themselves, known as self-gravitational force. In ground-based experimental conditions, the gravitational force due to earth plays a most significant role in the levitation and self-organizations of charged dust grains. In order to levitate charged dust grains in a plasma environment, this force is the one which needs to be counter balanced by all other forces acting on them. Typically, the sheath electric field provides this balance and make the charged dust particles levitate in the sheath or pre-sheath regions of the discharge plasmas.

(c) Drag forces

The drag force is typically defined as the time rate of momentum transfer between the charged dust grains and the plasma particles (i.e., electrons, ions, neutrals). There are two types of drag forces which may be present in a dusty plasma medium: (i) charge dependent ion drag force (since the collision cross sections between electrons and dust grains are very small and can be neglected) and (ii) charge independent neutral drag force.

i) Ion drag forces:

Ion drag forces typically originate from the scattering of the ions because of the electric fields of the charged grains and from the collection of ions in the surface of the dust. The bombardment of plasma ions on the surface of dust not only initiates the ion charging process but also transfers their momentum to the grains. The total ion drag force on the dust particles is then given by

$$\mathbf{F}_{ion} = \mathbf{F}_{coll} + \mathbf{F}_{Coul} \tag{1.7}$$

where the first term is associated with the adsorptions of ions (inelastic collisions) on the dust surfaces and the second one represents the force associated with the ions scattering by the grain field (elastic collisions). If the ion velocity distribution is isotropic (no directional flow of ions is present), the net ion momentum transfer to the grain is zero, i.e., the first term of equation 1.7 is significant only when there is a non-zero flow velocity of ions.

ii) Neutral drag forces:

The ionization fraction in a typical plasma discharge being very low, the neutral drag force is the most dominating frictional force present in the laboratory experiments. It represents the rate of momentum exchange between neutrals and dust grains because of their relative motions. The neutral drag force acting on a dust grain can be expressed as

$$\mathbf{F}_{dn} = -m_d \nu_{dn} \mathbf{v}_{dn} \tag{1.8}$$

where ν_{dn} and $\mathbf{v}_{dn}$ are the neutral drag coefficient and relative velocity between neutrals and grains, respectively. The negative sign represents that the drag force is acting in opposite direction to their relative velocity.

(d) Other forces

The asymmetry in the momentum transfer from neutrals may cause a net force experienced by the dust particles. This force is originated from the temperature (thermophoretic force) or pressure gradient in the background neutral gas. These forces are directed from higher gas temperature (or higher pressure) to lower temperature (lower pressure) region of the gas. There can also be radiation pressure force acting on dust grains along the direction of the incident radiation of photon flux.

1.4 Models to describe dusty plasmas

In typical laboratory conditions, because of the high charges on the dust grains, dusty plasmas are often found to be in the strongly coupled regime. The strongly coupled state of a dusty plasma system is generally defined by effective Coulomb coupling parameter Γ_{eff}, including the screening effect of plasma particles (electrons and ions). If $\Gamma_{eff} > 1$, then the medium is considered as a strongly coupled system. A host of independent theoretical models have been adopted to investigate the static and dynamical behavior of dusty plasmas in different physical regimes. Here, we will briefly discuss some of these methods have been employed to describe a dusty plasma medium.

(A) Generalized kinetic approach

The detail investigation on the kinetic theory of dusty plasmas has been reported by Tsytovich *et al.*, [58–61]. In this approach, the BogoliubovâĂŞKlimontovich model has been generalized for the case of dusty plasmas considering the discreteness of dust grain distribution. The electrons and ions were assumed to follow continuous kinetic equations, where, their absorption on the dust surfaces was also taken into account. Different aspects including dust charging process, dust-dust collisions, fluctuations of dust grain distribution and their effect on plasma properties, the effects of dust charge fluctuations on the dust interactions, Dust-plasma particles collisions, nature of forces on two test dust particles in the plasma environment, etc., have been studied. This theory is valid over a critical dust density where the binary collisions between plasma particles can be neglected with respect to the collisions with dust particles.

(B) Quasilocalized Charge Approximation (QLCA)

The QLCA model was proposed by Kalman and Golden [62,63] in order to obtain the dielectric response tensor and collective mode dispersion of strongly coupled

Coulomb liquids. The approach is based on the trapping of charged particles within the limits of relaxation time in local fluctuating potential wells [64,65]. The fluctuations in the potential create local potential minima at random locations. The relative positions of these potential wells are strongly correlated with each other. Particles are assumed to oscillate in these randomly distributed sites (local potential minima) exciting the phonon spectrum. The potential configurations are also evolving into the new potential structures on a longer time scale, leading to the slow diffusion of particles. This is the reason these dust particles are termed as "Quasilocalized Charge". One of the assumptions of this model is that the two associated time scales, i.e., time scale associated with the particle oscillations (phonon vibrations) in potential wells and the time scale associated with the rearrangement of potential configuration, are well separated. In this model, the amplitude of oscillations, as well as excursion due to the externally applied perturbation, are assumed to remain much smaller compared to the average inter-particle separation [65]. This limits the QLCA approach only up to linear response studies and is reliable for higher Γ (≥ 10). This model successfully explained different wave modes in strongly coupled dusty plasmas [66–68].

(C) Generalized Hydrodynamic (GHD) fluid description

The Generalized hydrodynamic approach is based on the continuum fluid model incorporating both elastic and viscous properties of the medium. In this model, the elastic nature (property of solids) has been coupled with the viscosity (characteristic of fluid) through the concept of *relaxation time* τ_m, phenomenologically. In a situation, where $t < \tau_m$, i.e., the time scale associated with a phenomenon is shorter (high-frequency response) than the relaxation time τ_m, the system retains the memory of its past configurations and elastic nature dominates in the dynamics of the medium. However, when the time scale is much longer compared to τ_m ($t > \tau_m$), the effect of viscosity plays a dominant role and the medium behaves like a typical charged fluid. Thus, in this model, a strongly coupled dusty plasma medium is described as a *visco-elastic* fluid. The viscoelastic nature of the medium is typically expressed by the following set of coupled equations

$$\frac{\partial n_d}{\partial t} + \boldsymbol{\nabla} \cdot (n_d \mathbf{v}_d) = 0 \tag{1.9}$$

$$\left[1+\tau_m\left(\frac{\partial}{\partial t}+\mathbf{v}_d\cdot\nabla\right)\right]\left[m_d n_d\left(\frac{\partial}{\partial t}+\mathbf{v}_d\cdot\nabla\right)\mathbf{v}_d+\nabla P+n_d Q\nabla\phi\right] = \eta\nabla^2\mathbf{v}_d+\left(\zeta+\frac{\eta}{3}\right)\nabla\left(\boldsymbol{\nabla}\cdot\mathbf{v}_d\right) \tag{1.10}$$

$$\nabla^2\phi = -\frac{1}{\epsilon_0}\Big(Z_i e n_i + Q n_d - e n_e\Big). \tag{1.11}$$

Here, equation 1.9, equation 1.10, and equation 1.11 are continuity equation, dust momentum equation, and Poisson's equation, respectively. The symbols η, ζ, $\mathbf{v}_d$, and Q represent the shear, bulk viscosity coefficients, dust fluid velocity, and charge on the dust grains (typically negative), respectively. This model has been successfully used to investigate low-frequency collective dynamics (both longitudinal and transverse) in a dusty plasma medium in both weak and strong coupling limits [23, 69].

(D) Viscoelastic-Density Functional (VEDF) model

Recently, Diaw and Murillo [70] have obtained a hydrodynamic description referred as viscoelastic-density functional (VEDF) model starting from the exact equations of the Bogoliubov-Born-Green-Kirkwood-Yvon hierarchy. They have used dynamical density functional theory in order to obtain this model which includes all the impacts of Coulomb coupling, viscous damping, and the viscoelastic response. They have compared there results with GHD model, QLCA, and MD simulations of Yukawa plasmas and found very good agreement for different strongly coupled systems.

(E) Particle-In-Cell (PIC) simulation approach

Particle-In-Cell (PIC) is one of the efficient computer simulation techniques to study very high density plasmas. In this approach, the original number of plasma particles is substituted by comparatively smaller number of super-particles (aggregation of many particles of same species). The concept of super-particles resales the number of plasma particles keeping the charge to mass ratio to have remained the same. The PIC technique has been used to model the dynamics of a dusty plasma medium including the effects of ions, electrons, and neutrals by several researchers [71–75]. One of the disadvantages of the PIC approach is that it can not capture the strong coupling effects, where the concept of super-particle does not work, such as crystallization, of the medium.

(F) Molecular Dynamic (MD) simulations

Molecular dynamics (MD is a method to simulate a many body complex system at the particle level. MD simulations are based on the exact dynamics of each particle governed from a given interaction potential. The phase space trajectories of each particle are evolved and determined by solving the Newton's equations of motion, numerically. This is also one of the most significant tools to explore the dynamics of a complex plasma system in the kinetic scales. In dusty plasma experiments, the positions of each dust particle can be tracked by standard video microscopes illuminating them with laser light. Thus, MD simulations directly mimic the experimental scenario. The macroscopic thermodynamic properties as well as phenomena associated with the particle level dynamics such as, strong coupling, transport phenomena, crystallization, etc., which can not be resolved by any other computer techniques, can be investigated using MD simulations. As discussed before, dusty plasma typically consists of three different charge species (electrons, ions, and charged dust grains) with a very wide range of time scales from electron-plasma period (ω_{pe}^{-1}, typically in the range of microsecond to nanosecond) to dust-plasma period (ω_{pd}^{-1}, typically of the order of few milliseconds). Thus, it is not feasible (being very computationally expensive) to simulate dusty plasmas with all three charged species. But one can adopt this method to study the dynamics associated with the dust grains only, where the exact dynamics of each electron and ion constituting the background plasma is not necessary but their effects can be incorporated through the dust interaction potential. Interestingly, this is possible for the case of dusty plasma medium. the charge to mass ratio (Q/m_d) of dust particles being very high, the response timescale associated with the dust dynamics become much slower compared to that of electrons and ions. Thus, while tracking the dust evolution, the response of electron and ion species can be considered as inertia-less and instantaneous. Their density can then be assumed to follow Boltzmann distribution. The charged of the individual dust grain can be assumed to be shielded by the lighter electrons and ions. Under this consideration, The inter-dust grain potential interaction can be modeled as shielded Coulomb, also termed as Yukawa potential of the form

$$U(r_i, r_j) = \frac{Q^2}{4\pi\epsilon_0 r_{ij}} \exp(-r_{ij}/\lambda_D). \tag{1.12}$$

Here, r_i and r_j are the positions of the ith particle and jth particle, respectively and $r_{ij} = |\mathbf{r_j} - \mathbf{r_i}|$ is the separation between them. The effect of background electrons and ions is taken care through the plasma Debye length λ_D.

Molecular dynamic simulation techniques have been extensively used to investigate kinetic processes associated with the transport properties of a strongly coupled dusty plasma medium including diffusion [76–78], thermal conductivity [79], viscosity [25, 78, 80–82], phase transitions [83, 84], etc.

In this thesis work, the dynamics of both equilibrium and non-equilibrium dusty plasma medium have been investigated using MD simulations by modeling the dusty plasma medium as a Yukawa system [41, 85]. The detail descriptions of the MD simulation technique have been provided in the respective chapters of the thesis.

1.5 Review of the earlier studies

The complexity, versatility and interdisciplinary features make the dusty plasma medium to be one of the most interesting and extensively studied topics in the research field. In this section, we will provide a brief summary of earlier works that have been made to understand the dusty plasma system in the context of this thesis work.

It was first W. L. Slattery and G. D. Doolen [86] and then H. Ichimaru [87] who predicted the possibility of Coulomb crystallization for the case of one-component plasma. They have suggested that there should exist a fluid-solid phase boundary at $\Gamma \geq 172$ (for $\kappa = 0$). H. Ikezi [88] first theoretically demonstrated that small particles in the plasma environment can form a Coulomb lattice and suggested that the conditions for the crystallization can be achieved more easily for the case of dusty plasmas. The research in strongly coupled dusty plasma received a great boost in 1994 when liquid and crystalline plasmas were discovered experimentally by three independent research group, Chu and I [32], Hayashi and Tachibana [48], and Thomas *et al.*, [31].

Rao *et al.* [13] presented for the first time the theoretical description for the existence of dust acoustic wave (DAW) which is the consequence of the collective dynamics of charged dust grains in the plasma medium. The existence of dust ion acoustic wave in a dusty plasma medium was first predicted and reported by Shukla *et al.*, [89]. Laboratory observation of DAW [90] and DIAW [19] was first time reported by Barkan *et al.* Different nonlinear collective dynamics displayed by the dusty plasma medium have investigated and reported by many authors in both simulation and experimental studies. These include dust acoustic solitons [13, 20–22, 91–93], dust ion acoustic solitons [94–96], shocks [27, 97–100], instabilities [29,30,101–103]. On the other hand, scattering phenomena where particle effects dominate over the collective dynamics of the medium was investigated by Marciante and Murillo [104] for the Yukawa systems.

The theoretical study of dust lattice waves in dusty plasma crystals was reported for the first time by F. Melandso [16]. Hamann *et al.* [37] reported their experimental study on laser-excited lattice waves in a plasma crystal. The experimental observation of transverse waves in a two-dimensional dusty plasma crystal was reported by Nunomura *et al.* [36]. Experimental study of transverse shear waves in a dusty plasma medium was reported by Pramanik *et al.* [105]. The visco-elastic properties and their consequences of strongly coupled dusty plasmas were investigated and reported by several researchers [23–25, 82, 106, 107].

Mach cones structures created by moving disturbances in a dusty plasma crystal, have been investigated by many authors including Samsonov *et al.* [26, 44], Miloch *et al.* [45]. The study of laser excited Mach cones and wake structures in a dusty plasma crystal was reported by Melzer *et al.* [108, 109], Nosenko *et al.* [43, 110]. Molecular dynamics study of Mach cones in two-dimensional Yukawa crystal was also reported by Ma *et al.* [111]. The study of fore-wake excitations from a charged object moving through the complex plasma was reported by Tiwari *et al.* [112]. Experimental observation of precursor solitons in a flowing dusty plasma was reported for the first time by Jaiswal *et al.* [113].

Dusty plasmas were also used as model systems to study phase transitions in condensed matter by several research groups. There are experiments [39, 114, 115] as well as simulations studies [40, 84, 116–118] on the melting transitions of dusty plasma crystals have been reported. Different structural configurations in dusty plasma crystals have been observed and reported by experimental studies [4, 34, 119–121]. Molecular dynamics study of layered structure formation of particles interacting via Yukawa pair potential in the presence of a one-dimensional parabolic potential ($(K/2)z^2$) was reported by Totsuji *et al.* [35, 122]. Reentrant transitions in Yukawa bilayers at zero temperature have been investigated by Messina and Lowen [33] using lattice sum minimization technique.

1.6 Organization of the thesis

In this doctoral thesis, we report the study of interplay between single particle effects and collective behavior of a dusty plasma system, where particles interacting via Yukawa pair potential, using molecular dynamics (MD) simulations. We have also explored the equilibrium configurations and their structural transitions under various external conditions of the medium. We provide below a chapterwise summary of this thesis work.

In Chapter 2, we discuss about the MD simulation description and set up which has been used extensively for various studies in this thesis. An equilibrium two-dimensional dusty plasma crystal layer has been formed with the help of simulations for a high value of the Coulomb coupling parameter. With the objective of studying the response of this equilibrated state to external perturbations, the crystal structure is perturbed by adding an extra charged particle. It is observed that the dusty plasma medium elicits both collective and single particle responses [41]. Furthermore, it has also been shown that there is a strong interplay between these two responses subsequently. At the location of inserted additional charge, a collective disturbance is seen. In addition, a few highly energetic dust particles get generated. They rapidly shoot outwards and deform and crack the crystal structure in their path. They perturb even those locations of the medium where the collective response has not had the time to reach. Subsequently, the interaction with the dust lattice reduces the energy of these dust particles and they slow down. In this phase, they are observed to excite secondary centers of collective excitation.

We have obtained the condition when the ballistic propagation of these energetic particles stops and they excite secondary collective responses in the medium. The effect of the strength of initial perturbations on both single particle and collective features has been studied by varying the charge of the externally inserted particle.

Chapter 3 discusses the effect of single particle features on different collective dynamics of the medium. Often in experiments [43, 44], as well as simulation observations [45, 46] highly charged objects (projectile) are moved through the dusty plasma medium and/or the medium itself is in motion with respect to such an obstacle. In this chapter, we have used MD to simulate this situation [41]. For this case too, we demonstrate that there is a strong interplay of single particle and collective effects. It is well known that when an object moves through a medium at speeds exceeding the speed of sound in the medium, it generates a shock wave ahead of it and a Mach cone wake structure behind it [43–45]. We have shown in our studies [41] that in this case too a few dust particles acquire a very high energy and shoot in random directions. These particles have a ballistic propagation producing cracking and deformations in the crystal structure. Thus, these energetic particles disturb the medium in those locations, which otherwise should have remained undisturbed. As a consequence, the tail region of the shock is observed to be deformed and no proper Mach cone structure is observed in the downstream region of the perturbing projectile object. At times energetic dust particles have also been observed to move ahead of the shock, cracking and deforming the crystal and ultimately generating secondary centers of collective perturbations in the crystal much ahead of the shock region. The temperature of a localized region disturbed by one of these energetic particles has been evaluated and observed to be much higher. This triggers a phase transition from crystallized to the visco-elastic fluid. Later on, when the shock and the projectile catches up with this region, it encounters an altogether different phase of the medium. The changed characteristics of the medium effects the projectile and shock dynamics. We have also studied the role of neutral damping for both single particle and collective features displayed in these simulations. The frictional drag and random kicks to the dust grains by neutral atoms have been considered. As expected, it has been shown that with increasing damping both the cracking lengths and time taken to excite secondary centers of collective excitations by energetic particles get reduced.

In the Chapter 4, we focus on the formation of dust crystal in three-dimensions [85]. Three-dimensional molecular dynamics simulations have been performed with Yukawa pair potential between dust grains for this purpose. Beside the pair interaction each dust particles are also subjected to forces (a) due to gravity, $m\boldsymbol{g}$ (acting vertically downward, i.e., along $-\hat{z}$), and (b) force due to externally applied sheath electric field, $Q\mathbf{E}_{ext}(z) = QA\exp(-\alpha z)\hat{z}$. The details of the simulation parameters chosen for these simulations have been discussed in the chapter. The 2-D dust layer formation has been illustrated through simulations. The single dust layer forms at the minima of external potential. However, when one varies the parameters α and κ (the screening distance of Yukawa potential) transformation to bi-layer and multiple layers are observed. The underlying physics of layer formation and its dependence on α and κ parameters have been elucidated.

In Chapter 5, it has been demonstrated that for certain range of α and κ values, particles chose to levitate in two different layers along $\hat{z}$, instead of filling up the whole simulation box, thereby forming a bi-layer crystal structure. In this chapter, the internal structures of these bilayers have been characterized [85]. The radial distribution function and Voronoi diagrams are employed for the purpose. It is shown that for some values of α and κ, the dust particles settle on a lattice structure with hexagonal (triangular) symmetry. With increasing values of α and κ, however, the lattice structure changes to a square (rhombic) form. By calculating the lattice angle in each layer, we have been able to discern the values of α and κ for which these structural transitions happen. We, however, observe that the transition is not sudden from a bond angle of $60°$ (representing hexagonal lattice) to $90°$ (corresponding to square lattice). For an intermediate value of α and κ, the crystal phase seems to pass through a disordered phase with an average bond angle which is in between $60°$ to $90°$.

In Chapter 6, we provide the summary of the thesis work along with future directions emphasizing the relevance of the work to other areas of physics.

2

Dynamical response to a static perturbation in 2-D dusty plasma crystal

Srimanta Maity, Amita Das, Sandeep Kumar, and Sanat Kumar Tiwari, Physics of Plasmas, 25, 043705 (2018)

The objective of this chapter is to study the response of dusty plasma in equilibrium to external perturbations. It is demonstrated through Molecular Dynamics simulations that the interplay of both single particle effects and the collective response of the dusty medium determine the dynamical response of the medium.

2.1 Introduction

Dusty plasma offers itself as an ideal model system to study various natural phenomena involving many particles at the fundamental atomistic level. The Collective responses in the context of dusty plasma medium have been investigated thoroughly by many authors. These include new acoustic modes originating from a balance of the dust particle inertia and plasma pressure, e.g. linear dust acoustic waves [13, 19, 89, 90], dust acoustic solitary waves [13, 20, 21, 91–96], Korteweg-de Vries (KdV) solitons [22], spiral waves [123, 124], different dust lattice modes [15–17, 36, 37, 105] and so on . Mack cone wake structures behind a moving disturbance [26, 43–45, 108–111], precursor solitons and shocks have also been reported by both simulation [112] and experimental studies [113]. On the other hand, the scattering phenomena where particle effects dominate instead of collective features, has been studied only recently by Murillo et al., [104], for the Yukawa system. The length and time scales (in the range of tens of milliseconds) associated with typical dusty plasma medium makes the study of this medium very interesting as they fall in a regime of direct human perception without requiring sophisticated diagnostics for visualizing them. Furthermore, since the discovery of plasma crystals in 1994 [31, 32, 48], the investigation of the atomistic processes triggering crystallization and melting transitions has attracted interests forging interdisciplinary areas of interest. The dusty plasma medium can be prepared in a strongly coupled state wherein it acquires distinctive features of soft matter, viscoelastic fluid systems etc., which have been important areas of interest. It is ideal medium to investigate the emergence of collective phenomena from single particle response.

In this chapter, we present the equilibrium study of two-dimensional (2-D) dusty plasma crystal where the dust grains interact via Yukawa pair potential. Our main objective is to study the response of this equilibrated state to external perturbations [41]. The external disturbance has been introduced by putting an extra particle in the system with different and a much higher charge compared to the individual dust particles. The potential disturbance due to this additional particle can in fact be considered to mimic an applied voltage of a biased probe inserted in the plasma experimentally. It has been shown in our numerical studies that the disturbances induced in a dusty plasma crystal elicits both single particle and collective responses. Beside the collective excitation of wave, few energetic particles are observed to generate from the point of initial perturbation. Furthermore, as these individual energetic particles propagate, the dust crystal is observed to crack along their path. These are the indications of single particle response of the medium. It is also seen that ultimately the energy of these highly energetic dust particles gets dissipated due to its interaction with the background dust lattice. When they slow down at an appropriate speed (which is quantified by us in this chapter), these particles excite secondary centers of collective disturbances. This exhibits a strong interplay between the single particle and collective responses in the medium.

2.2 Molecular Dynamics (MD) simulation details

Two-dimensional (2-D) molecular dynamics (MD) simulations have been carried out with 26,000 charged point particles (dust grains), each having mass $m_d = 6.99 \times 10^{-13}$ kg and charge $Q = 11940e$ (where e is an electronic charge). An open source classical MD code, Large-scale Atomic/Molecular Massively Parallel

Simulator (LAMMPS) [125] has been used in these simulation studies. Initially, particles have been distributed randomly inside a 2-D (x-y) simulation box with length $L_x = 285.8a$ and $L_y = 285.8a$ along $\hat{x}$ and $\hat{y}$ directions, respectively. Here a is the 2-D Wigner-Seitz radius, defined as, $a = (\pi n_{2d})^{(-1/2)}$, where n_{2d} is the density of dust grains in two-dimensions. In these studies, density of dust grains n_{2d} is kept to be $1.0 \times 10^6\ m^{-2}$, so that the value of average inter-particle separation $a = 5.6418 \times 10^{-4}$ m. The typical Debye length (λ_D) has been chosen to be $\lambda_D = 5.6418 \times 10^{-4}$ m, which is the same as a. Although, in some cases of our simulation studies the vale of λ_D has been varied accordingly. The dynamics of lighter electron and ion species have not been considered directly in our simulation studies. However, there contribution has been taken into account in the screening factor with parameter $\kappa = a/\lambda_D$. For these parameters, The characteristic frequency associated with the dust dynamics (in 2-D) is given by $\omega_{pd} = \sqrt{Q^2/2\pi\epsilon_0 m_d a^3} \simeq 22.8914\ s^{-1}$, corresponds to the dust plasma period $T_d = 0.2745\ s$.

Now, our next target is to achieve the thermodynamic equilibrium state of the system for a given value of Γ. Canonical ensemble has been used in the presence of a Nose-Hoover [126, 127] thermostat to obtain the positions and velocities of each particle in thermal equilibrium. Nose-Hoover [126, 127] thermostat has been used to obtain, as well as maintain the equilibrium temperature corresponding to a desired value of Γ.

The time evolution of temperature and total energy of the system in canonical ensemble (NVT) have been shown in the subplots (a1) and (a2) of Fig. 2.1, respectively. When the system finally reaches to the thermodynamic equilibrium state with a desire temperature, we have disconnected the canonical thermostat and

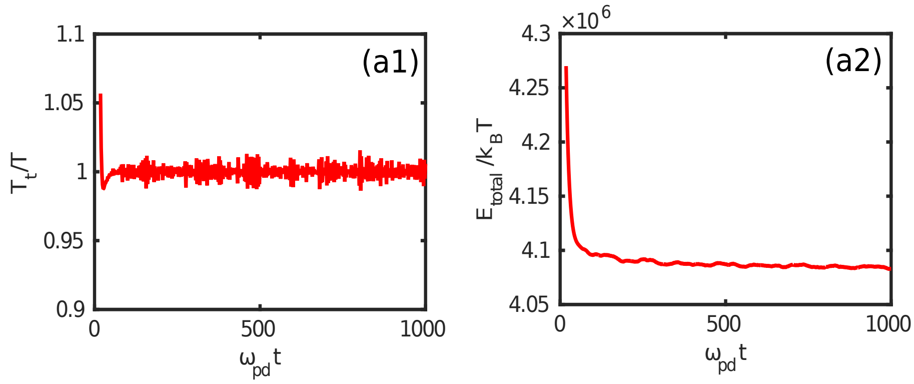

Figure 2.1: The time evolutions of (a1) Temperature (T_t) and (a2) total energy (E_{total}) of the system for canonical (NVT) simulation with the value $\Gamma = 1000$ and $\kappa = 1.0$.

allowed the system to evolve in micro-canonical (NVE) ensemble for an additional time of $1000\omega_{pd}^{-1}$. The purpose of using micro-canonical ensemble is to maintain the total energy of the system to be constant. The time evolution of temperature and total energy in this state has been shown in the subplots of Fig. 2.2. This prepares the medium as an equilibrium system which is ready for studying the evolution of external perturbations.

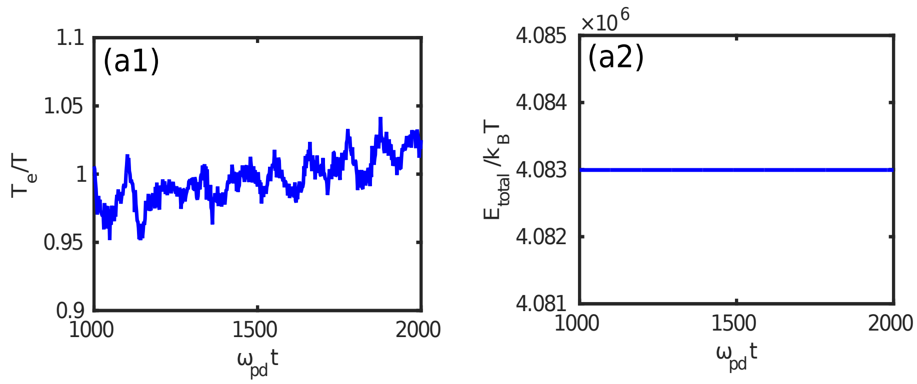

Figure 2.2: The time evolution of (a1) Temperature (T_e) and (a2) total energy (E_{total}) of the system in micro-canonical (NVE) ensemble with the value $\Gamma = 1000$ and $\kappa = 1.0$.

We have also shown the velocity distribution of particles at time $\omega_{pd}t = 2000$ for both $\hat{x}$ and $\hat{y}$ components in the subplots (a1) and (a2) of Fig. 2.3, respectively. It is clearly seen that both the components of the velocity of particles independently follow the Gaussian distribution. This indicates that the system is indeed in the statistical equilibrium and ready for further explorations.

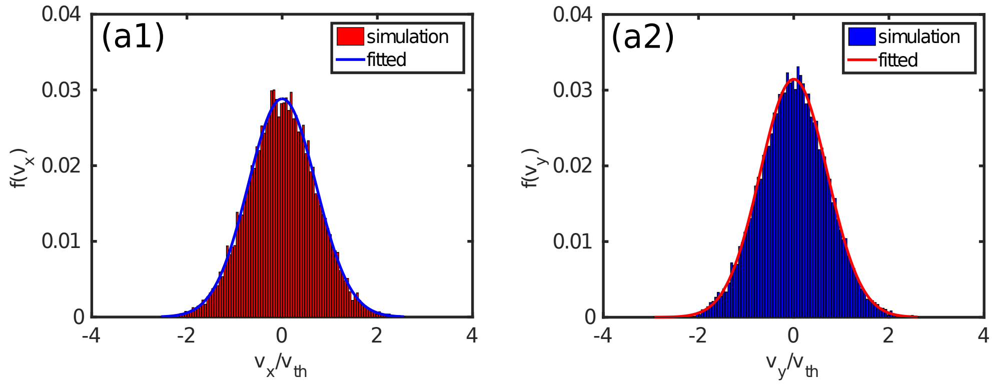

Figure 2.3: Velocity distribution of particles in NVE equilibrium for both x and y components at $\omega_{pd}t = 2000$ (subplots (a1) and (a2), respectively). Here, $v_{th} = \sqrt{2k_BT/m_d}$ is the thermal speed of particles.

2.3 Equilibrium study

It is now time to explore the internal configurational properties of these 2-D Yukawa systems in equilibrium. Structural properties of a dusty plasma medium have been investigated by several researcher in both simulation and experimental studies [4, 34, 119–121]. Here, we will review briefly some of these properties concerning the equilibrium phases of a dusty plasma system for a wide range of the parameter Γ.

2.3.1 Mean Square Displacement (MSD)

One of the distinct ways to separate crystalline phase from a fluid is the particle mean square displacement (MSD), defined as,

$$R^2(t) = \left\langle \frac{1}{N} \sum_{i=1}^{N} (\mathbf{r}_i(t) - \mathbf{r}_i(0))^2 \right\rangle, \tag{2.1}$$

where $\langle ... \rangle$ represents the average over multiple runs and different initial conditions. Here, N is the total number of particles of the system, and $r_i(t)$ represents the position of the ith particle at time t. The MSD as a function of t for different values of Γ and at a fixed $\kappa = 1.0$ is given in Fig. 2.4. It is clearly seen that for $\Gamma \leq 100$, MSD ($R^2(t)$) gradually increases with time even after a large time scale. It is also evident from the Fig. 2.4 that, the value of MSD exceeds the average inter-particle distance a for $\Gamma \leq 100$. Clearly, this is the feature of a liquid (generally known as visco-elastic [24, 25, 106] liquid).

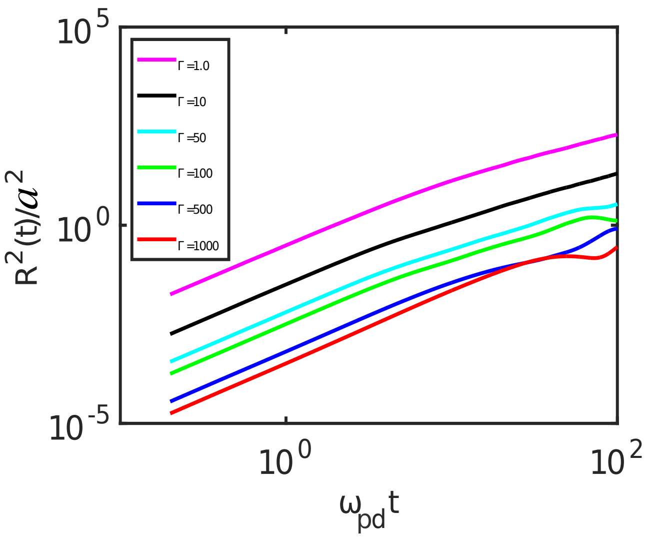

Figure 2.4: Mean square displacement (MSD) of particles for different values of coupling parameter Γ with a fixed $\kappa = 1.0$.

For $\Gamma = 500$ and 1000, the value of MSD decreases considerably and approaches a constant value at a large time scale. From Fig. 2.4 it is clearly seen that even after a long time, the value of MSD never exceeds the value of a. This is a characteristic feature of the crystalline phase, where particles can only vibrate (because of their thermal motions) around there equilibrium positions. This is more apparent from the particle trajectories plots of Fig. 2.5, where we are showing the evolution of particle's positions (for a time interval $\omega_{pd}t = 50$) in a $x-y$ plane for $\Gamma = 50$ and 1000 (subplots (a1) and (a2), respectively). It can be clearly seen that the particle's motions for $\Gamma = 50$ is diffusive, whereas at $\Gamma = 1000$ particle's positions are only fluctuating around there equilibrium positions.

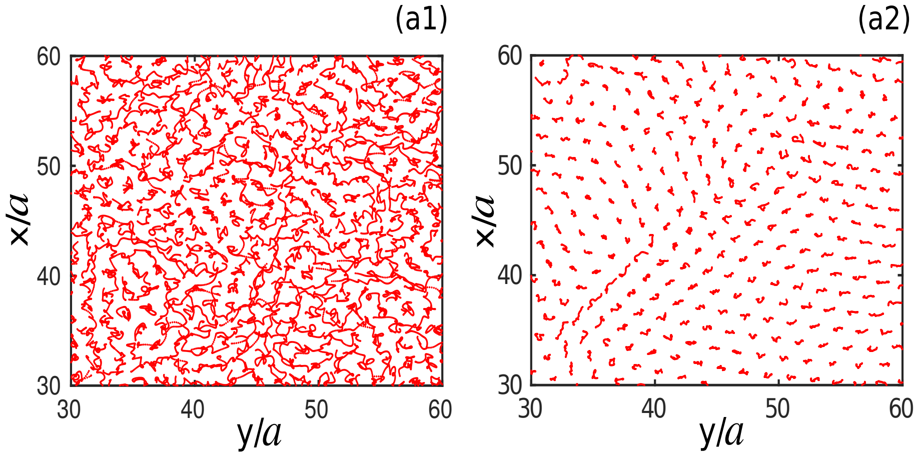

Figure 2.5: Particle's trajectories for (a1) $\Gamma = 50$ and (a2) $\Gamma = 1000$ with a fixed $\kappa = 1.0$. Trajectories are shown here for a time interval $\omega_{pd}t = 50$ in a small portion of the actual simulation box.

2.3.2 Pair correlation function ($g(r)$)

One of the important diagnostic tools to examine the different structural phases of an equilibrated system is pair correlation function $g(r)$. It is defined as,

$$g(r) = \left\langle \frac{N_r(r, dr)}{n_{2d} 2\pi r dr} \right\rangle, \tag{2.2}$$

where $\langle ... \rangle$ represents the ensemble average over all the particles for multiple simulation runs and different initial conditions. Here $n_{2d} = N/A$, is the average number density of particles in the 2-D (x-y) plane, where N is the total number of particles and $A = L_x L_y$ is the area of this 2-D plane. $N_r(r, dr)$ represents the number of particles located within a distance of r and $r + dr$ ($dr = 0.015a$) away from a reference particle.

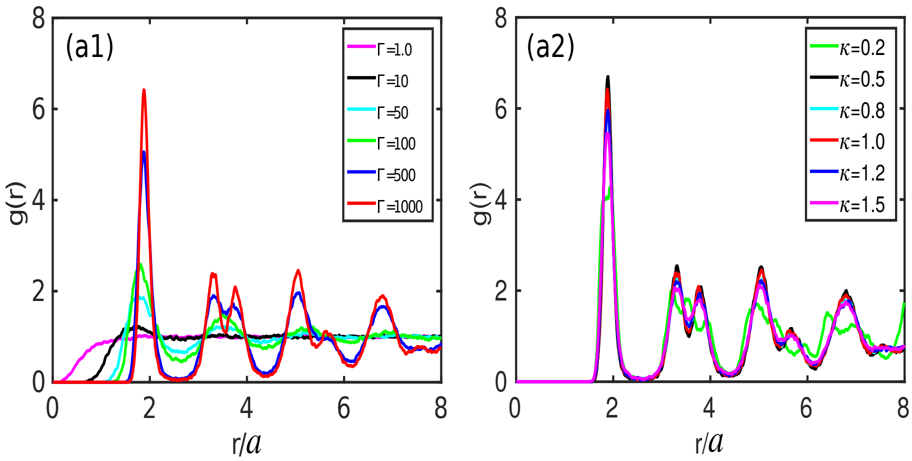

Figure 2.6: Pair correlation function $g(r)$. Subplot (a1) shows $g(r)$ for different coupling parameters Γ at a fixed $\kappa = 1.0$. Subplot (a2) represents same for different screening parameters κ at a constant $\Gamma = 1000$.

The pair correlation functions $g(r)$ for different coupling parameters Γ and screening parameters $\kappa = 1.0$ are shown in Fig. 2.6. From subplot (a1) of Fig. 2.6, it can be observed that for $\Gamma = 1.0$, after a certain distance (typically, one inter-particle distance) $g(r)$ becomes almost constant. which is a characteristic feature of a gaseous phase. For $1.0 < \Gamma > 100$, multiple peaks appear in the profile of $g(r)$, which indicates that particles have chosen to distribute themselves in specific shells around any test particle. It is also seen that the height of the peaks increases and width decreases with the increasing values of coupling parameter. Thus, it can be concluded that the structural order increases with the increasing values of Γ. From Fig. 2.6 (a1), it can also be observed that the oscillations in peaks of $g(r)$ increase for higher values of Γ ($\Gamma = 500$ and 1000), indicating the appearance of crystalline order in the system. The pair correlation functions for different values of screening parameter κ for a fixed value of $\Gamma = 1000$ are also shown in subplot (a2) of Fig. 2.6. It is seen that for all the cases there exist sharp multiple peaks in $g(r)$, indicating the crystalline state. Although, the height and oscillations of the peaks changes a little but the structural phases of the system seem to be remained the same with the changing values of κ.

2.3.3 The Voronoi diagrams

The form of crystalline structure of any order system can be easily distinguished from Voronoi diagrams. The Voronoi diagrams for different values of Γ and κ are shown in Fig. 2.7 and 2.8. For $\Gamma = 1.0$ (subplot (a1) of Fig. 2.7), no structural order is observed to be found in medium. The coexistence of both ordered and disordered phases are observed for $\Gamma = 50$ and 100, indicating the visco-elastic liquid phase of the system, as shown in subplots (a2) and (b1) of Fig. 2.7. Voronoi diagram in subplot (b2) clearly depicts the formation of a nearly hexagonal crystalline structure (with some deformations). In subplots of Fig. 2.8, we have shown the Voronoi diagrams for different values of screening parameter κ at a fixed $\Gamma = 1000$. It is clearly seen that for all these cases particles arrange themselves in nearly hexagonal lattice configurations with some deformations, as has been indicated from $g(r)$.

Thus, it can be concluded that for $\Gamma = 1000$ and for $\kappa = 1.0$, the equilibrium configuration of particles is hexagonal lattice configuration. Wherever it is not explicitly mentioned, We will use these values of Γ and κ in all of our future studies.

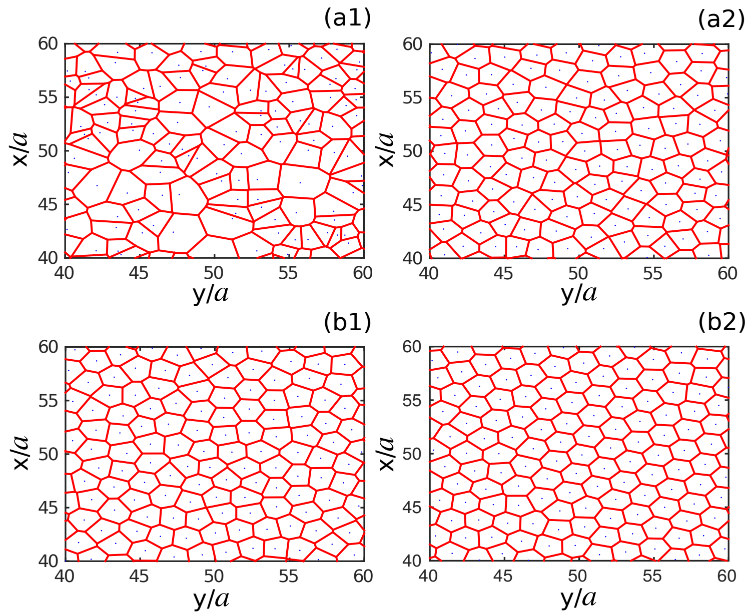

Figure 2.7: Voronoi diagrams for different values of Γ at a fixed $\kappa = 1.0$. Subplots (a1), (a2), (b1), and (b2) are for $\Gamma = 1.0$, 50, 100, and 1000, respectively. We have shown here the Voronoi diagrams of only a small portion of the simulation box.

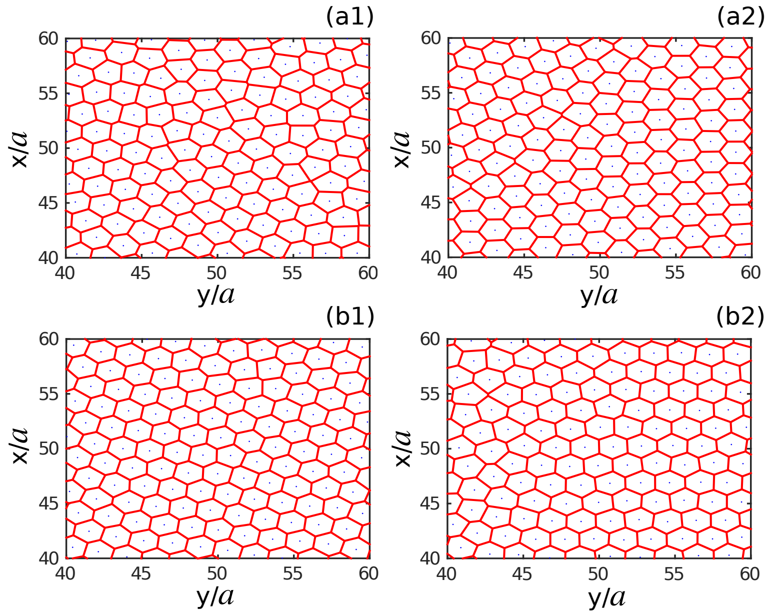

Figure 2.8: Voronoi tessellations for different values of κ at a fixed $\Gamma = 1000$. Subplots (a1), (a2), (b1), and (b2) are for $\kappa = 0.2$, 0.5, 1.0, and 1.5, respectively.

2.4 Effect of external perturbation

With the objective of studying the response of these equilibrated crystalline states to external perturbations, we now add an extra particle to the medium with a charge of $Q_p = fQ$ (i.e. the charge of the inserted particle is chosen to be f times the charge of the individual dust grains. In our simulations, f has been varied from a value of unity to 150). The addition of this particle can be considered as similar to inserting a probe with a biased voltage in the medium experimentally.

2.4.1 High energetic particle generation

The insertion of an extra particle disturbs the equilibrium and triggers a response from the dust medium. It is observed that when the charge of this external particle is much higher compared to the background dust particles, a few dust particles suffer rapid displacement (Fig. 2.9(a)). The collective response of the medium is also observed to be present (Fig. 2.9((b)-(d))), however, the speed of the particles involved in this is comparatively very slow. The velocity quiver plot of Fig. 2.10((a)-(d)) also clearly shows that a few particles move very rapidly. Their movement through the medium generate cracks and defects in the crystal structure along their path. Subsequently, they seem to loose their kinetic energy and significantly slow down. At their slow phase, these particles form secondary centers from where the collective response of the dust medium emanates. These secondary centers are at locations which are significantly separated from the region where the external particle was introduced. This is clearly evident from Fig. 2.10((b)-(d)). The highly energetic particles, which are few in number, get generated as soon as the medium is disturbed. They are essentially single particle scattering response from the potential disturbance introduced by inserting the extra particle.

The velocity quiver plots (Fig. 2.10) show that few particles are ejected in random directions with very high velocities. The fastest particle reaches furthermost from the original disturbance as can be observed from zoomed plot of indicating their velocities in Fig. 2.10(a) shown at $\omega_{pd}t = 5.0$. As these energetic particles trace their way through the crystal, they interact with the lattice. During the initial phase, they seem to generate cracks in the crystal and also tend to generate secondary energetic particles. As a result of such encounters, the original particle subsequently slows down. It is observed that after losing a significant amount of energy it creates a secondary center of collective excitation in the medium (Fig. 2.10(c)).

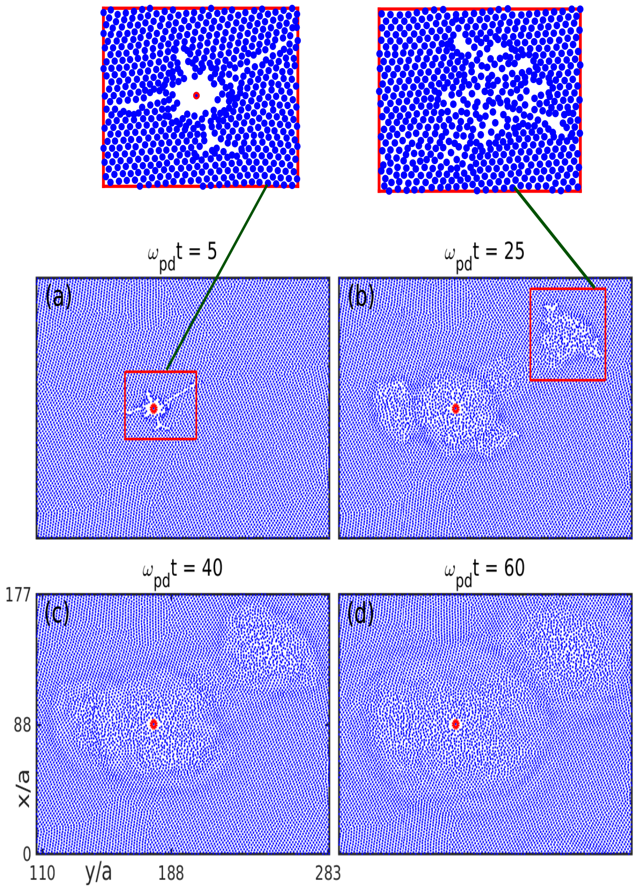

Figure 2.9: Time lapse sequence of particle configuration in position space after adding an extra particle with charge, $Q_p = 100Q$ in the system. Generation of cracks and deformations in the crystal structure made by some high energetic particles traveling through the crystal is shown in (a). The excitation and propagation of collective modes are shown in (b)-(d).

2.4.2 Condition to excite secondary centers

We now try to understand the condition when the ballistic propagation of the energetic particle stops and it excites collective disturbance in the medium. For this purpose, we chose to track four distinct particles in the order of increasing energy (created by the initial external disturbance in the medium). They are marked as $p1, p2, p3, p4$ and are identified by in Fig. 2.11(a) by various symbols.

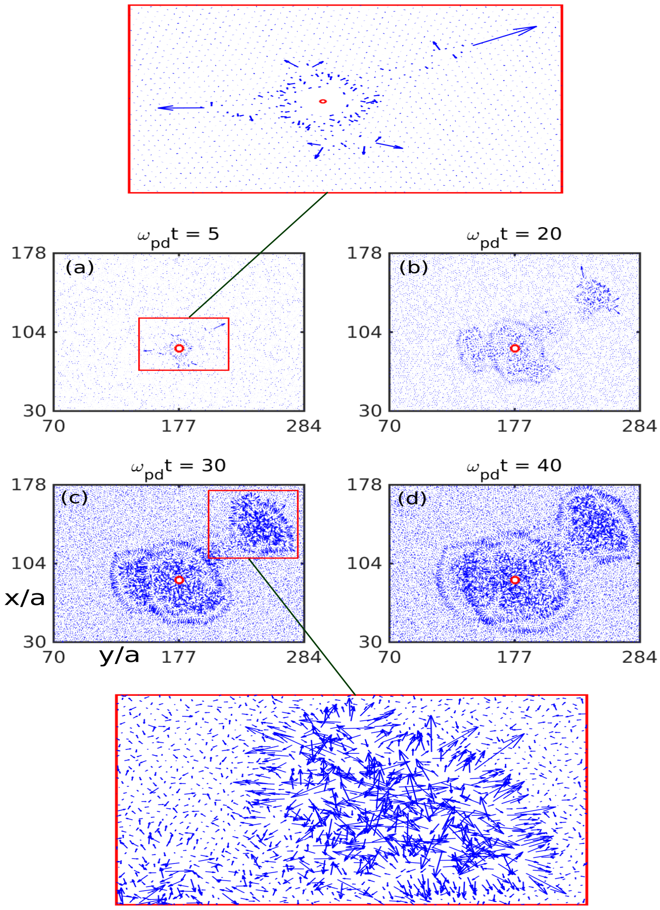

Figure 2.10: Time evolution of the velocity of particles. Length of the arrow represents velocity amplitude of the particle. The ejection of high energetic particles in random directions is shown in (a). These high energetic particles travel through the medium creating cracks and defects in the crystal and finally generates collective disturbances far from the initial perturbation as shown in (b)-(d).

The size of the arrow associated with these four particles has also been drawn which indicates their respective speeds v. In Fig. 2.11((b)-(e)) we show the evolution of $R = kv/\omega_{pd}$ for all the four particles. Here $k = 2\pi/a$ is the wavenumber associated with the lattice spacing a and v is the speed of the particle that one is tracking. Hence, $(kv)^{-1}$ is the typical time scale associated with the energetic particles. When the collective modes of the system have similar response time, then they can get excited. It is observed that initially the value of $R = kv/\omega_{pd}$ is much higher than unity. After that there is a steady decrease of kv/ω_{pd} for each particle and ultimately it reaches the value of unity for each of them and hovers around it. Thus only when the time scale associated with the energetic particle movement is similar to the collective response of the medium, the collective modes get excited.

The inset of the subplots ((b), (c), (d), (e)) of Fig. 2.11 demonstrates it in a clear fashion. In subplot (b) of Fig. 2.11 we have shown the evolution of R_{p1}, where $p1$ is the particle with slowest speed. It can be observed that R_{p1} has already reached the value of unity before $\omega_{pd}t \sim 10$. For other three particles (viz., $p2, p3, p4$) $R_{pi} > 1$ for $(i = 2, 3, 4)$. The inset of Fig. 2.11(b) shows that while the collective response at the location of $p1$ at $\omega_{pd}t = 10$ has already been initiated , the other three particles are still marching ballistically ahead in the crystal. This gets further confirmed from the inset of other subplots ((c), (d), (e)).

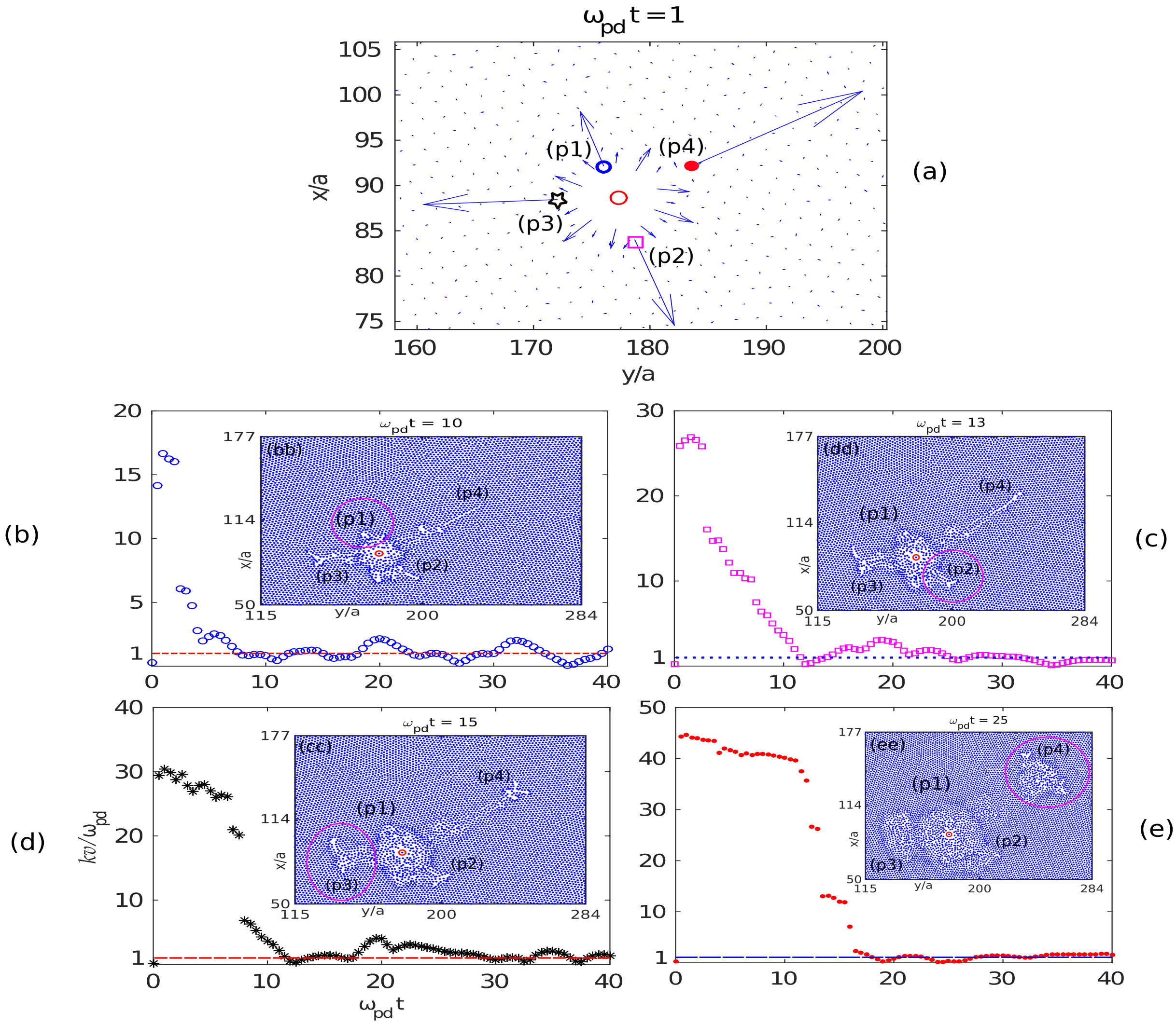

Figure 2.11: (a) Shows the velocity quiver plot of particles at $\omega_{pd}t = 1$, after inserting an extra charged particle (red marked circle) with $Q_p = 100Q$ in the medium. Here the length of the arrow represents the relative amplitude of the velocity of particle. (b)-(e) show the time evolution of frequencies associated with perturbations made by high energetic particle, $(p1)$, $(p2)$, $(p3)$ and $(p4)$ respectively. Insets (bb)-(ee) represent the particle configurations, showing the excitation of collective disturbance (pink marked region) caused by each of these high energetic particles ($(p1)$, $(p2)$, $(p3)$ and $(p4)$), respectively.

For instance, in Fig. 2.11((c), (d)) the inset shows the particle picture at $\omega_{pd}t =$ 13 and 15. At these times R for all the three particles are close to unity except the 4th particle. It should be noted that the crystal shows collective response around all the three particles in these subplots, except the fourth one. The 4th particle is still moving ballistically ahead. In subplot (d) the inset is shown at $\omega_{pd}t = 25$. At this time even R_{p4} has touched the value of unity and it can be observed that there are secondary collective disturbances around this 4th particle as well. The secondary center excited by each of the energetic particle forms at a random location depending on the angle and velocity with which they got scattered initially.

2.4.3 Effects of the initial strength of perturbation

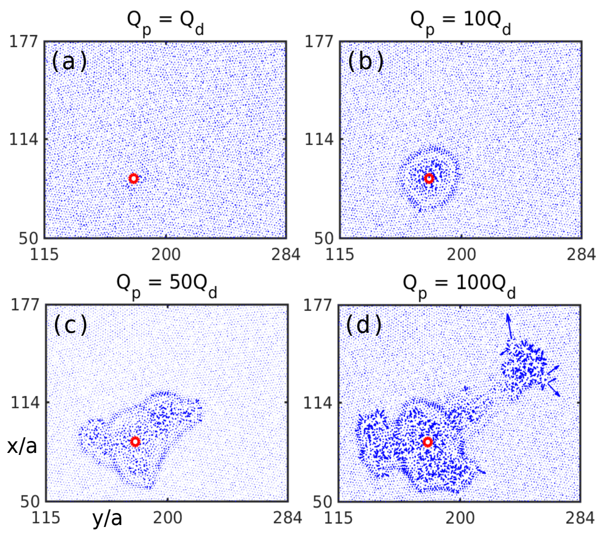

Figure 2.12: velocity quiver diagrams of particles after inserting an extra particle in the medium with charge (a) $Q_p = Q$, (b) $Q_p = 10Q$, (c) $Q_p = 50Q$ and (d) $Q_p = 100Q$ at $\omega_{pd}t = 20$. Almost no disturbance is made in the system as we insert the extra particle having same charge as that in the medium as shown in (a). Collective disturbance propagating isotropically around the point of intertion as shown in (b). Disturbances get anisotropic for higher amount of charges as shown in (c) and (d).

We have also investigated the role of the initial strength of perturbation on both the collective and single particle features by varying the charge of the extra particle which was added in the medium. It can be clearly seen from the velocity quiver plots shown at $\omega_{pd}t = 20$ in Fig. 2.12 that when we put the extra particle having a charge equal to the dust grains ($Q_p = Q$, i.e. $f = 1$) there is hardly any disturbance which persists in the medium (Fig. 2.12(a)). This is expected, as the extra particle is same as the background dust grains of the medium and hence they easily adjust in the equilibrated system. When the charge is ten times the charge of the background dust, merely collective response around the extra charge is observed to develop. The symmetric form of the collective disturbance around the added particle (Fig. 2.12(b)) bears testimony to this.

However, with increasing charge (e.g. $f = 50, 100$) the disturbances get anisotropic. The shape is essentially governed by the paths taken by the few energetic particles which get generated by the individual scattering events, and which ultimately trigger the collective response from secondary centers when their speeds get slower significantly to match with the time scale of collective response. A comparison of $f = 50$ and $f = 100$ shows that higher the charge of the added particle, the secondary center forms at a location which is further away from the originally inserted particle. This is essential because the maximum energy acquired by the individual scattering events increases with the charge of the particle that has been added in the medium. This is more clearly shown in Fig. 2.13, where the radial distributions of kinetic energy of particles ($E_k = (1/2)m_d(v_x^2 + v_y^2)$) from the point of initial perturbation for different charges of externally added particle are shown. Here, r_0 is the initial separation (at $\omega_{pd}t = 0$) of particles from the externally added particle. The kinetic energy E_k has been calculated at time $\omega_{pd}t = 0.5$. It is clearly seen that those particles which were initially close to the externally inserted particle, acquire higher energies. It is also observed from Fig. 2.13 that, with increasing the charge of the externally added particle, the scattering processes become more energetic, i.e., particles scattered with higher initial energies. This is more apparent from the inset of Fig. 2.13, where we are showing the time evolution of a single particle which was initially the nearest one of the extra added particle.

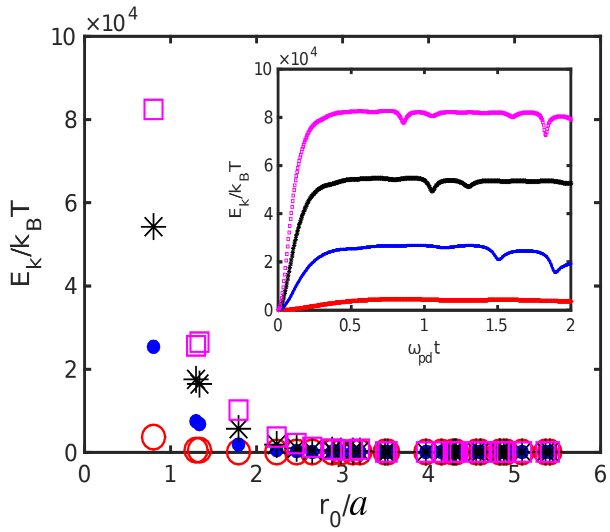

Figure 2.13: Radial distribution of the kinetic energy E_k of particles calculated at time $\omega_{pd}t = 0.5$ after adding an extra particle to the medium. Here, r_0 is the initial separation (at $\omega_{pd}t = 0$) of particles from the externally added particle. Magenta squares, black stars, blue dot, and red circles are for $f = 150, 100, 50,$ and 10, respectively. The inset shows the time evolution of E_k of the particle which was initially the nearest one of the extra added particle for four different charge ($f = 150, 100, 50,$ and 10) of the added particle.

The scattering strength will also dependent on the value of screening parameter κ, as it defines the range of the inter-particle interactions. In order to verify this, we have shown the radial distribution of kinetic energies, as well as kinetic energy evolution of nearest neighbor particle, as in the previous case, for different values of κ in Fig. 2.14. Here also one can observe that with increasing κ, the scattering processes become less energetic. This is expected, as with increasing κ the strength of the effective inter-particle interactions become less.

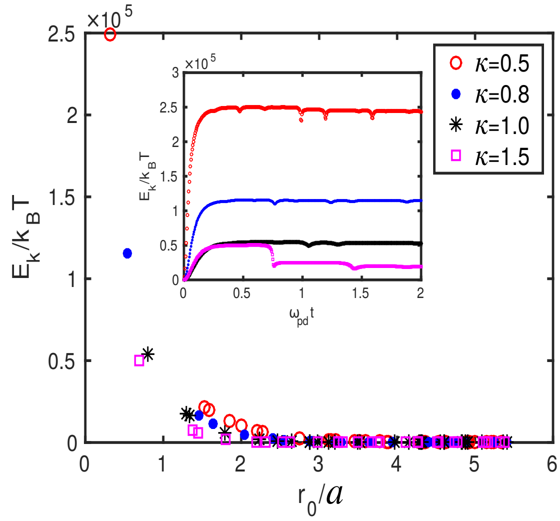

Figure 2.14: Radial distribution of the kinetic energy E_k of particles calculated at time $\omega_{pd}t = 0.5$ after adding an extra particle to the medium. Here, r_0 is the initial separation (at $\omega_{pd}t = 0$) of particles from the externally added particle. The inset shows the time evolution of E_k of the initially nearest neighbor particle of the extra added one.

2.5 Conclusions

We have considered a dusty plasma medium for which the dust grains interact amongst themselves via Yukawa interaction. The equilibrium properties of these Yukawa systems have been studied briefly and benchmarked with previous studies. We have also carried out MD simulations to investigate the response of such a dusty plasma medium to an imposed disturbance. We created disturbance in the medium by adding an extra charged (unity to 150 times the charge in each dust particles) particle. It is observed that medium has two distinct modes of response. The initial fast response arises through individual particle scattering by the imposed potential. Subsequently, the medium also shows the collective response in terms of acoustic waves, fore-shock generation, etc. It has been observed that the scattering response can often lead to a generation of a few very energetic particles. These particles move very rapidly in the medium. Such fast particles, as they move ballistically in the medium, introduce cracks and defects in their paths. However, when they slow down they invoke a collective response in the medium at localized regions. These locations have been termed as the secondary centers by us. For these cases, where the secondary center is ahead of the primary disturbance induced by the projectile, the primary disturbance will encounter a disturbed medium as it propagates. This influences their subsequent development. It has thus been shown by our simulations that the dusty plasma responds to any externally imposed disturbances in two distinct ways. These are single particle scattering events (often leading to the generation of energetic particles) as well as the collective response. Subsequently, however, the overall evolution strongly depends on the interplay of these two responses in the medium.

3

Dynamical response to an externally introduced moving charged particle in dusty plasma

Srimanta Maity, Amita Das, Sandeep Kumar, and Sanat Kumar Tiwari, Physics of Plasmas, 25, 043705 (2018)

In this chapter, we have considered a situation when a charged object moves through the dusty plasma medium with the supersonic speed. A detailed study using Molecular Dynamics simulation has been carried out to investigate both single particle and collective response that get generated in the dusty plasma medium.

3.1 Introduction

The dynamics of complex plasma systems flowing past a charged object and/or phenomena associated with a moving charged object in the plasma medium are interesting research topics in physics. It is well known that for a fluid which is flowing around an obstacle, or alternatively when an object moves through a fluid, shocks get formed when the relative velocity of the medium and the object exceeds the acoustic speed of the medium. There are many features associated with such a physical situation. For instance, Mach Cone structures, precursor solitons/shocks, density waves etc., which originate when such disturbances propagate through the plasma.

The existence of Mach cones in a dusty plasma was initially predicted by Havnes *et al.* [128, 129]. Mach cones structures excited by a charged projectile moving spontaneously beneath a 2-D dusty plasma crystal were observed and reported by Samsonov *et al.* [26, 44]. Laser excited compressional Mack cones and shear wave Mach cones were studied by Melzer *et al.* [108, 109], and Nosenko *et al.* [43, 110], respectively. It is to be noted that these wakes structures in the dusty plasma medium are very different from the ship's wakes in the water. A ship's wake is produced because of the transverse surface gravity waves (non-acoustic), where the cone angle does not vary with the speed of the ship in the water [130]. The experimental observation of precursor solitons in a flowing complex plasma has been reported recently by Jaiswal *et al.* [113]. The numerical study of the precursor nonlinear structure formations from moving charged particle in a dusty plasma liquid has been reported by Tiwari *et al.* [112, 131]. We aim at understanding the generation of these features using molecular dynamics simulations for a dusty plasma medium where the dust charges interact via screened Yukawa potential.

Thus, in this chapter, we provide a detailed simulation and discussion of different dynamical phenomena originating from a moving charged particle through a dusty plasma medium. Molecular dynamics simulations have been carried out to understand the response of the dusty plasma medium when a point charge particle (or a collection of such particles) are inserted in the plasma [41]. These particles (we often term them as projectiles) move with a definite velocity through the equilibrium dusty plasma crystal ($\Gamma = 1000$, $\kappa = 1.0$). Multiple simulations have been carried out with varying charges and velocity of the projectiles. The variety of collective phenomena excited in the medium when disturbed by such projectiles, such as Mach cone wake structures, precursor density waves, and pinned structures, moving along with the projectile have been studied. Beside these collective phenomena, single particle responses have also been shown to get triggered in the medium as shown in chapter 2. The consequence of the single particle response in influencing the collective response of the medium has also been studied.

This chapter is organized as follows. In the next section (Sec. 3.2), we provide the study of different chareteristic features of the collective response of the medium and their dependency on the projectile's velocity and charge. In Sec. 3.3, we discuss the single particle dynamics of the medium. Section 3.4 is concerned with the effect of neutral damping on both the single particle and collective features of the medium. Finally, a brief summary has been provided in Sec. 3.5.

3.2 Collective dynamics associated with the moving charged object

3.2.1 Variation with Mach number

The Mach number is defined by the ratio of the projectile velocity to the dust acoustic speed of the medium, i.e., $M = v_p/C_s$. The dust acoustic speed for the medium is evaluated by introducing a linear (small amplitude) electric field perturbation (along $\hat{y}$) to the system to excite dust acoustic wave. Then from the slope, (dy/dt) of the plot of the trajectory along $\hat{y}$ (after averaging in x) with respect to time, we have calculated the acoustic speed of the medium. It turns out that the dust acoustic wave speed (C_s) of the medium for $\Gamma = 1000$ and $\kappa = 1.0$ is equal to the 9.2×10^{-3} (m/sec). The dust acoustic speed was also calculated from the dispersion relation $(\omega - k)$ of the longitudinal wave spectra. The wave spectra of the longitudinal mode were obtained from the longitudinal current correlation functions calculated using the equilibrium particle's positions and velocities. The dust acoustic speed of the medium with $\omega_{pd} = 22.8914\ s^{-1}$ and $\kappa = 1.0$, obtained using this technique, is equal to the 9.22×10^{-3} (m/sec). Thus the quantitative estimate of the dust acoustic speed obtained from both the technique matches quite well.

We then introduce a charged particle moving with a certain velocity in the medium. The speed of the introduced particle is varied and the response to this perturbation is studied in detail in the simulation. The response of the medium is shown in the velocity quiver plots of Fig. 3.1. The dark blue regions correspond to the higher velocities of particles. The Mach number (v_p/C_s) of the projectile with charge $Q_p = 100Q$ has been varied from the value $M = 1.01$ to $M = 2.3$ (subplots (a1)-(b2) of Fig. 3.1). It is observed that there are two distinct types of collective phenomena which get initiated when the charged object is moving at supersonic speed. In the upstream region of the projectile, a bow-shaped density crest with splitting long tails get created. It is clearly seen that with increasing Mach number of the projectile, the angle of this bow-shaped structure decreases. At very high Mach number of the projectile, this bow-shaped structure forms a compressional Mack cone which follows the typical Mach-cone-angle relation, $\sin\mu = C_s/v_p$. Another Mack cone structure is also observed to be formed in the downstream region (wake region) of the projectile. The Mack cone angle μ (as defined in the inset of Fig. 3.2) of this wake structure also decreases with increasing projectile's velocity. The variation of μ of this second Mach cone structure (wake structure) with the velocity of the projectile is shown in Fig. 3.2. When a charged particle is moving through the dusty plasma medium, it pushes the particles of the medium away from its path creating a small void around the projectile. As a result, particles are pushed collectively in the forward direction forming a bow-shaped compressed structure in the precursor region of the projectile. There will be particles moving back toward their equilibrium undisturbed positions behind the projectile, forming a V-shaped structure in the wake region (second cone). This Mack cone wake structure, which is not observed in typical gas dynamics, has been produced as a consequence of the restoring force between the nearest neighbors in a crystalline state.

A detail investigation on the dynamics of the medium in the precursor region of the projectile will be discussed now. The 1-D (along the $\hat{y}$) density profiles of the medium have been shown in subplots (a1)-(b2) of Fig. 3.3 for different Mach

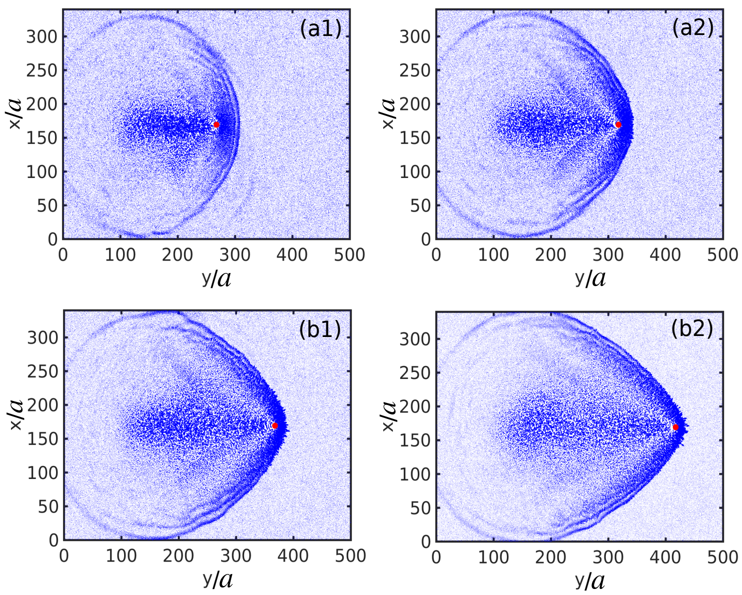

Figure 3.1: Velocity quiver plots with a projectile (red solid point) having charge $Q_p = 100Q$ moving through the dusty plasma medium with Mach number (a1) $M = 1.1$; (a2) $M = 1.5$; (b1) $M = 1.9$; (b2) $M = 2.3$. All these subplots are at the same time $\omega_{pd}t = 175$.

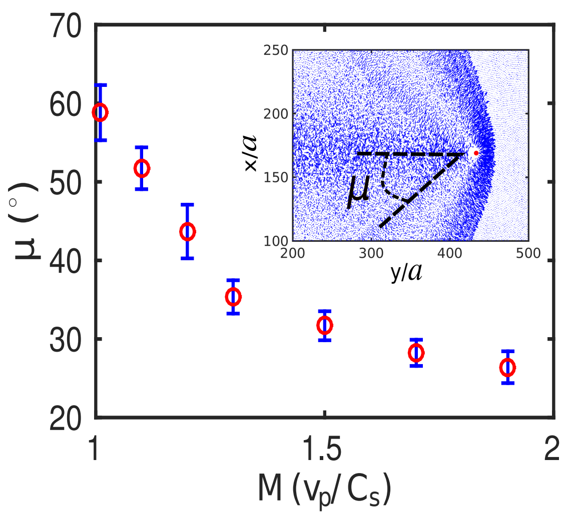

Figure 3.2: Variation of the Mach cone angle μ of the wake structure with the Mach number M of the projectile having charge $Q_p = 100Q$. The inset shows the way μ is defined.

numbers ($M = 1.1$, 1.5, 1.9, and 2.3, respectively) of the projectile having charge $Q_p = 100Q$. The density profile n along the $\hat{y}$ direction has been obtained by binning the system along $\hat{y}$ and averaging over a narrow strip along $\hat{x}$ around the projectile, as shown in the inset of subplot (b2) of Fig. 3.3. In the profile of n, the low-density region with larger fluctuations corresponds to the randomized wake channel produced behind the projectile along its path in the medium. The density hump represents the precursor density crest produced ahead of the projectile. It is clearly seen that with increasing M, the amplitude as well as the sharpness of this precursor density structure increases. For lower values of M ($M = 1.1$, 1.5), multiple peaks are observed to form in the crest of the density profile.

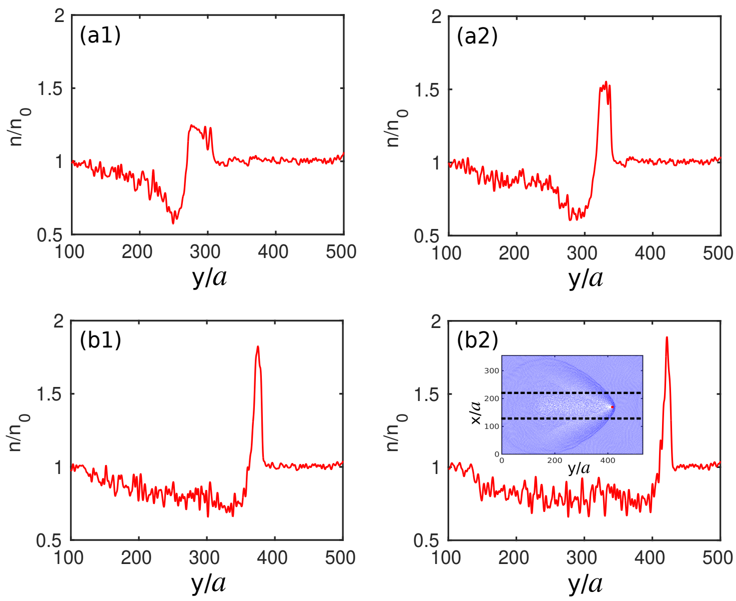

Figure 3.3: Particle density n after averaging over a narrow strip (with $dx = 50a$) along $\hat{x}$ arond the projectile. Here n_0 is the equilibrium dust density. Subplots (a1), (a2), (b1), and (b2) are for the projectile with Mach number $M = 1.1$, 1.5, 1.9, and 2.3, respectively. All the subplots showing here are at the same time $\omega_{pd}t = 175$.

The time evolution of the width (d) of the precursor density structure for various Mach number of the projectile has been shown in the subplot (a1) of Fig. 3.4. The

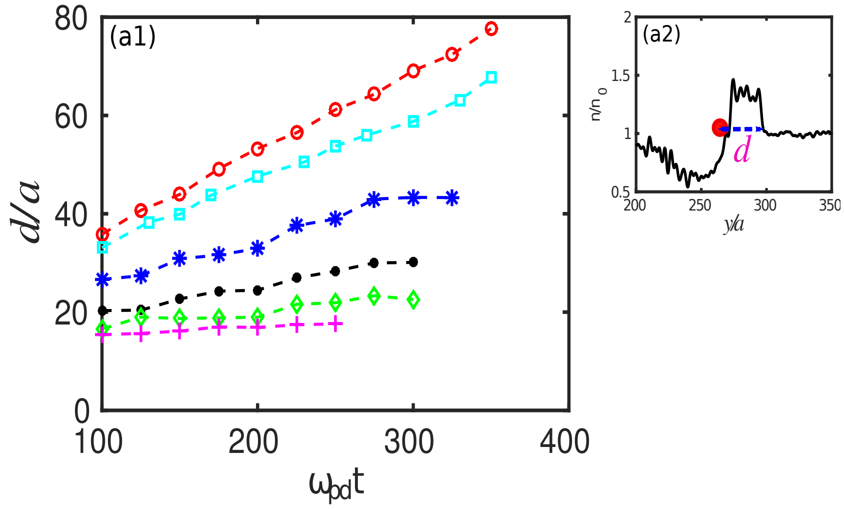

Figure 3.4: Time evolution of the width d (along $\hat{y}$) of precursor density crest with respect to the projectile position is shown in subplot (a1) for different Mach number of the prjectile with charge $Q_p = 100Q$. The way d is defined and measured has been shown in subplot (a2), where red solid dot represents the projectile. In subplot (a1), red, cyan, blue, black, green, and magenta colored symbols are for different Mach number $M = 1.01$, 1.1, 1.3, 1.5, 1.7, and 1.9, respectively.

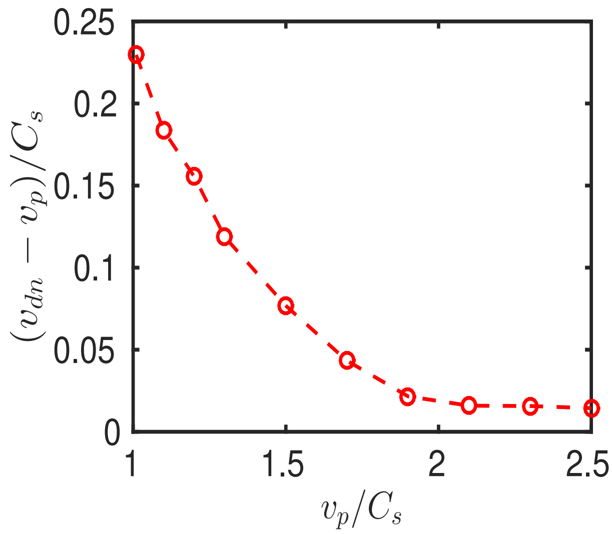

Figure 3.5: propagation velocity of the front of the density crest v_{dn} relative to the projectile speed v_p for different Mach numbers of the projectile with fixed charge $Q_p = 100Q$. Here, the normalization has been done by the dust acoustic speed of the medium C_s.

width d has been calculated with respect to the projectile's position (y-coordinate) at different times, as shown in the subplot (a2) of Fig. 3.4. It is observed that for lower values of Mach number (M = 1.01-1.3), the width of the density structure increases rapidly with time. The value of d also decreases with increasing Mach number. This was also shown in Fig. 3.3. It is also clearly seen that with increasing M, the time rate of increase in the width of the precursor density crest decreases. For $M = 1.7$ and 1.9, The width d become nearly constant in time. This certainly indicates that the relative speed of the leading front of precursor density structure should decrease with increasing Mach number of the projectile. In order to verify this, the relative velocity of the forefront of the density structure with respect to the projectile speed ($v_{dn} - v_p$) has been calculated and depicted in Fig. 3.5. It is indeed seen that the relative speed decreases with increasing Mach number. For Mach number $M \geq 1.7$, the relative speed of the crest becomes very low. Consequently, The width does not change measurably with time, as shown in Fig. 3.4.

The formation of different density structures in the upstream region of the projectile with various Mach numbers can be understood by the following arguments. When a highly charged particle moves through the medium, it pushes away particles of the medium from its path because of the repulsive force (in our case shielded Coulomb) among them. As a result, a nonlinear collective density compression will be initiated in the forward direction when the projectile's speed exceeds the value of dust acoustic speed of the medium. This nonlinear density crest will move and spread with a certain velocity in the precursor region of the projectile. The width of the precursor density crest increases with time as long as the rate of spreading of this density structure exceeds the value of projectile's speed, as shown in Fig.

3.4 and 3.5. For lower values of M, i.e., when the relative speed of the density crest is much larger, they get enough time to spread in the forward direction. As a result of that, at very low Mach numbers, multiple peaks and broader structure of the crest in density profile are observed, as shown in Fig. 3.3. When the velocity of this precursor structure becomes equal or less than compared to the projectile's speed, the width remains constant in time. In that case, the precursor density crest will move along with the projectile as a pinned structure. This has been clearly depicted in Fig. 3.3 and Fig. 3.4.

3.2.2 Variation with the charge of the projectile

In order to study the effect of projectile's charge on the collective structure, the charge of the projectile moving with a fixed Mach number $M = 1.1$ has been varied from $Q_p = 10Q$ to $150Q$. The time evolution of the width d of the precursor density crest for various values of the charge on the projectile has been shown in Fig. 3.6. In the inset of Fig. 3.6, the relative velocity of the forefront of density crest $(v_{dn} - v_p)$ has been shown for different charges on the projectile. It is observed that the velocity does not change much (varying only between $0.155 - 0.19$) with the choice of the range of charge between $10Q$ to $150Q$ of the projectile. Consequently, the value of width d at a given time, as well as the rate of change of d does not change much with the charge of the projectile. It is also observed that for $Q_p = 10Q$, the values of d at different times get reduced significantly compared to the cases with $Q_p > 50Q$. This may be because of the significant decrease in the strength of the perturbation caused by the projectile with a very low charge. Single particle responses which will be discussed in the next section (Sec. 3.3), are often also responsible for the increase in the width d for the higher values of charge of the projectile.

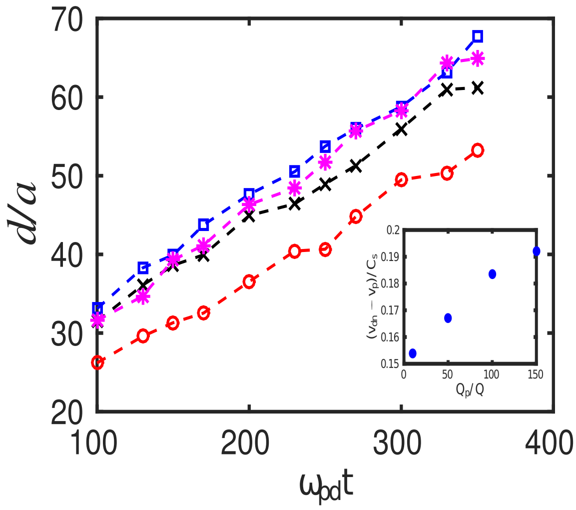

Figure 3.6: Time variation of the width of the precursor density crest d for different values of charge of the projectile moving with the fixed Mach number $M = 1.1$. Here, magenta, blue, black, and red colors are for $Q_p = 150Q$, $100Q$, $50Q$, and $10Q$. Inset shows the relative velocity of the density-crest front with respect to the projectile speed for different values of the projectile's charge.

The particle density profiles n along the $\hat{y}$ have been shown in the Fig. 3.7 at different times for $M = 1.1$. It is indeed seen that with time the width (d) of the density compressed structure increases. This is because, for this particular Mach number ($M = 1.1$) of the projectile, the spreading rate of the density structure (relative velocity of the forefront) is higher compared to the projectile's speed. Consequently, it is also observed that the appearance of multiple peaks and the inter-peak separation in the density compressed structure are becoming more prominent with time. Certainly, these results reveal great insights and detail understandings in the recently reported study of precursor solitons and/or dispersive shocks in the dusty plasma medium.

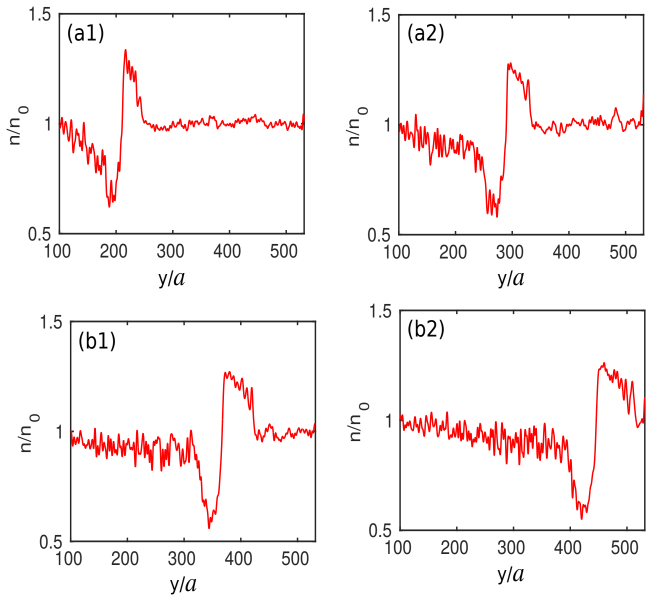

Figure 3.7: Particle density profile with the projectile having charge $Q_p = 100Q$ and Mach number $M = 1.1$. Subplots (a1), (a2), (b1), and (b2) represent the same at time $\omega_{pd}t = 100$, $\omega_{pd}t = 200$, $\omega_{pd}t = 300$, and $\omega_{pd}t = 400$.

3.3 Single particle features

In Chapter 2, the energetic particle generation originating from the single particle scattering events and its consequences in the dynamics of the medium have been discussed. We believe that these observations, in turn, would have far reaching consequences to many kinds of collective phenomena that has so far been observed in the context of dusty plasma medium. For instance, when a charged projectile moving with the supersonic speed through the dusty plasma crystal, it produces Mack cone wake structures behind the projectile, as well as precursor density crest moving ahead of the projectile, as have been discussed in the previous section of this Chapter. A charged projectile in the medium should also elicit single particle scattering events leading to energetic particle generation. These faster particles can disturb the medium ahead of the shock region which otherwise should have remained undisturbed. Though the location of secondary centers is a random event and may not necessarily form exactly ahead of the initial inserted projectile particle, but, it is quite likely that in these random events the medium ahead of the projectile gets disturbed even before the sound or the shock has had a chance to reach there. We now carry out simulations to ascertain whether this indeed happens.

3.3.1 Generation of high energetic particles

We insert a charged particle in the system with $Q_p = 100Q$ and a velocity $v_p = 1.3 \times 10^{-2}$ m/sec, associated with the Mach number, $M = 1.41$.

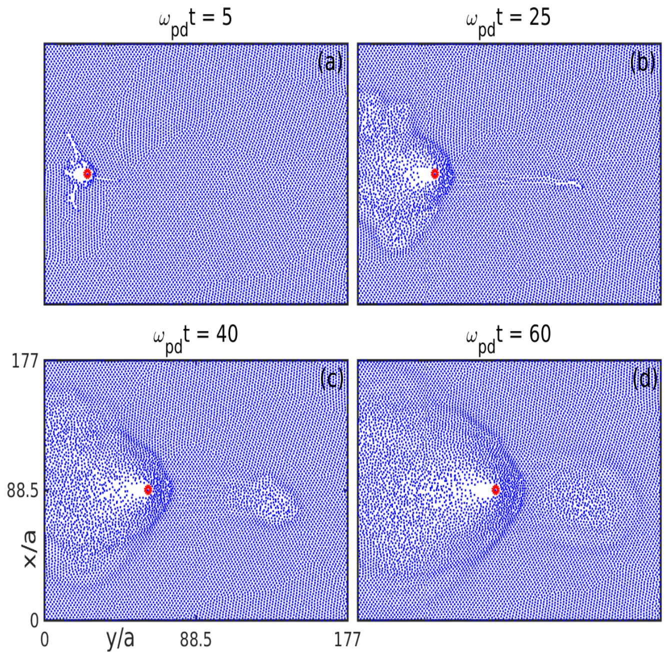

Figure 3.8: Time lapse sequence of the snapshots of particle configurations when a projectile (red marked circle) with charge $Q_p = 100Q$ and velocity $v_p = 1.3 \times 10^{-2}$ m/sec (Mach number, $M = 1.41$) moving through the medium. Single particle scattering is shown in (a) and (b) -(d) shows the occurrence of deformations and disturbances far ahead of the precursor shock.

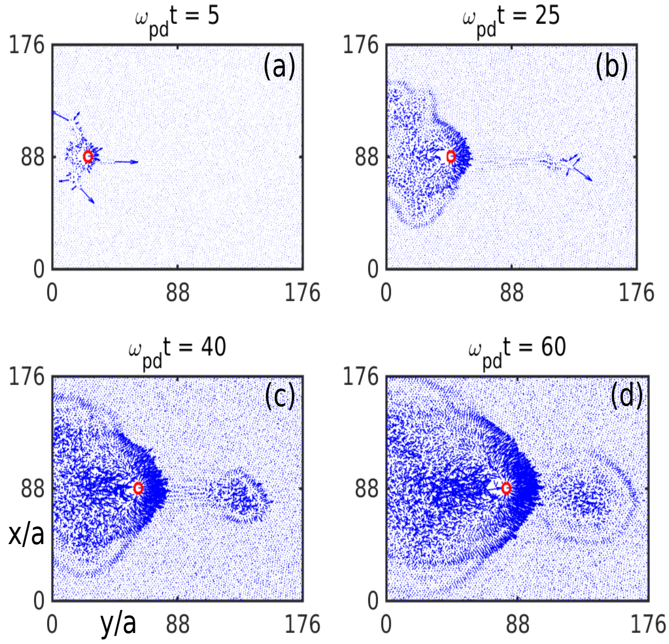

Figure 3.9: Time series of velocity quiver plots with a projectile (red marked circle) having charge $Q_p = 100Q$ and velocity $v_p = 1.3 \times 10^{-2}$ m/sec ($M = 1.41$).

It can be observed from Fig. 3.8, that at $\omega_{pd}t = 5$ the dust particles get evacuated from the neighborhood of the projectile and a few dust grains acquire high velocities. They move very rapidly away from the projectile. This is more apparent from the velocity quiver plot of Fig. 3.9. A shock structure is also observed to form ahead of the projectile. However, the energetic particles disturb the unshocked crystalline medium beforehand. Thus when the shock region catches up, it encounters not the original medium but a disturbed crystal. In these simulations also, energetic particle has a ballistic propagation in the medium in the beginning wherein it creates cracks and defects along its path. Subsequently, however, as it slows down it excites a collective response in the medium around a point which is located considerably apart from the position of the projectile.

3.3.2 Single particle induced phase transition

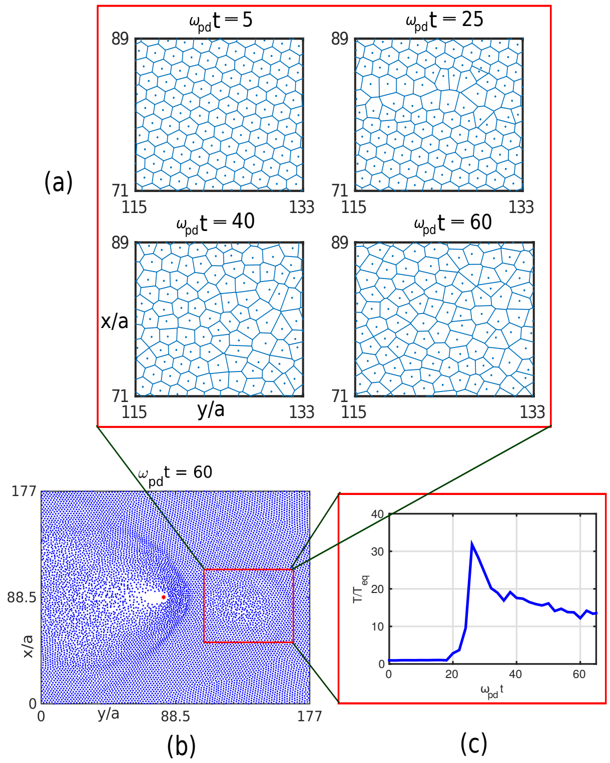

Figure 3.10: Occurrence of phase transitions in a local region (red marked quadrilateral in (b)) far-ahead of the precursor. Time series of Voronoi diagram indicates the breaking of crystal symmetry, as shown in (a). Time evolution of temperature of the local region is shown in (c).

The collective excitations at the secondary centers triggered by these energetic particles change the properties of the medium in the neighborhood, as well as beforehand of the precursor waves (Fig. 3.9). We have illustrated this with the help of Voronoi plots (Fig. 3.10(a)). The initial lattice has an ordered hexagonal form. However, after it gets disturbed, the lattice structure breaks down and system appears to take a disordered form.

We have also evaluated the temperature of the localized region disturbed by one of the energetic particles much ahead of the projectile. In Fig. 3.10(c) the time evolution of the temperature of this localized region has been shown. It is observed that the temperature of this region increases almost 30 times when the energetic particles reach there. Subsequently, however, the temperature appears to steadily decrease. However, it still remains quite high (about 10 times) when the shock associated with the projectile arrives at this location. This would correspond to an effective $\Gamma = 100$ for this local region. This value of Γ corresponds to an intermediate phase of complex fluid between liquid and solid states, which has often been characterized as visco - elastic medium. Thus, instead of a regular crystal structure, the shock propagating with the projectile would encounter a region of visco-elastic [23–25, 106] medium rather than a crystal state. Thus, the propagation of precursor solitons and/or dispersive shock, which are moving ahead of the projectile at comparatively slower time scale, will encounter patches of disturbed medium in an altogether different phase. This will effect their dynamics considerably.

3.3.3 Varying charge of the projectile

The velocity quiver plots in Fig. 3.11 are showing the velocity map of the particles in the medium with different charge of the projectile. It is seen that for $Q_p = 10Q$ (subplot (a1)), the perturbation strength is not enough to trigger the single particle responses in the medium. Thus, when a projectile with charge $Q_p \leq 10Q$ moves through the dusty plasma crystal with supersonic speed , it can only initiate the collective phenomena in terms of Mach cone wake and precursor shock in the medium, as can be seen in the subplot (a1) of Fig. 3.11. But for higher charged projectile ($Q_p \geq 50Q$), besides these collective dynamics, single particle responses in terms of generation of the few energetic particles, have also been initiated in the medium. These high energetic particles may excite the secondary collective disturbances ahead of the precursor density crest, as shown in the subplots (a2)-(b2) of Fig. 3.11. These secondary collective excitations change the properties of the medium (Fig. 3.10), as well as may affect the structure of precursor density crest, as mentioned in the section 3.2.2.

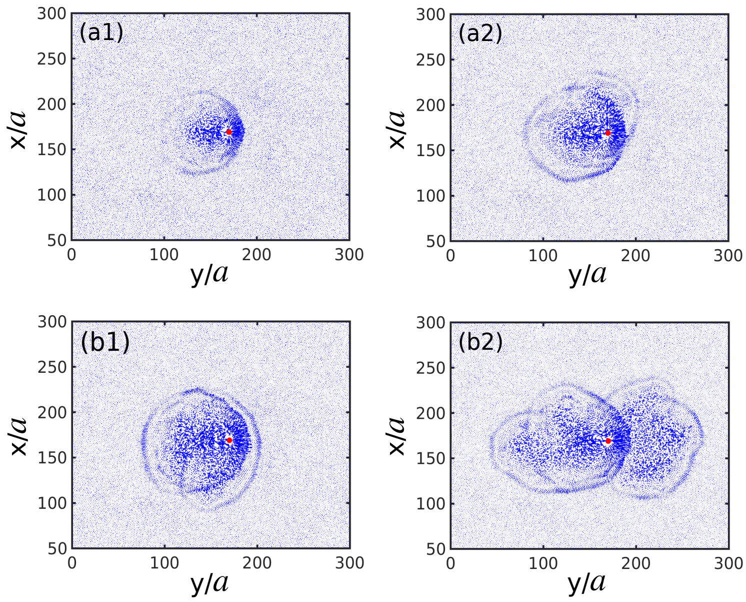

Figure 3.11: Velocity quiver diagrams with the projectile (red solid dots) having charge (a1) $Q_p = 10Q$; (a2) $Q_p = 50Q$; (b1) $Q_p = 100Q$; (b2) $Q_p = 150Q$ moving with the constant speed $M = 1.1$ along $\hat{y}$. All the subplots are at the same time $\omega_{pd}t = 50$.

3.3.4 Multiple projectiles

We have also simulated a case with multiple projectiles [112], all of them having the same high charge ($Q_p = 100Q$) and moving with the same velocity along $\hat{y}$. This choice helps preserve periodicity condition along $\hat{x}$ direction. Furthermore, with an increased number of such projectile particles, one essentially mocks up a moving wire having a potential bias (frequently used in experiments [113]). For

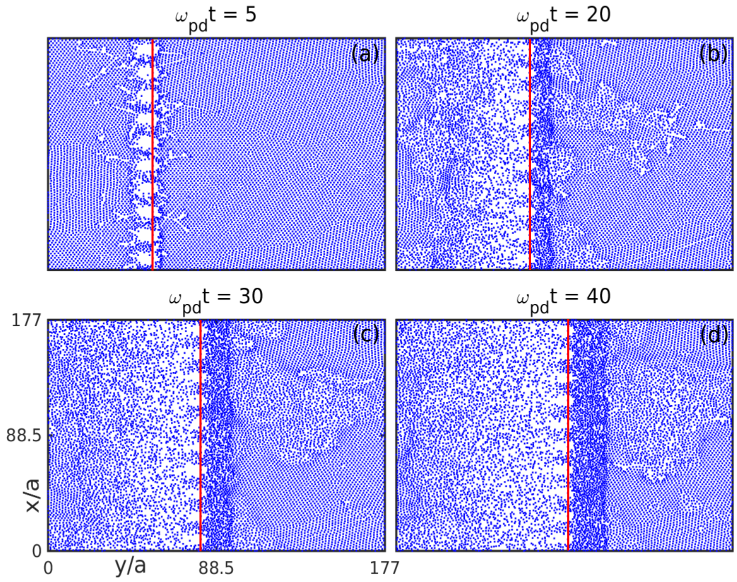

Figure 3.12: Time series of particle configurations of the system when an array of 10 particles (red marked line) each with charge, $Q_p = 100Q$ and velocity, $v_p = 1.3 \times 10^{-2}$ m/sec (associated Mach number, $M = 1.41$) moving along $\hat{y}$ direction through the medium.

this case too one observes a few energetic particle shoot ahead of the projectile initially creating disturbances in the medium ahead. A planar shock gets formed which then encounters a disturbed medium. This has been shown in Fig. 3.12.

3.4 Effect of neutral damping

The effect of gas damping on both the single particle and collective response has also been studied in this work. It is observed that the energy acquired by the particles in single particle scattering events decreases faster in the presence of damping due to neutral gas. As a result, the energetic particles travel comparatively shorter distance through the crystal and the distance of the secondary centers of collective excitations occur at a reduced distance. Furthermore, the time to excite secondary

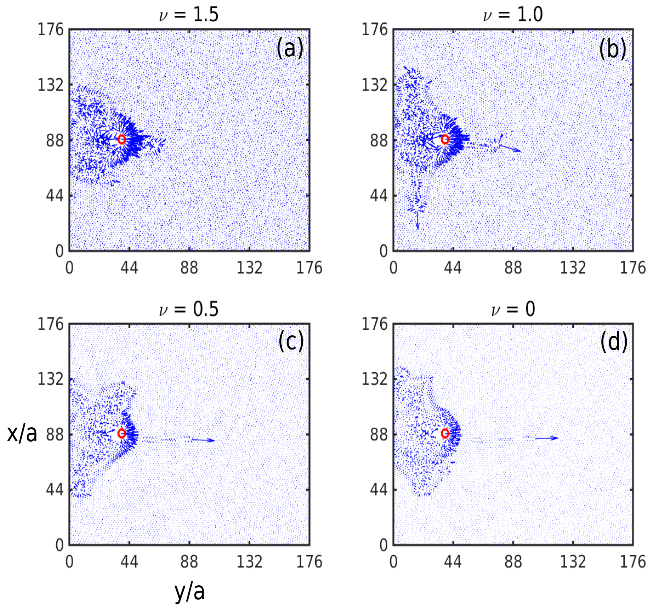

Figure 3.13: Velocity quiver plots of particles for various damping coefficients (ν in sec^{-1}) when a projectile (red marked circle) with charge $Q_p = 100Q$ and velocity $v_p = 1.3 \times 10^{-2}$ m/sec ($M = 1.41$) moves through the crystal. All these plots are taken at time $\omega_{pd}t = 18$.

centers also gets reduced. These features have been clearly illustrated in the velocity quiver plots of Fig. 3.13.

3.5 Conclusion

The dynamical features of dusty plasma medium associated with a charged projectile moving with the supersonic speed through the medium have been investigated using molecular dynamics simulations. Dust particles are assumed to interact among themselves via screened Coulomb potential. It has been demonstrated that both the collective and single particle responses have been initiated in the medium from the moving charged projectile. A Mach cone wake structure is observed behind the projectile and has been characterized with the various Mach number of the projectile. The formation of nonlinear bow-shaped density structures in the precursor region of the projectile has been observed and reported. The time evolution of these density crests has been analyzed and elucidated with various Mach number and charge of the projectile. The transition from the precursor moving disturbance to the pinned structure of this nonlinear density crest with respect to the projectile has been captured. These are the collective responses of the medium triggered by the moving charged projectile. The single particle responses of the medium have also been demonstrated in this work. A few energetic particles are observed to generate because of the scattering events caused by the charged projectile in the medium. The phase transitions in few localized regions have been observed to trigger by some of these high energetic particles. It has also been demonstrated that these energetic particles can move with much more higher velocities compared to the precursor density structure. The effect of neutral damping on both the single particle and collective responses of the medium has also been studied. It has been shown that with increasing damping coefficient, the energy of the both the dynamics of the medium gets reduced. The time taken to excite the secondary collective centers by the energetic particles also gets reduced with increasing neutral damping.

4

Crystalline layer formations in 3-D dusty plasma medium

Srimanta Maity and Amita Das, Physics of Plasmas, 26, 023703 (2019)

In laboratory experiments typically (unlike micro-gravity experiments on space-craft) the dust particles levitate at a height where gravity balances the sheath electric field. In the strongly coupled limit 2-D crystal layer gets formed. The formation of multiple 2-D crystal layers have been illustrated with the help of MD (Molecular Dynamics) simulations. The conditions for the formation of such multiple layers along with their equilibrium structural properties have been studied in detail.

4.1 Introduction

Dusty plasmas have proven to be an ideal model system to study the strong coupling effects in laboratory experiments. The high charge on each of the dust grains often leads the average inter-grain potential energy to exceed the value of average thermal energy, driving the medium to the strongly coupled state in the typical laboratory conditions. One of the interesting consequence of this is the arrangement of particles in ordered structures with the characteristic features of a crystalline medium. The first experimental observations of dusty plasma crystal (Coulomb crystal) were reported in 1994 in radio frequency (rf) discharge plasma by four independent research groups, Chu *et al.*, [32], Hayashi and Tachibana [48], Thomas *et al.*, [31], and Melzer *et al.*, [132]. Later on, plasma crystals were found and reported by Fortov *et al.*, [133] in a direct current (dc) glow discharge plasma experiment.

Coulomb crystallization was also been observed in colloidal suspensions. But there are certain disadvantages in the study of crystalline properties using colloidal crystal as a model system. Colloidal crystal typically consists of negatively charged almost mono-dispersive micron sized particles suspended in an electrolyte. The inter-particle interaction is shielded by the ions of both signs of the electrolyte, similar to the case of dusty plasma medium. The typical screening radius being very small, in a colloidal suspensions a rather high particle number density is required for crystallization (unlike dusty plasma crystals). Consequently, colloidal crystals are usually opaque making it difficult to have a detailed experimental investigation of there bulk properties. Another drawback in the study of the colloidal crystals is that they have very long equilibrium relaxation time (several weeks) in the typical experimental conditions.

The dynamics of the individual particles of a dusty plasma medium are, however, easily observable and can be traced even by normal charge-coupled devices. The response time scale of a dust-plasma system to the variations of experimental conditions is also fast (few seconds) in contrast to that for a colloidal suspension. Thus, dusty plasma crystals appear to be particularly suited as model systems for the investigation of various statistical phenomena in condensed matter studies in the laboratory conditions.

Another unique aspect of a dusty plasma system is that additional forces such as gravity etc., (as discussed in Chapter 1), which are typically insignificant in the conventional electron-ion plasma experiments, may play important roles in the characteristic properties of the medium. Particles can be confined in a wide range of configurations with different geometries by utilizing these forces in a controlled way. In this part of the thesis, we have performed equilibrium three-dimensional (3-D) molecular dynamics simulations in order to explore the effects of two most important forces, (a) force due to gravity ($m_d\boldsymbol{g}$) and (b) force due to the sheath electric field ($Q\mathbf{E}_{ext}$). These two forces are typically present in all ground-based dusty plasma experiments, responsible for the levitation of charged dust grains in the plasma environment. In this study, the layered crystal formation in dusty plasma medium with Yukawa interaction amidst dust grains has been investigated [85]. The mechanism behind the formation of multilayer structures, in the presence of a combined gravitational and external electric field force (representing the sheath field in experiments) has been investigated. A detailed study of the dependence of the number of layer formation, their width, etc., on various system parameters (viz., the external field profile and the screening length of Yukawa interaction) have been analyzed. The configurational properties of each of these layers have also been studied for some cases.

4.2 Molecular dynamics simulation descriptions

Three-dimensional (3-D) Molecular Dynamic (MD) simulations have been carried out using an open source classical MD code LAMMPS [125]. Initially, 500 identical point particles, each having a mass $m_d = 6.99 \times 10^{-13}$ kg and charge $Q = 11940e$ (where e is an electronic charge), is chosen to be distributed randomly in a 3-D simulation box. The boundary conditions are chosen to be periodic. The length of the simulation box $L_x = L_y = L_z = 12.7943a$. Here $a = (3/(4\pi n))^{(1/3)}$ is the Wigner-Seitz radius in three dimensions and n is the average 3-D density of particles for the whole simulation box. It should thus be noted here that $a \propto n^{-1/3}$, thus increasing density is tantamount to decreasing a. In our simulations, n is kept to be 2×10^7 m^{-3}, so that the value of $a = 2.2854 \times 10^{-3}$ m. The magnitude of inter-particle unscreened electric field associated with this value of a is $E_0 = Q/4\pi\epsilon_0 a^2 = 3.2918$ V/m. The interaction potential between particles (dust grains), as indicated in section I, is taken to be Yukawa (screened Coulomb). Beside the Yukawa interaction, particles are also subjected to the external force due to gravity $m_d g(-\hat{\mathbf{z}})$ (i.e. acting vertically downward) and the force exerted by the electric field $Q\mathbf{E}_{ext}(z) = QA\exp(-\alpha z)\hat{\mathbf{z}}$ (which acts vertically upward for negatively charged dust particles), as shown in the schematic of Fig. 4.1. The magnitude of the electric field is adjusted by A in a fashion so as to have the potential minima of these external force at the middle of the simulation box at $L_z/2$. The value of A is thus calculated from, $A = (m_d g/Q)\exp(\alpha L_z/2)$ for a given value of α in our simulations. This ensures that for all values of α, the two external forces $m_d\boldsymbol{g}$ and $Q\mathbf{E}_{ext}$ can balance each other exactly at $z = L_z/2$. The potential minima, as shown on Fig. 4.2 appears at $L_z/2$. It should be noted that even if one keeps the value of A to be constant for different values of α, it does not change any phenomena. It merely provides a vertical shift in the position of dust layers. Thus, this choice is mainly to ensure that the equilibrium location of the dust particles under the external forcing is at the center of the simulation box for convenience. For the chosen set of parameters the characteristic frequency $\omega_{pd} = (nQ^2/\epsilon_0 m_d)^{(1/2)} \simeq 3.4389\ s^{-1}$, associated with the dust plasma period of $T_d = 1.8271\ s$. This is typically the fastest frequency associated with the dust medium and hence its inverse is chosen to normalization time. We have chosen our simulation time step to be $0.01\omega_{pd}^{-1}$, which can thus resolve the time scale of any phenomena associated with dust response.

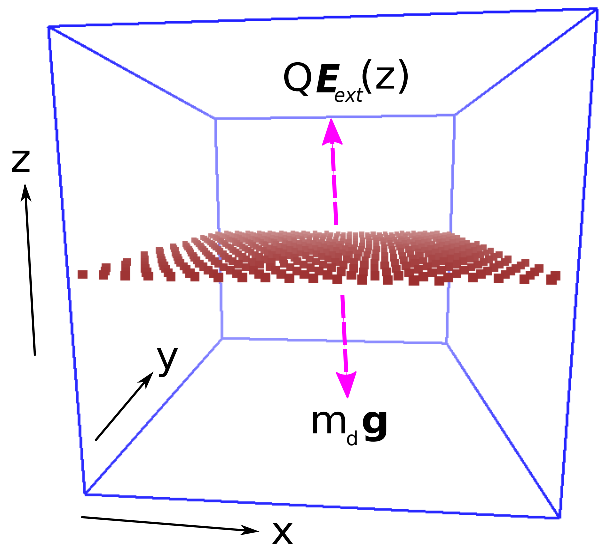

Figure 4.1: Shows the schematic of simulation configuration with two oppositely directed external force (a) force due to gravity $m_d\boldsymbol{g}$ and (b) force due to externally applied electric field $Q\mathbf{E}_{ext}$.

Positions and velocities of each particle have been generated from the canonical ensemble (NVT) in the presence of a Nose-Hoover thermostat [126, 127]. The purpose of using Nose-Hoover thermostat is to achieve thermodynamic equilibrium state for a given value of Γ. We have continued our simulations connecting this thermostat for about $4000\omega_{pd}^{-1}$ time for all cases. In every case, it has been checked that the system achieved the assigned equilibrium temperature much before this time. For all of our simulation studies, we have chosen Γ $(= Q^2/4\pi\epsilon_0 a k_B T)$ to be 3000.

4.3 Numerical observations

4.3.1 Layer formation

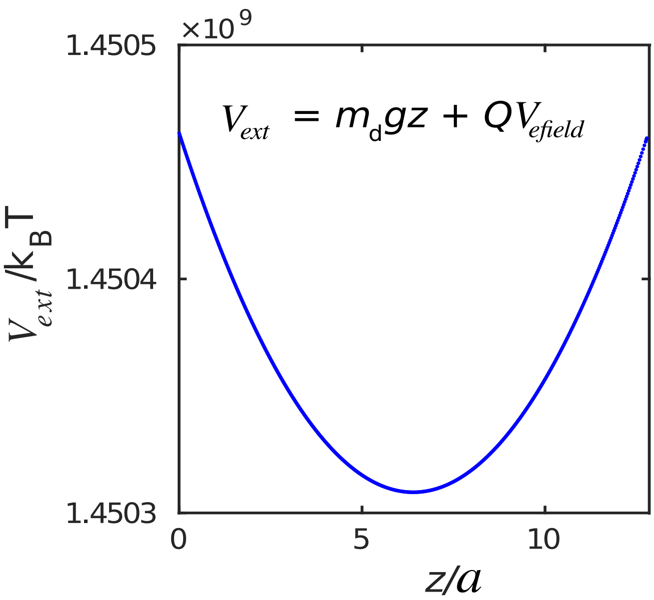

Figure 4.2: Shows total external potential energy, V_{ext} along z for $V_{efield} = -\int E_{ext}(z)dz = (A/\alpha)\exp(-\alpha z)$, with $\alpha a = 2.2854 \times 10^{-3}$ and $A/E_0 = -1.105 \times 10^3$.

The total potential energy associated with each particle V_{ext} at any vertical position z, has contributions from the gravitational potential energy $m_d gz$ and the electrostatic energy associated with the externally applied electric field $E_{ext}(z) =$

$A\exp(-\alpha z)$. The plot of the external potential energy V_{ext} experienced by the dust particles as a function of z is shown in Fig. 4.2, for $\alpha a = 2.2854 \times 10^{-3}$ and $A/E_0 = -1.105 \times 10^3$. It is clearly seen that the minimum in the potential energy profile occurs at $z/a \approx 6.4$. The minimum is sharper when the value of α representative of how rapidly the external electric field falls, is high. A single dust grain will always reside on the z location where the potential energy is minimum. As the number density of the dust grains is increased, they would try to equilibrate at this location so long as the inter-dust interaction has considerably smaller effect than the external potential. In such a case, single dust layer gets formed. However, with increasing number density, the dust particles start experiencing the Yukawa interaction and automatically try to arrange themselves in a two-dimensional (2-D) crystal formation for which the inter-dust distance is larger for the Yukawa potential amidst them to be effective.

The multilayer formation starts when besides experiencing the external force field, inter-particle Yukawa pair potential starts becoming important. As the initially randomly distributed particles now try to achieve equilibrium in the external potential as well as the self consistent interaction potential. The interplay of these two defines the multiple layer formation. In our system the sheath potential profile is defined by α and the Yukawa interaction by the parameter κ. We study the equilibrium layer formation in terms of α and κ parameters.

In Fig. 4.3, equilibrium configurations of particles have been shown for different α and κ values. It has been observed that particles choose to levitate at different heights along $\hat{z}$ forming layered structure, instead of randomly filling up the entire simulation box. Though there is only one minimum of external potential for all values of κ and α, there are more than one layer which get formed, as can be

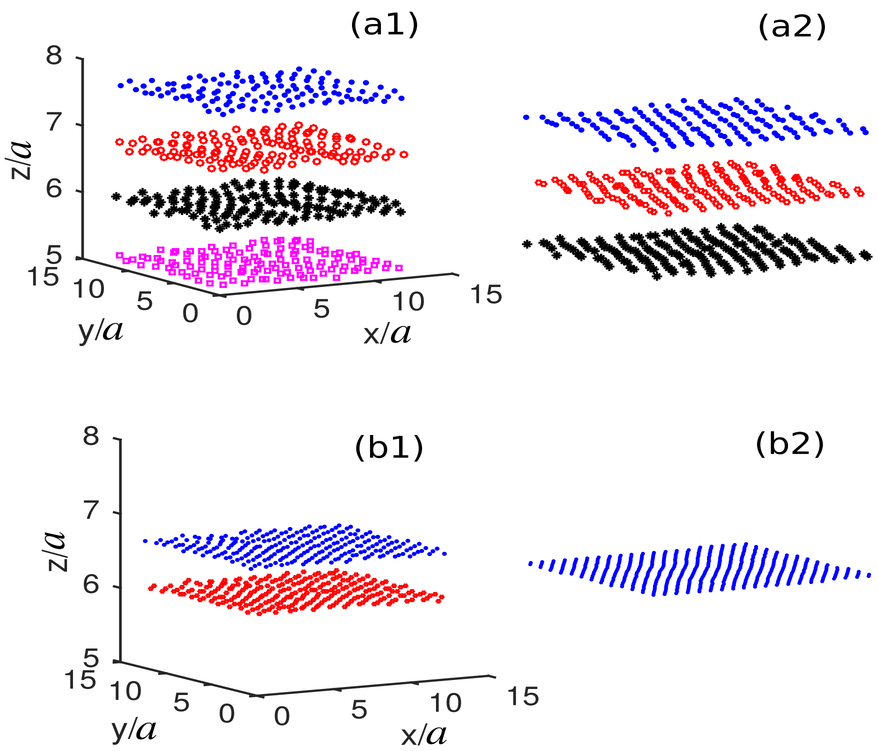

Figure 4.3: Shows layers formation for different κ and α values. Subplots (a1) and (a2) are for $\kappa = 1.0$ and 1.5, respectively with a fixed $\alpha a = 2.2854 \times 10^{-3}$. Subplots (b1) and (b2) are for $\alpha a = 5.7134 \times 10^{-3}$ and 38.852×10^{-3}, respectively with fixed value of $\kappa = 2.5$. Different color symbols represent dust particles levitating in different layers.

observed from Fig. 4.3. The external forces of gravity and sheath electric field try to confine particles at the location of the minimum of V_{ext}, the location of potential energy minimum as depicted in Fig. 4.2. However, the repulsive force associated with the pair potential tries to maintain a certain inter-grain distance. If such an inter-grain distance can not be maintained by a single layer, the layer first gets a little broader and then ultimately splits and forms clear two layers as shown in Fig. 4.4. The layer increases in number by first broadening itself and subsequently forming an additional clear layer. This fact is also clearly shown in Fig. 4.5 by the density profile of particles f(z) along the vertical z-axis (blue color line). We have obtained f(z) by binning the whole system along the z-axis and then counted the number of particles in each bin. Function, f(z) has been normalized by the total number of particles in the system, such that $\int_0^{L_z} f(z)dz = 1$, where L_z is the length of the simulation box along z.

The number of layers, thus gets determined by a competition between external confining potential and the repulsive pair potential $U(r)$. This fact is clearly depicted in Fig. 4.3 and Fig. 4.4.

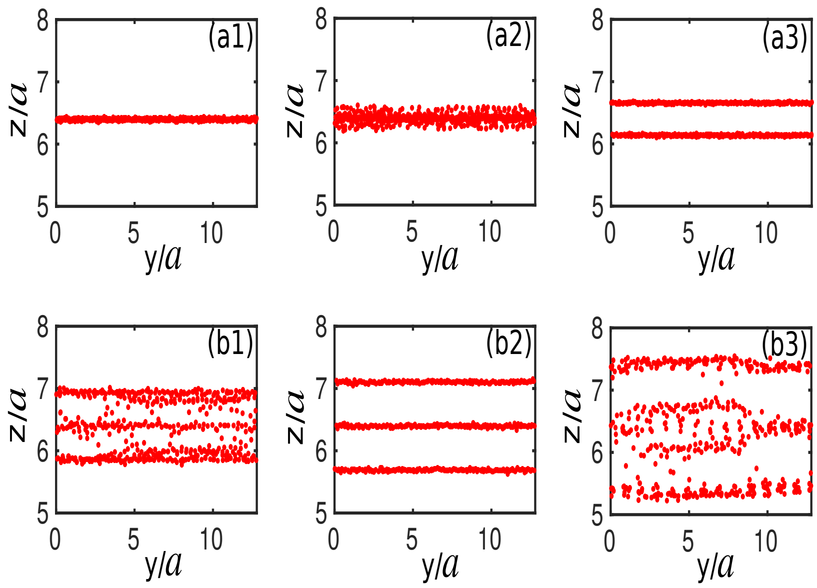

Figure 4.4: Shows side view of particle's positions (red points). Subplots (a1) $\kappa = 8.0$, (a2) $\kappa = 7.0$, (a3) $\kappa = 4.5$, (b1) $\kappa = 2.75$, (b2) $\kappa = 2.0$, and (b3) $\kappa = 1.29$. All the subplots are for a constant $\alpha a = 2.2854 \times 10^{-3}$.

4.3.2 Characterization of layered structure

It should be noted that while α defines the sheath profile of the external electric field, κ represents the range of the interaction distance amidst the dust grains. For a fixed value of parameter κ, as α increases, the external potential profile becomes sharper. Thus particles have to be confined within a short height. As a result, the

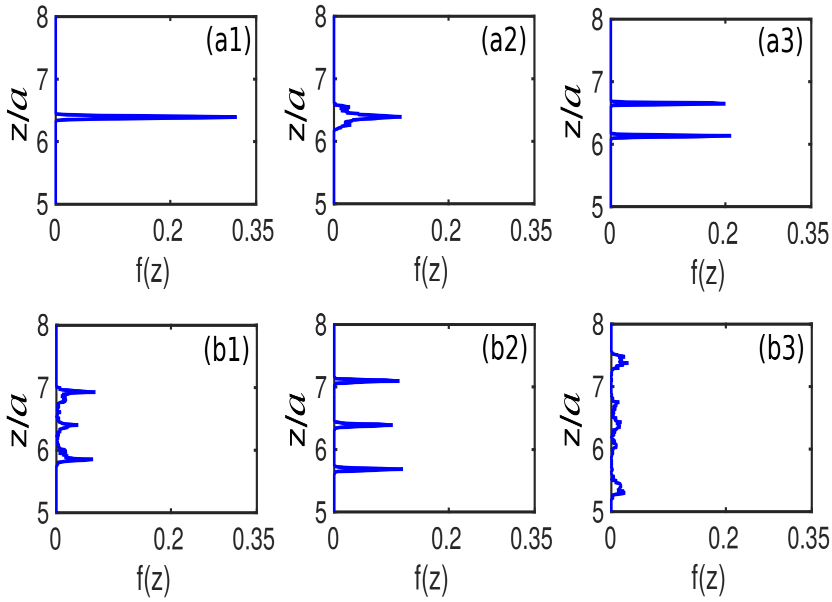

Figure 4.5: The density profile of particles, f(z) (blue lines) along $\hat{z}$. Normalization has been done in such a way that $\int_0^{L_z} f(z)dz = 1$, where L_z is the length of the simulation box along $\hat{z}$. Subplots (a1) $\kappa = 8.0$, (a2) $\kappa = 7.0$, (a3) $\kappa = 4.5$, (b1) $\kappa = 2.75$, (b2) $\kappa = 2.0$, and (b3) $\kappa = 1.29$. All the subplots are for a constant $\alpha a = 2.2854 \times 10^{-3}$.

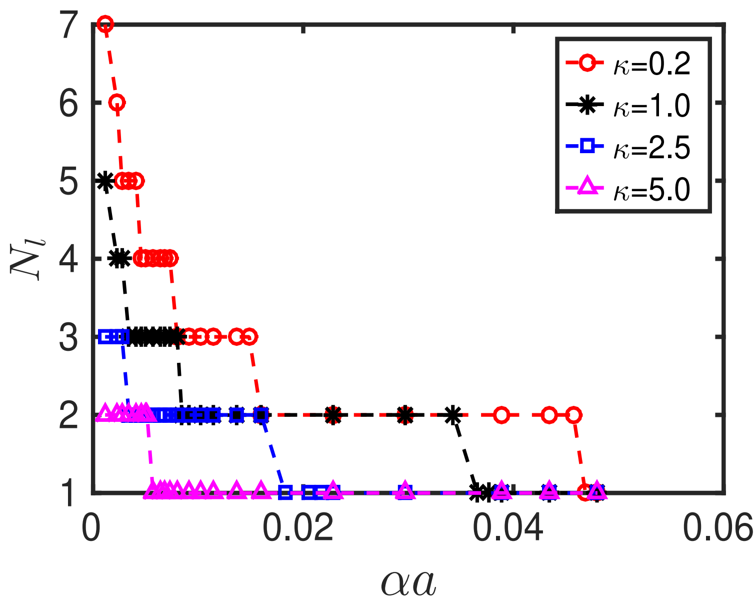

Figure 4.6: Variation of number of layers N_l with α at different fixed values of κ.

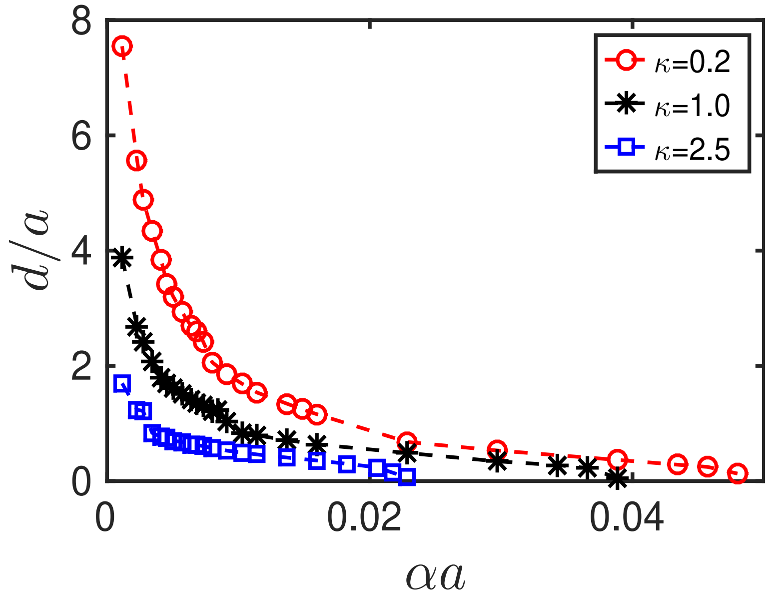

Figure 4.7: Variation of the width of the particle distribution along $\hat{z}$ with α at fixed values of κ.

number of layers and the width of particle distribution d along $\hat{z}$ decreases with increasing value of α, as shown in Fig. 4.6 and Fig. 4.7. As κ increases, the mutual repulsive force between particles gets weaker. Consequently, both the number of layers Nl and the thickness d decreases with increasing κ, for fixed values of α. This has also been depicted in Fig. 4.6 and Fig. 4.7.

Next, we want to understand the effect of thermal energy of particles on these layered structures. it is quite obvious that if the thermal energy of the particles is increased, they can easily overcome the total effective potential barrier, contributed from both the pair repulsion and total externally applied potential and make the system to be homogeneous. Side view (y-z plane) of particle positions (red dots) for different values of Γ with fixed $\kappa = 1.5$ and $\alpha a = 2.2854 \times 10^{-3}$ is shown in Fig. 4.8. It is clearly seen that at sufficiently high temperature ($\Gamma = 10$) particles choose to distribute with a width around the location of minimum in the potential

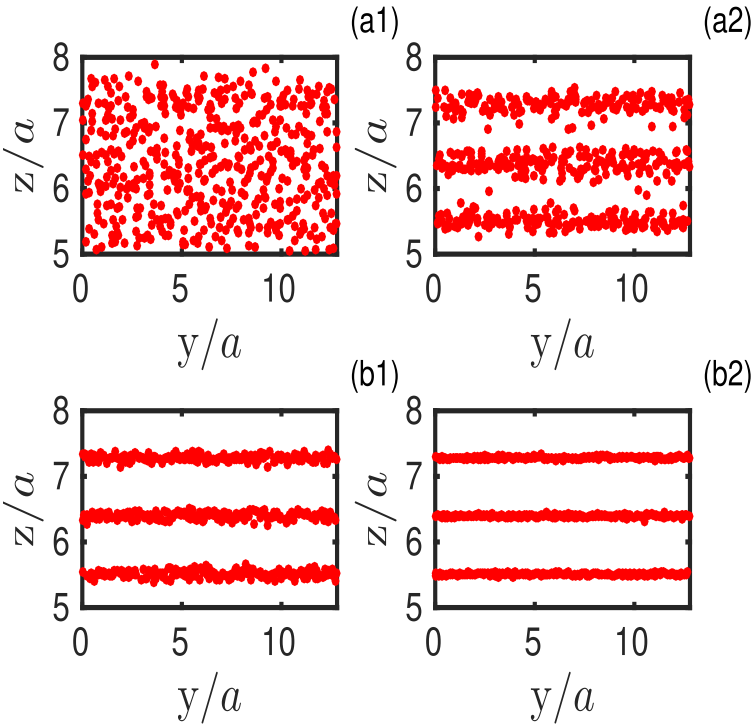

Figure 4.8: Side view of particle positions (solid red points) for different values of Γ. Subplots (a1), (a2), (b1), and (b2) are for $\Gamma = 10$, 100, 300, and 3000, respectively, with fixed values of $\kappa = 1.5$ and $\alpha a = 2.2854 \times 10^{-3}$.

energy profile ($z/a \approx 6.4$) forming a homogeneous cloud. As we increase the values of Γ, microscopic structures along $\hat{z}$ start to appear in this homogeneous cloud, as can be seen form subplots (a2) and (b1) of Fig. 4.8. This is expected as with increasing Γ, the temperature of the dust grains decreases and the mutual repulsive interactions will start to dominate over the thermal diffusive force in order to form layered structures. At sufficiently low temperature (subplot (b2)), particles are observed to organize themselves into distinct sharp layers. This is more apparent from the Fig. 4.9, where we have shown the particle distribution profile $f(z)$ along $\hat{z}$. It is clearly seen that the width of the peaks of the density profile, representative of distinct layers, increases with decreasing Γ. This is because the thermal fluctuations of particles around the each layer increase as we decrease Γ. For $\Gamma = 10$, no peak but a flat profile (black line) is observed in the density distribution of particles, representing a homogeneous cloud of particles.

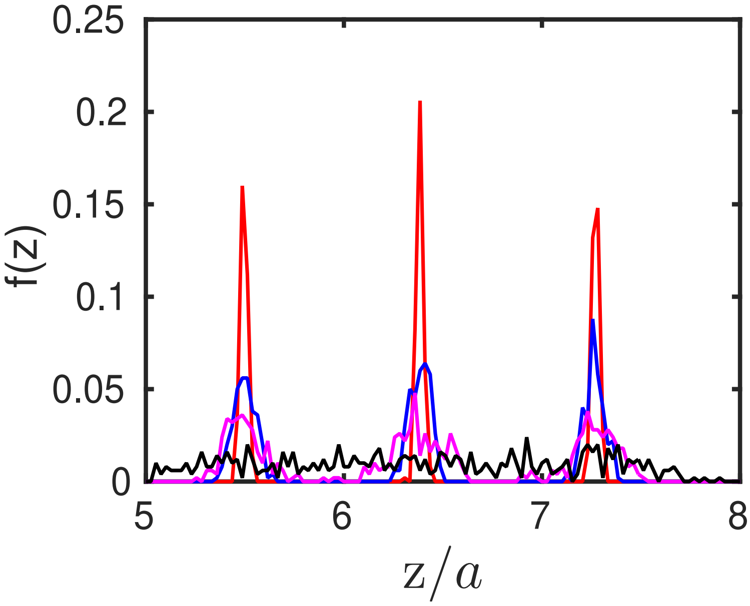

Figure 4.9: Density profile of particles $f(z)$ along $\hat{z}$ for different values of Γ with fixed values of $\kappa = 1.5$ and $\alpha a = 2.2854 \times 10^{-3}$. Colors black, magenta, blue, and red are for $\Gamma = 10$, 100, 300, and 3000, respectively.

4.4 Structural analysis of layered crystal

In this section of this chapter we will discuss some of the structural properties of these layered structures for a few cases. By obtaining the coordinates of individual particles levitating in different layers, one can analyse the internal configurations of these layers. There are several diagnostics to examine the structural properties of a ordered system. One of such tools is radial distribution function, also known as pair correlation function $g(r)$, as defined in chapter 1. It represents the probability of finding particles between r and $r + dr$ from any reference particle and so measures the translational order in the structure. Radial distribution function for two different values of κ (κ = 1.5 & 2.5) is shown in Fig. 4.10 at a fixed $\alpha a = 2.2854 \times 10^{-3}$ and $\Gamma = 3000$. Particles coordinates have been picked up separately for each of the layers and used them to obtain the pair correlation function for individual layer. It is clearly seen that for all the cases there are sharp multiple peaks exist in the profile of $g(r)$. Each crest in the profile of $g(r)$ represents the locations where the probability of finding particles is higher. Thus, the oscillations in the pair correlation functions indicate that particles arrange themselves in crystalline order structure in each of these distinct layers.

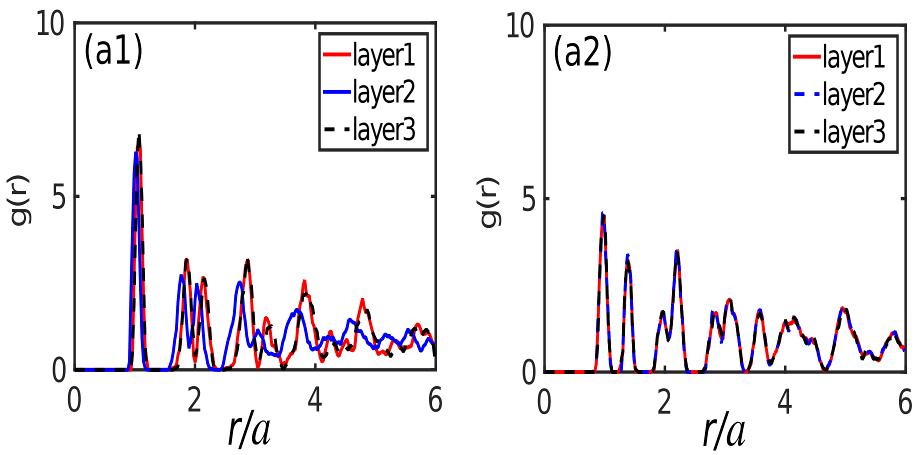

Figure 4.10: Radial distribution functions of all the three layers for two different cases: (a1) $\kappa = 1.5$, (a2) $\kappa = 2.5$ with a fixed $\alpha a = 2.2854 \times 10^{-3}$ and $\Gamma = 3000$.

In order to identify different possible lattice types in these layered structures, particle's coordinates in adjacent horizontal layers have been superimposed sequentially in a 2-D (x-y) plane. Two different types of crystal structure have been found to observe and Fig. 4.11 illustrates them. In Fig. 4.11, we have shown these superimposed particle's coordinates for two different cases, where we have changed the value of κ from 1.5 (subplot (a1)) to 2.5 (subplot (a2)), with fixed $\alpha a = 2.2854 \times 10^{-3}$ and $\Gamma = 3000$. Red solid dots, blue circles, and black stars represent the particle positions of three consecutive layers, respectively. It is seen from subplot (a1) that, for $\kappa = 1.5$, particles arrange themselves in the hexagonal closely packed (hcp) structures with the triangular configurations in each individual layers. For $\kappa = 2.5$, particle configurations consist of a typical face centered cubic (fcc) structure with the arrangement in square lattice structures in each individual layers. The fundamental origins behind these structural transitions will be discussed in more details in the next chapter (chapter 5) of this thesis.

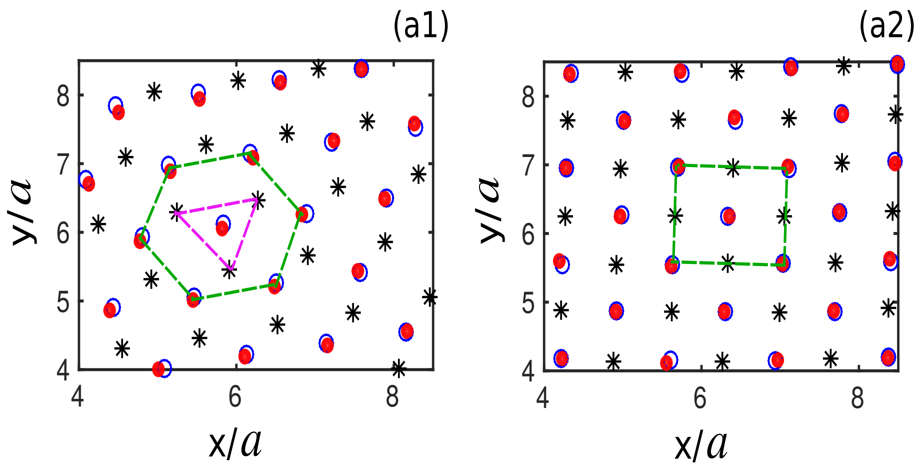

Figure 4.11: Particle's positions at three distinct layers viewing from the top (along z) for (a1) $\kappa = 1.5$ and (a2) $\kappa = 2.5$, with a fixed $\alpha a = 2.2854 \times 10^{-3}$. Red solid dots, black stars, and blue circles represent particles levitating in first, second, and third (counting from top) layer, respectively. Subplot (a1) shows a typical hexagonal closely packed (hcp) structures, where as subplot (a2) represents a typical face centered cubic (fcc) lattice structure.

4.5 Conclusions

Three-dimensional (3-D) constant temperature molecular dynamics simulations been carried out to investigate the equilibrium configurations of charged point particles (dust grains). In our simulation studies, dust grains are assumed to interact amongst themselves via screened Coulomb interaction, also known as Yukawa interaction. In typical ground-based experiments, beside the pair interactions, the dynamics of these charged micro-particles are strongly affected by the force due to gravity and sheath electric field. Thus, in order to replicate a real experimental situation, in our simulation studies, each dust particles are also subjected to the force due to gravity (vertically downward, i.e., along $-\hat{z}$) and force associated with an externally applied electric field (along $\hat{z}$), which mimics the cathode-sheath electric field in experiments. It has been shown in our simulations that in thermal equilibrium particles levitate in different discrete crystalline layers along $\hat{z}$. The mechanism behind the transitions to a new crystalline layer has been investigated in details. The number of layers and vertical width (along $\hat{z}$) of particle distribution have been characterized by two independent parameters κ and α. Here, κ defines the range of the pair interactions and α represents the sharpness of total external potential. The effect of thermal motions of particles on the discrete nature of layers has also been investigated with the changing values of Γ. The intralayer configurations of particles has been studied for some cases using pair correlation functions and directly from particle positions residing in different layers. Both fcc and hcp crystal structures are observed in the equilibrium particle configurations.

5

Structural phase transitions in a dusty plasma bilayer

Srimanta Maity and Amita Das, Physics of Plasmas, 26, 023703 (2019)

The objective of this chapter is to study in detail the structural properties of a crystalline bilayer using molecular dynamics simulations for dusty plasma medium. The conditions and mechanism behind the structural phase transitions from hexagonal configuration to square lattice symmetry have been investigated for a wide range of system parameters.

5.1 Introduction

In a typical ground-based complex plasma experiments, a dusty plasma crystal can be formed when charged dust particles are levitated in the cathode sheath region by balancing the force of gravity and repulsive electrostatic force of the sheath electric field. As discussed in the Chapter 1, the charge on the dust grain is typically shielded by the ambient plasma particles (electrons and ions). Thus, instead of Coulomb interaction, the dust particles interact amongst themselves with a repulsive shielded Coulomb potential, also known as Yukawa pair potential. This repulsive Yukawa pair potential can be characterized by a dimensionless parameter, known as screening parameter $\kappa = a/\lambda_D$, where a is the Wigner-Seitz radius in 3-D and λ_D is the typical Debye length of the background plasma. Thus, the screening parameter κ depends upon the plasma discharge conditions, as well as dust grain density. Any change in the discharge conditions, i.e., discharge voltage, background neutral pressure, etc., changes the plasma density, potential, and temperature. Consequently, plasma Debye length λ_D and screening parameter κ both will change accordingly. Again with the change of discharge conditions, the cathode sheath potential will also change. Thus, with changing experimental conditions, the dust particles can be levitated at different heights of the experimental chamber with a wide range of structural configurations.

In the context of plasmas, the structural phase transitions were first investigated and reported by Dubin [134] for a trapped Coulomb crystal for a one-component plasma (OCP) system. The layered structure transitions have been studied theoretically by Totsuji *et al.*, [35, 122] and Qiao *et al.*, [135, 136] for a Yukawa system in 1-D parabolic confining potential. The phase diagram of crystalline bilayer of particles interacting via Yukawa pair potential has been reported by Messina and Lowen [33]. They have also investigated reentrant structural phase transitions at zero temperature in these Yukawa bilayers using lattice sum minimization technique.

In this work, we focus on studying the properties of dust crystalline bilayer formations for a realistic choice of the gravitational and sheath potentials using three-dimensional molecular dynamics simulations [85]. The structural properties of each layer of the bilayer system has been investigated using various diagnostic tools. We also report the observations of the structural phase transitions observed in our simulations with the changing values of system parameters. The origin of these structural transitions is investigated in details.

5.2 Yukawa bilayer formation

In this section, we will explore some phenomena associated with the different structural properties of a Yukawa bilayer system using constant temperature MD simulations. In Chapter 4, we have shown that for a given κ and α value, particles can be made to levitate at different heights forming one or more crystalline layers. It was demonstrated that for a certain range of κ and α values crystalline bilayers can be formed. In this chapter we have focused our attention on the bilayers and have studied their characteristics in detail. In these studies, we have kept all the simulation parameters to be same as mentioned in the Chapter 4 (e.g. $\Gamma = 3000$). However, the values of κ and α have been chosen with in a range $3.0 \leq \kappa \geq 6.0$ and $0.002 \leq \alpha a \geq 0.013$.

The number density profile of particles, f(z) along the vertical z-axis for different values of κ and α is shown in Fig. 5.1. The density profile shows two sharp peaks, which are corresponding to two different layers. We have counted the number of particles in each layer and found it to be $N/2$ for all the cases, where N is the total number of dust grains in the system. Since simulation box size along x and y directions are kept constant, the mean inter-particle distance a_{xy} in each layer is the same for all the cases.

From Fig. 5.1 also it can be seen that vertical distance (along $\hat{z}$) between two layers reduces with increasing values of κ and α as depicted in subplots (a1) and (a2) respectively of this figure. This can be physically understood as follows. With increasing values of κ, the range of repulsive Yukawa interaction decreases. The layers can then choose to lie as close as possible in the vicinity of the minima of external potential without requiring additional energy to overcome the repulsion amongst themselves. Similarly, when α is increased the external potential energy minima is steeper and moving further from it requires energy. Thus, the competition between the shape of the external potential and the mutual repulsion due to Yukawa interaction essentially decides the location of the two layers.

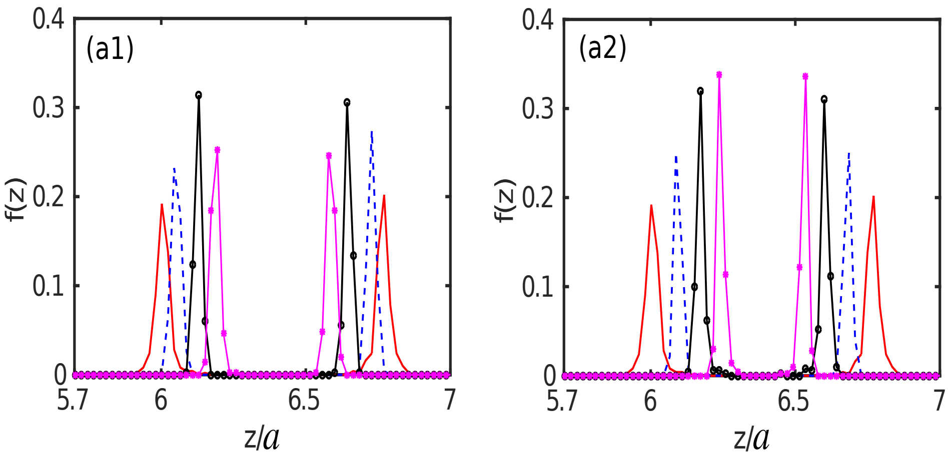

Figure 5.1: Density profile of particles, $f(z)$ along $\hat{z}$. In subplot (a1), red line represents the density profile for $\kappa = 3.0$; blue line is for $\kappa = 3.5$; black and magenta are for $\kappa = 4.5$ and 5.5, respectively with a fixed value of $\alpha a = 2.2854 \times 10^{-3}$. In (a2), red, blue , black, and magenta colors are for $\alpha a = 2.2854 \times 10^{-3}$, 4.57×10^{-3}, 7.998×10^{-3}, and 12.569×10^{-3}, respectively with a fixed $\kappa = 3.0$.

5.3 Structural properties of crystalline bilayers

5.3.1 Particle's coordinate analysis

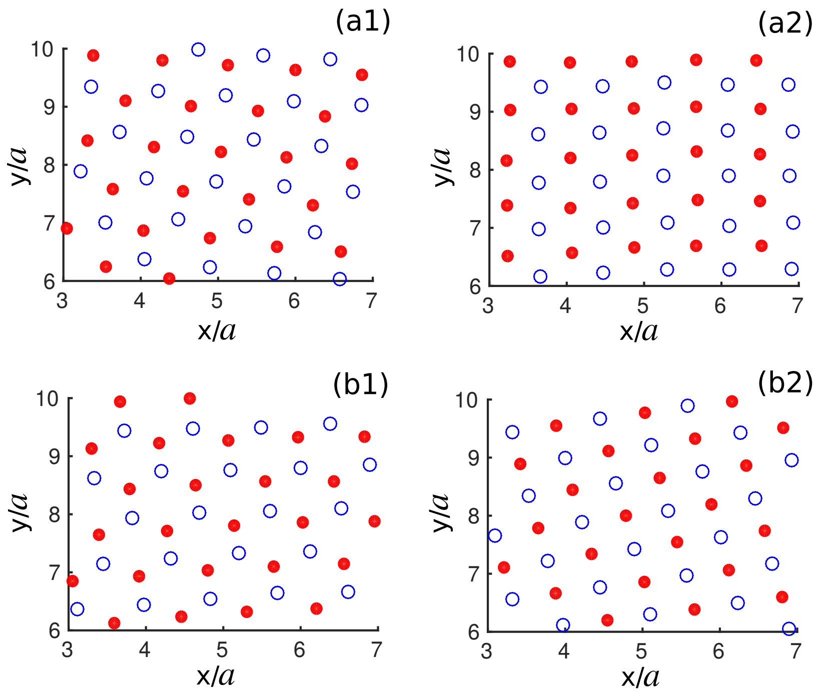

Figure 5.2: Particle positions at two different layers viewing from the top (along z). Red solid points represent particles at upper layer (layer1) and blue circles represent same at lower layer (layer2). Subplots (a1) and (a2) are for $\kappa = 3.0$ and $\kappa = 5.3$, respectively with fixed $\alpha a = 2.2854 \times 10^{-3}$. (b1) and (b2) are for $\alpha a = 3.428 \times 10^{-3}$ and $\alpha a = 11.427 \times 10^{-3}$, respectively with fixed $\kappa = 3.0$.

To analyze the structural properties of the whole system, all the particle's positions have been superimposed in a 2-D x-y plane. These superimposed coordinates are shown for different κ and α values in Fig. 5.2, where red solid dots are particle's locations in layer1 (upper) and blue circles represent the same in layer2 (lower). From Fig. 5.2, it is seen that in some cases, particles are distributed in both the layers with triangular configurations and in some other cases, they get organized in a square (or rhombic) lattice configurations. It is also clear that a vertical string structure, with particles in two layers aligned vertically (along $\hat{z}$) is not observed. Instead, particles in different layers are always found to be displaced in the transverse $x - y$ plane. This happens because for a given inter-layer separation, the inter-particle distance between two particles in two different layers is relatively higher when there is no vertical alignment. This causes the inter-particle interaction energy to be lower. Thus, the minimum energy configuration does not favor particles to be located exactly one below the other particle in a bilayer system.

There are, however, experimental evidences of particles being aligned vertically. This typically happens when there is an ion flow along vertical direction. Due to ion focusing below the particles in the upper layer, particles in lower layer would like to be trapped in the wake of the upper one, causing the vertical string like structural arrangement [137]. In fact in those experiments where the effect of ion flow was insignificant, the absence of vertical alignment had been reported [34,138].

5.3.2 Pair correlation function

One of the important tools to characterize the structural properties of any ordered system is radial distribution function, also known as pair correlation function $g(r)$, defined as,

$$g(r) = \left\langle \frac{N_{2d}(r, dr)}{\rho 2\pi r dr} \right\rangle, \tag{5.1}$$

where $\langle ... \rangle$ represents the ensemble average over all the particles. Here $\rho = N_{2d}/A$, is the average number density of particles in the 2-D (x-y) plane, where N_{2d} is the total number of particles in a 2-D planer layer and $A = L_x L_y$ is the area of this plane. $N_{2d}(r, dr)$ represents the number of particles located within a distance of r and r + dr ($dr = 0.015a$) away from a reference particle in a given layer.

Radial distribution functions $g(r)$ in the 2-D plane for both the layers (red and

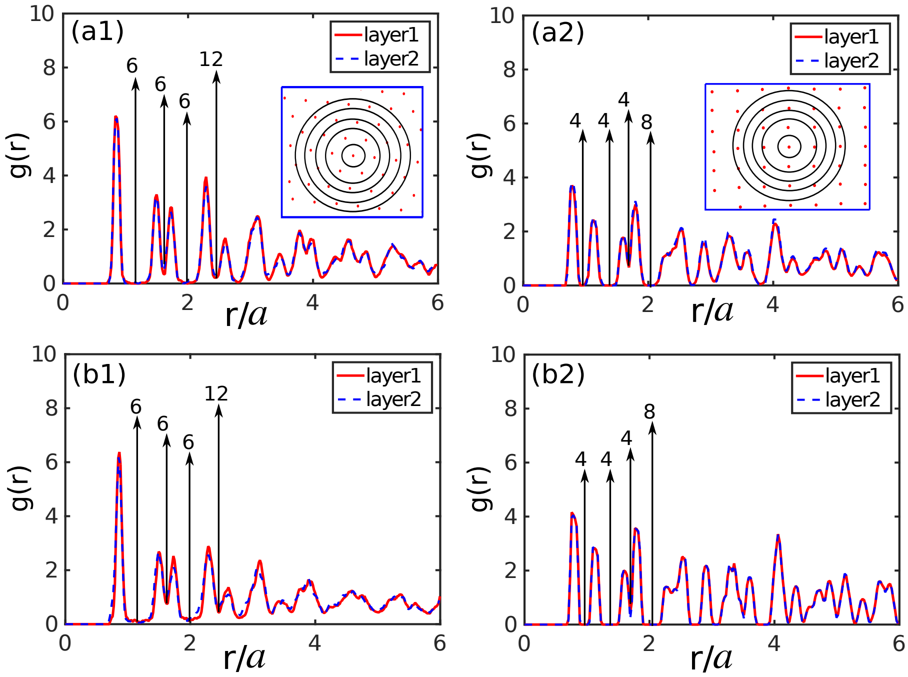

Figure 5.3: Radial distribution function $g(r)$ for each individual layer with different κ and α values. Subplots (a1) and (a2) are for $\kappa = 3.0$ and $\kappa = 5.3$, respectively with a fixed $\alpha a = 2.2854 \times 10^{-3}$. For subplots (b1) and (b2) $\alpha a = 3.428 \times 10^{-3}$ and 11.427×10^{-3}, respectively with constant $\kappa = 3.0$. Sharp multiple peaks in all the cases indicate that individual layers are in the crystalline state. The number marked arrows represent the number of particles residing at different successive circular shells around a reference particle in a given layer. Schematic representation of such shells are shown in the inset of subplots (a1) and (a2).

blue lines) have been shown in Fig. 5.3 for different κ and α values. It can be observed that the radial distribution function is identical for the two layers. Sharp multiple peaks in all the cases confirm that layers are in the crystalline state.

If we observe the pair correlation functions given in Fig. 5.3, carefully, it is seen that the profile of $g(r)$ changes with the changing values of κ and α. In order to understand this quantitatively, we have counted the average number of particles located at different successive shells away from a reference particle. By successive shells, we mean the circular strips with radial width dr between two consecutive minima in the profile of $g(r)$, as shown by the schematic diagrams in the insets of

Fig. 5.3 (subplots (a1) and (a2)). The number of particles located at such different shells has been counted by radially binning the each layer, as we did in calculating $g(r)$. The numbered marked arrows in all the subplots represent those number for different cases. For example, in subplot (a1) and (b1) of Fig. 5.3, the first arrow has a number '6' indicates that there are 6 particles located up to the distance (r) of first minimum of $g(r)$ (first shell) from any reference particle in a particular layer. Similarly, the second arrow has a number '6' tells that there are 6 particles resided between the first minima and second minima of $g(r)$ (second shell) and so on. This is more apparent from the inset of subplot (a1), where it is seen that first shell has number six, second and third shells also contain six particles, and the number of particles resided in fourth shell is twelve. This is a typical configuration of a hexagonal structure. From subplots (a2) and (b2), it is seen that the number of particles located in the nearest shell of any reference particle is four, second and third shells also contain four particles, and fourth shell has eight particles. This is also shown in the inset of subplot (a2) for this particular case. Such a distribution of particles away from a reference particle is a typical configuration of square (or rhombic) lattice structure. Thus, this is a clear indication of structural phase transitions triggered due to the change in κ and α values.

5.3.3 Voronoi diagram

The form of the crystalline structure can be easily discerned from the Voronoi diagrams. In Fig. 5.4, the subplots in the two columns show the internal structure of the two layers for two different values of κ ($\kappa = 3.0$ & 5.3) for $\alpha a = 2.2854 \times 10^{-3}$. It is observed that for $\kappa = 3.0$, particles arrange themselves in hexagonal (triangular) lattice configuration (except at the boundaries) for both the layers as

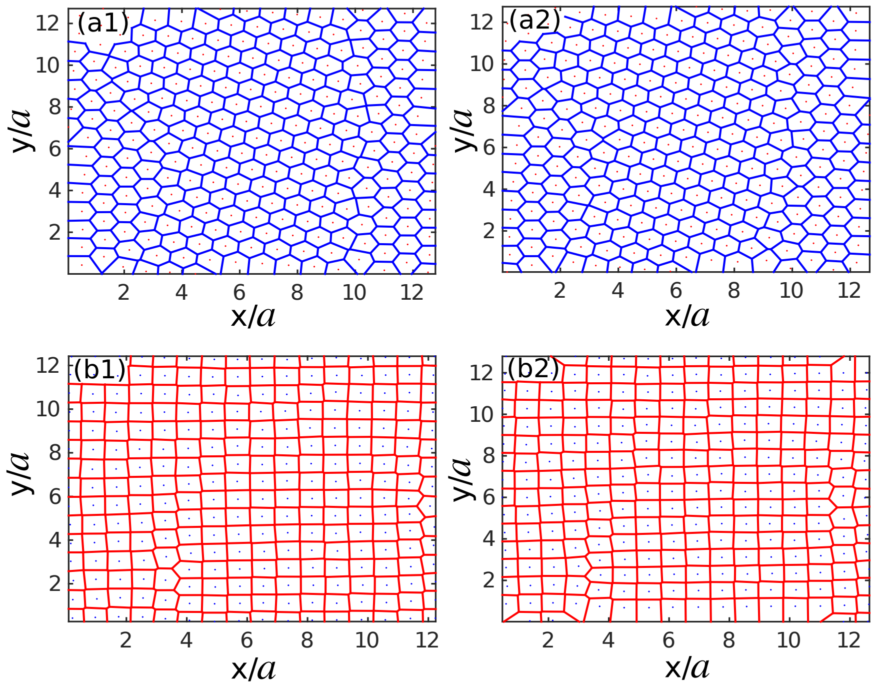

Figure 5.4: Voronoi diagrams for different κ values at fixed $\alpha a = 2.2854 \times 10^{-3}$. Subplots (a1) and (a2) correspond to layer1 and layer2 respectively for $\kappa = 3.0$. Subplots (b1) and (b2) represent same for $\kappa = 5.3$

shown in subplots (a1) & (a2). Whereas, for the value of $\kappa = 5.3$, the equilibrium configuration of particles in each layer turns into a square lattice form (subplots (b1) & (b2) of Fig. 5.4). The same transition of crystal structure from hexagonal to square pattern can be observed when α is increased and κ is held constant. This has been shown by Voronoi diagrams in Fig. 5.5. Clearly the role of κ and α are interchangeable. This is because κ governs the inter-particle energetics and α describes the form of the external potential. The structural phase transition observed with increasing α or κ values can be understood as follows. With increasing values of these two parameters, the two layers come closer, as has been shown in Fig. 5.1. When the layers come closer, particles from the two layers start feeling the repulsive interaction amongst themselves. The lattice tries to arrange in such a fashion so as to maximize the spacing between the particles of the two layers.

This is evident from the fact that the particles in the bilayers are not vertically stacked one above the other as shown in Fig. 5.2. The 2-D lattices of the two layers instead are shifted with respect to each other as shown by the solid and hollow circles in Fig. 5.2. The square lattice maximizes the inter-particle distance amidst the two layers and hence, is energetically favorable when the layers come close by. The hexagonal structure forms when only particles in the 2-D plane are interacting with each other. However, as soon as particles stacked in the third dimension (along $\hat{z}$) also start interacting, this structure does not remain a minimum energy configuration.

The fundamental reason behind these structural transitions with the changing values of κ and α will be discussed in more details in the next section.

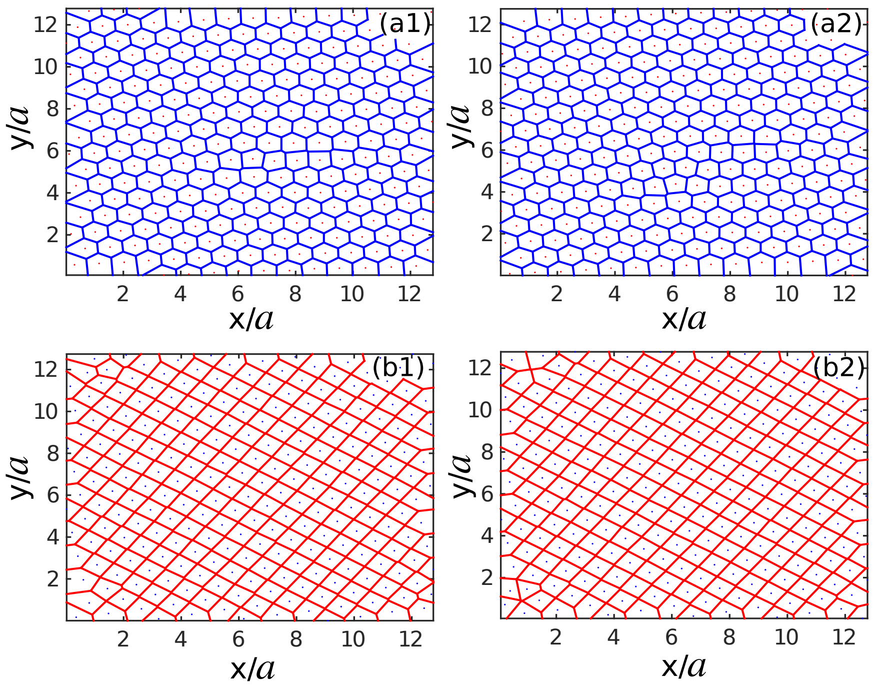

Figure 5.5: Voronoi tessellations for different α values at fixed $\kappa = 3.0$. Subplots (a1) and (a2) correspond to layer1 and layer2 respectively for $\alpha a = 3.428 \times 10^{-3}$. Subplots (b1) and (b2) represent same for $\alpha a = 11.427 \times 10^{-3}$.

5.4 Structural phase transition

As the mean inter-particle distance in a given layer (a_{xy}) does not change with the changing values of κ and α, these structural transitions should be associated with the reentrant behavior of particles. In order to investigate exactly for what values of the parameters such a phase transition occurs, we have calculated the average angle θ between lattice vectors in each layer, defined as,

$$\theta = \left\langle \frac{1}{N_r} \sum_{i=1}^{N_r} \theta_i \right\rangle. \tag{5.2}$$

Here N_r is the number of nearest neighbors of a reference particle in a given layer and θ_i is the angle between two consecutive bonds, made by a reference particle and its nearest neighbors, as shown in the inset of Fig. 5.6 (subplot (a1)). The nearest neighbors of any reference particle in a given layer had been marked up to the distance of the first minimum of $g(r)$ of that layer. Variation of θ and standard deviation (std) with varying κ and α values are shown in Fig. 5.6. Subplots (a1) and (a2) are for upper and lower layer, respectively with a fixed value of $\alpha a = 2.2854 \times 10^{-3}$. While, (b1) and (b2) are that with changing values of α at a constant $\kappa = 3.0$. From subplot (a1) and (a2), it is seen that up to a certain value of κ ($\simeq 4.3$), the value of θ is approximately 60°. This value of θ is associated with the triangular lattice. While, for $\kappa > 4.7$ it is seen that the value of $\theta \approx 90^\circ$, which is corresponding to the square lattice. And θ lies in between 60° and 90° in the intermediate region $4.3 < \kappa > 4.7$. Subplots (b1) and (b2) of Fig. 5.6 also shows the transition of order parameter θ from the value approximately 60° to 90°, associated with a phase transition from triangular to rhombic crystal structures. Here also there is an intermediate region of α, where no conventional lattice structure is found to exist. The Voronoi diagrams for one of these intermediate values of κ and α are shown in Fig. 5.7.

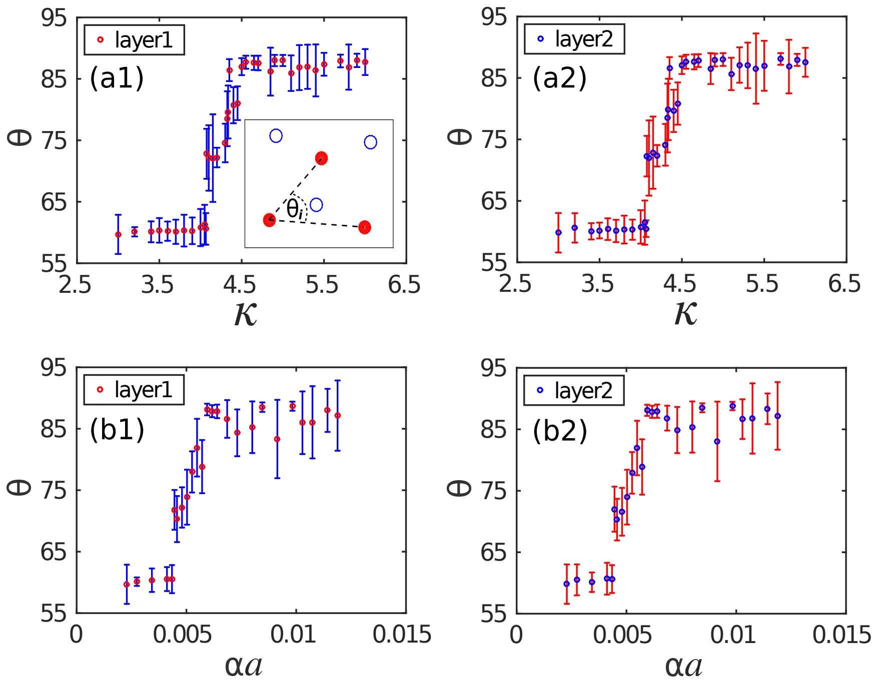

Figure 5.6: Shows the values of angle θ (points) between unit vectors of lattice with standard deviations (lines) for different α and κ values for both the layers. The inset of subplot (a1) shows the way θ is defined. Subplots (a1) and (a2) are for a fixed $\alpha a = 2.2854 \times 10^{-3}$. (b1) and (b2) are for a fixed $\kappa = 3.0$. In all the subplots it is seen that there is a jump of the angle from $\theta \approx 60$ to $\theta \approx 90$, which clearly indicates a phase transition from triangular (hexagonal) to square lattice structure simultaneously in both layers.

The reason behind these structural transitions can be understood by the following arguments. For lower values of κ and α, two layers are significantly separated from each other. Thus, the internal structural configuration of a given layer does not effected much by the presence of another layer in a bilayer system. This makes the structural configurations of each individual layers to be hexagonal (as in the case of two-dimensional dusty plasma crystal). One of these cases has been shown in subplots (a1) and (a2) of Figs. 5.4 and 5.5. As we increase the values of κ and α, the inter-layer distance decreases, as shown in Fig. 5.1. Thus, after certain limit, as we increase the values of κ and α, particles in given layer will also be effected strongly by the interaction with the particles in another layer. This makes particles to move in such a direction so that they can maintain the maximum possible inter-particle distance with its neighboring particles (in the same layer, as well as in another layer). Thus, the lattice angle θ changes accordingly, as shown in Fig. 5.6. In the extreme limit of κ and α values, when two layers are very close to each other, the lattice angle θ for each layer become approximately 90°, corresponding to the square (or rhombic) structure. One of these configurations has been shown in subplots (b1) and (b2) of Figs. 5.4 and 5.5.

It is also shown in Fig. 5.6 that there is an intermediate region of κ and α values for which θ has values in between 60° and 90°. To analyze the internal structural properties of each layer in these intermediate values of κ and α, we have used the Voronoi diagrams technique, as shown in Fig. 5.7. The structural configuration of a particular layer (another layer also has an almost similar configuration) for two different cases, where the values of κ and α are lying in that intermediate region ($\theta = 78°$ and 79°, respectively) have been shown in Fig. 5.7. It can be observed that the lattice structures do not have any pure square and/or hexagonal configurations. Instead, they appear frustrated with both kinds of structures appearing mixed up in various patches.

The variation of the order parameter θ clearly indicates that phase transitions due to the changing values of κ and α are indeed a reentrant type. It is to be realized that with the formation of another new layer (third layer), these structural transitions, from square to triangular symmetry repeat alternatively in each layer with the changing values of α and κ. The structural transition from hcp to fcc lattice symmetry, as mentioned in the previous Chapter (Chapter 4), is nothing but the consequence of such alternative changes of particle's configurations in each layer.

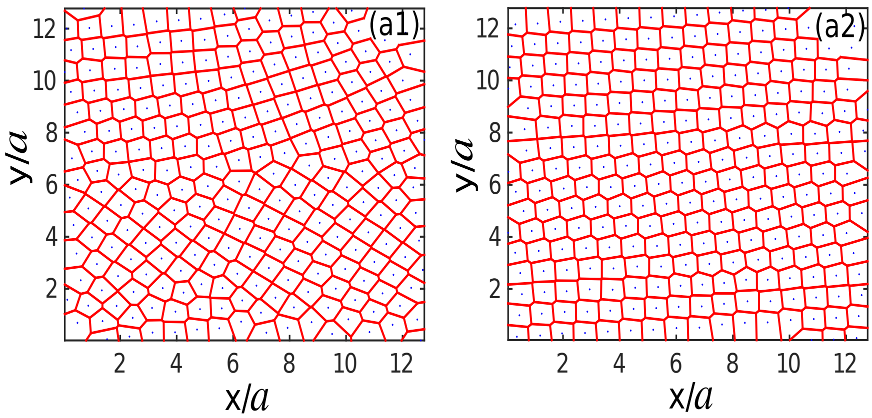

Figure 5.7: Voronoi diagrams of particles at layer1 for (a1) $\kappa = 4.6$; $\alpha a = 2.2854 \times 10^{-3}$ ($\theta \simeq 78°$) and (b1) $\kappa = 3.0$; $\alpha a = 5.7134 \times 10^{-3}$ ($\theta \simeq 79°$).

5.5 Conclusions

We have considered a dusty plasma system where charged dust particles interact via Yukawa pair potential. A constant temperature three dimensional molecular dynamics simulation has been performed with periodic boundary conditions. Our simulation studies include not only pair interaction force, gravitational force and force associated with an externally applied electric field, which mimics the sheath electric force in the real experiments have also been incorporated. We have defined two dimensionless parameters in our studies. One is the screening parameter κ, which defines the length scale of repulsive pair interactions. Another one is αa (a is the typical Wigner-Seitz radius), which represents the sharpness of total external potential (contributed from both gravitational potential and potential of the externally applied electric field). It is shown in our studies that for a certain range of κ and α values, particles can be made to levitate in two distinct layers forming bilayer structures. The internal structural properties of these crystalline bilayers have been characterized in details using radial distribution functions and Voronoi diagrams. It has been shown that for certain range of κ and α values, the dust particles organize on a lattice structure with hexagonal symmetry (triangular configuration). However, with increasing values of κ and α, when the three-dimensional effects arising from the repulsive interactions amidst particles levitating in different layers become important, the lattice structure in each layer changes to the square (or rhombic) form. By calculating the ensemble averaged angle between the lattice vectors (lattice angle) in each layer over a wide range of α and κ values, we have been able to discern the location in the $\alpha - \kappa$ space where these structural transitions happen. It is observed that the transition is not sudden from a lattice bond angle of $60°$ (representing hexagonal lattice with triangular configurations) to $90°$ (corresponding to square lattice). There exists an intermediate region of κ and α values, where the crystal phase seems to pass through a disorder phase with an average lattice angle in between $60°$ to $90°$.

6
Conclusion

In this thesis work, both the equilibrium structures and dynamical features of a dusty plasma medium under external perturbations have been investigated. The dusty plasma medium is an ideal test bed to understand the underlying physics of various macroscopic phenomena emerging from the microscopic dynamics of individual particle that can visually be tracked. In this thesis molecular dynamics (MD) simulations have been carried out to investigate various phenomena in two and three-dimensions. In 2-D studies the equilibrium structure are perturbed by the insertion of external charged particles. The relaxation dynamics of the medium has been observed which illustrates the role of both collective and single particle dynamics. The interplay of these two effects leads to interesting dynamical features which has been observed in simulations and has been highlighted. The 3-D studies involve a complete characterization of the formation of various equilibrium structures. The physics of multiple layer formation and the inter-layer structural patterns have been addressed in our studies.

A summary of the interesting findings obtained from this research work has been provided in section 6.1. The future scope related to this thesis work has been discussed briefly in section 6.2.

6.1 Important findings of the thesis

6.1.1 Two-dimensional studies

Two-dimensional (2-D) MD simulations have been performed to investigate the equilibrium structural properties and dynamical response of a 2-D dusty plasma system. Periodic boundary conditions have been used in these simulation studies. The dynamics associated with the electron and ion particles in the plasma have not been followed up through simulations, as they are considerably lighter than the dust species. Their response in comparison to the dust species can, therefore, be treated as instantaneous. It is assumed that the lighter species instantaneously shield the dust particles giving rise to Yukawa interactions amidst the dust species (Chapter 1).

A Nose-Hoover thermostat has been used to achieve the thermodynamic equilibrium state of a system dust particles interacting via Yukawa potential. The thermodynamic equilibration of this dust grain system has been verified by studying the total energy, temperature and the velocity distribution of particles. The main results of this study are summarized below.

- **Equilibrium study of 2-D dusty plasma systems**

  The structural properties concerning equilibrium phases of a 2-D dusty plasma system have been explored over a wide range of Coulomb coupling parameter Γ and screening parameter κ (Chapter 2). From the time evolution of particle trajectories and mean square displacement (MSD) of the particles, the equilibrium phases have been diagnosed for different values of Γ at fixed κ value. The pair correlation function $g(r)$ and Voronoi diagrams have been used to characterize the equilibrium particle configurations for different values of Γ and κ. It has been shown that as we increase Γ for a fixed κ value, the structural order of the medium increases. It is also shown that for $\Gamma = 1000$, as we change κ, the structural phase of the system does not change. In the crystalline regime ($\Gamma = 1000$ and $\kappa = 1.0$ for these studies), it is shown that a 2-D dusty plasma system in equilibrium always prefers hexagonal lattice configuration.

- **Effect of static perturbations in the medium**

  The MD simulations are then carried out to investigate the response of dusty plasma crystals in the presence of an external static perturbation (Chapter 2). The equilibrium crystalline medium has been disturbed by adding an extra charged particle to the medium. The potential disturbance produced by this extra charged particle can be considered to mimic the applied voltage of a biased probe inserted in the medium experimentally. It has been shown for the first time that medium has two distinctly different response. A few particles of the medium are observed to move in random directions with very high kinetic energy. These are the fast single particle response of the medium emerging through the close scattering events triggered by the externally imposed potential disturbance. The collective response of the medium has also been observed. In this case a collective disturbance propagates at the characteristic response time of the medium. These correspond to the dust plasma frequency in the medium (of the order of ω_{pd}^{-1}). The consequence of the fast single particle responses of the medium has been investigated in details. It has been shown that during initially these energetic particles move ballistically in the medium creating cracks and defects in the crystalline structure along their paths. As a result of which they slow down and subsequently invoke collective response of the medium at different locations. These new locations of collective disturbances triggered by the energetic particles have been termed as *secondary centers*. By tracking these energetic particles, it has been demonstrated that when the time scale associated with these high energetic particles become of the order of collective response time scale of the medium (ω_{pd}^{-1}), their ballistic propagation stops and excite the secondary centers of collective disturbance. The effect of the strength of initial perturbations on the dynamics of the medium has been studied by varying the charge of the externally inserted particle as well as the screening parameter κ. It has been shown that as the charge of the externally inserted particle is increased or κ is decreased, the scattering events become more energetic, i.e., particles generated from the single particle scattering events acquire higher initial energy and hence can disturb the medium further away from the originally inserted perturbation.

- **Effect of moving disturbance in the dusty plasma crystal**

  Molecular dynamics simulation technique has also been adopted to simulate a situation when a highly charged object moves through a dusty plasma medium (Chapter 3). It has been shown that when the speed of the charged projectile exceeds the sound speed of the medium, it generates precursor density waves ahead of it and a Mack cone wake structure behind it. The dynamical features of theses collective structures have been studied and characterized over a wide range of Mack number and charge of the projectile. In this case also a strong interplay of single particle and collective effects has been demonstrated. Few energetic particles have been observed to propagate in the random directions producing cracks and deformations in the medium. Their dynamics affect the characteristic properties of the shock and Mach cone structures. The temperature evolution of a localized region disturbed by one of the energetic particles demonstrates a melting transition undergone by the medium from crystalline to visco-elastic liquid phase. Voronoi diagrams confirm this transition from ordered state to a disordered state in a localized region of the medium triggered by energetic particles as they slow down.

The role of neutral damping on these features have also been studied. It is observed that secondary excitation centers get formed at a reduced distance. The time to excite secondary centers also gets reduced with the increasing value of neutral damping. This is because the energetic particles suffers an additional damping wherein its speed decreases much faster to reach the limit wherein secondary excitations can be triggered.

6.1.2 Three-dimensional studies

The process of crystallization and the possibility of the formation of different variety of crystal structures have been investigated extensively using three-dimensional MD simulations. In this study, the dusty plasma medium is considered, where particles interact via screened Coulomb or Yukawa pair potential. Besides the pair interactions, each dust particles are also subjected to the gravitational force and the force due to an externally applied electric field, which is typically the cathode sheath electric field in experiments. The interesting findings from this study are as follows.

- **Layered structure formation**

  The equilibrium configurations of particles have been investigated in details for different κ and α values. Here, κ is the screening constant of the Yukawa pair potential amidst the two dust charges. The parameter α defines profile of the external electric field which balances the gravitational force acting on the dust particles. The sharpness of total external potential energy contributed from both gravity and externally applied electric field (Chapter 4) gets defined by this parameter. It has been shown that in thermal equilibrium, particles levitate at different crystalline layers. The number of layers has been characterized with these two parameters κ and α. The mechanism and underlying physics behind these layered structure formation and the transition from a particular number of layers to a higher number have been explored in details. The configuration showing the distribution of the particles in each of the layers has also been analyzed using pair correlation function and Voronoi diagrams. The observations of hexagonal close packing (hcp) and face-centered cubic (fcc) structure have been reported.

- **Structural properties and phase transitions**

  This thesis work also includes the study of structural properties and structural phase transitions in crystalline bilayers (Chapter 5). The range of κ and α values for which the charged dust particles will form a bilayer structure has been identified. Internal particle configurations of each of the individual layers of these bilayer systems have been characterized with the help of pair correlation functions and Voronoi diagrams. It has been shown that the inter-layer separation decreases with increasing κ and α values. With varying κ and α values, it has been demonstrated that a structural phase transition from hexagonal to square lattice configuration can be triggered in each of the layers of this bilayer system, simultaneously. By calculating the ensemble averaged lattice angle in each layer, the exact range of α and κ values for which these structural transitions happen has been recognized.

6.2 Future scope

This thesis work reveals a lot of possibilities and directions to be explored in the field of dusty plasmas as well as other strongly coupled systems. A brief discussion about some of these future studies that can be carried out as an extension of this thesis work has been mentioned below:

- In this thesis work, the generation of high energetic particles which essentially leads to the cracks and defects in the crystalline structure, has been reported. The extensive study of the properties of these cracks and their propagation through the crystalline structure in both longitudinal and transverse directions can be an interesting research topic in the field of plasma crystals as well as other soft matter system.

- The collective features in the magnetized dusty plasma medium have been explored extensively. But the effect of magnetic field on both the single particle scattering events and their dynamics in the medium is still unexplored and an interesting research work which could be carried out in future along this direction.

- The three-dimensional layered structure formations have been investigated in this study where the lighter electrons and ions are assumed as inertialess species. The effects of ion streaming, which often exists in the typical dusty plasma experiments, on these structures can be studied in details as a part of the future works.

- The dynamical response of the 3-D structures to external perturbations can be studied to understand the possibility of phase transition amidst different forms of the lattice structure, the criteria of melting in two and three-dimensions also need to be explored.

- Throughout this thesis work, the charge on the dust grain is assumed to be constant. In real experiments, these charges may change with time. The effects of charge fluctuation on both the equilibrium configurations and dynamical features of the dust grain system are interesting topics to explore.

- Only one type of charged dust species has been considered throughout this study. Thus, the study of the equilibrium structures of a multi-component charged grain system such as binary mixtures is an interesting future work to be done.

- In this study, equilibrium particle configurations have been explored in the presence of external vertical confinement (combine effect of gravity and externally applied electric field). In the horizontal plane (X and Y), the periodic boundary conditions have been used in the simulations. In laboratory experiments, charged dust particles are also confined in the horizontal plane by using a ring-shaped wire. The extensive molecular dynamics simulations can be performed in the presence of both vertical and horizontal confinements to investigate the structural properties of the system.

Bibliography

[1] G Praburam and J Goree. Experimental observation of very low-frequency macroscopic modes in a dusty plasma. *Physics of Plasmas*, 3(4):1212–1219, 1996.

[2] Tonuj Deka, A Boruah, SK Sharma, and H Bailung. Observation of self-excited dust acoustic wave in dusty plasma with nanometer size dust grains. *Physics of Plasmas*, 24(9):093706, 2017.

[3] A Barkan, N D'angelo, and Robert L Merlino. Charging of dust grains in a plasma. *Physical Review Letters*, 73(23):3093, 1994.

[4] RA Quinn, C Cui, J Goree, JB Pieper, H Thomas, and GE Morfill. Structural analysis of a coulomb lattice in a dusty plasma. *Physical Review E*, 53(3):R2049, 1996.

[5] CK Goertz. Dusty plasmas in the solar system. *Reviews of Geophysics*, 27(2):271–292, 1989.

[6] Frank Verheest. Waves and instabilities in dusty space plasmas. *Space Science Reviews*, 77(3-4):267–302, 1996.

[7] Robert L Merlino and John A Goree. Dusty plasmas in the laboratory, industry, and space. *PHYSICS TODAY.*, 57(7):32–39, 2004.

[8] R Bingham and VN Tsytovich. New mechanism of dust growth and gravitation-like instabilities in astrophysical plasmas. *Astronomy & Astrophysics*, 376(3):L43–L47, 2001.

[9] Gary S Selwyn, J Singh, and RS Bennett. I nsitu laser diagnostic studies of plasma-generated particulate contamination. *Journal of Vacuum Science & Technology A: Vacuum, Surfaces, and Films*, 7(4):2758–2765, 1989.

[10] II Beilis, M Keidar, RL Boxman, and S Goldsmith. Macroparticle separation and plasma collimation in positively biased ducts in filtered vacuum arc deposition systems. *Journal of applied physics*, 85(3):1358–1365, 1999.

[11] A Bouchoule and L Boufendi. Particulate formation and dusty plasma behaviour in argon-silane rf discharge. *Plasma Sources Science and Technology*, 2(3):204, 1993.

[12] Vadim N Tsytovich and J Winter. On the role of dust in fusion devices. *Physics-Uspekhi*, 41(8):815, 1998.

[13] NN Rao, PK Shukla, and M Yu Yu. Dust-acoustic waves in dusty plasmas. *Planetary and space science*, 38(4):543–546, 1990.

[14] PK Shukla. A survey of dusty plasma physics. *Physics of Plasmas*, 8(5):1791–1803, 2001.

[15] JB Pieper and J Goree. Dispersion of plasma dust acoustic waves in the strong-coupling regime. *Physical review letters*, 77(15):3137, 1996.

[16] Frank Melandso/. Lattice waves in dust plasma crystals. *Physics of Plasmas*, 3(11):3890–3901, 1996.

[17] T Misawa, N Ohno, K Asano, M Sawai, S Takamura, and PK Kaw. Experimental observation of vertically polarized transverse dust-lattice wave propagating in a one-dimensional strongly coupled dust chain. *Physical review letters*, 86(7):1219, 2001.

[18] N d'Angelo. Ion-acoustic waves in dusty plasmas. *Planetary and Space Science*, 42(6):507–511, 1994.

[19] A Barkan, N D'angelo, and RL Merlino. Experiments on ion-acoustic waves in dusty plasmas. *Planetary and Space Science*, 44(3):239–242, 1996.

[20] SK Sharma, A Boruah, and H Bailung. Head-on collision of dust-acoustic solitons in a strongly coupled dusty plasma. *Physical Review E*, 89(1):013110, 2014.

[21] P Harvey, C Durniak, D Samsonov, and G Morfill. Soliton interaction in a complex plasma. *Physical Review E*, 81(5):057401, 2010.

[22] Sandeep Kumar, Sanat Kumar Tiwari, and Amita Das. Observation of the korteweg-de vries soliton in molecular dynamics simulations of a dusty plasma medium. *Physics of Plasmas*, 24(3):033711, 2017.

[23] PK Kaw and A Sen. Low frequency modes in strongly coupled dusty plasmas. *Physics of Plasmas*, 5(10):3552–3559, 1998.

[24] Yan Feng, J Goree, and Bin Liu. Viscoelasticity of 2d liquids quantified in a dusty plasma experiment. *Physical review letters*, 105(2):025002, 2010.

[25] Peter Hartmann, Máté Csaba Sándor, Anikó Kovács, and Zoltán Donkó. Static and dynamic shear viscosity of a single-layer complex plasma. *Physical Review E*, 84(1):016404, 2011.

[26] D Samsonov, J Goree, ZW Ma, A Bhattacharjee, HM Thomas, and GE Morfill. Mach cones in a coulomb lattice and a dusty plasma. *Physical review letters*, 83(18):3649, 1999.

[27] PK Shukla and AA Mamun. Solitons, shocks and vortices in dusty plasmas. *New Journal of Physics*, 5(1):17, 2003.

[28] Sandeep Kumar and Amita Das. Molecular dynamics simulations of spiral waves in driven strongly coupled dusty plasma medium. *arXiv preprint arXiv:1711.02081*, 2017.

[29] D Samsonov and J Goree. Instabilities in a dusty plasma with ion drag and ionization. *Physical Review E*, 59(1):1047, 1999.

[30] Sanat Kumar Tiwari, Amita Das, Dilip Angom, Bhavesh G Patel, and Predhiman Kaw. Kelvin-helmholtz instability in a strongly coupled dusty plasma medium. *Physics of Plasmas*, 19(7):073703, 2012.

[31] H Thomas, GE Morfill, V Demmel, J Goree, B Feuerbacher, and D Möhlmann. Plasma crystal: Coulomb crystallization in a dusty plasma. *Physical Review Letters*, 73(5):652, 1994.

[32] JH Chu and I Lin. Direct observation of coulomb crystals and liquids in strongly coupled rf dusty plasmas. *Physical review letters*, 72(25):4009, 1994.

[33] René Messina and Hartmut Löwen. Reentrant transitions in colloidal or dusty plasma bilayers. *Physical review letters*, 91(14):146101, 2003.

[34] M Zuzic, AV Ivlev, J Goree, GE Morfill, HM Thomas, H Rothermel, U Konopka, R Sütterlin, and DD Goldbeck. Three-dimensional strongly coupled plasma crystal under gravity conditions. *Physical review letters*, 85(19):4064, 2000.

[35] Hiroo Totsuji, Tokunari Kishimoto, and Chieko Totsuji. Structure of confined yukawa system (dusty plasma). *Physical review letters*, 78(16):3113, 1997.

[36] S Nunomura, D Samsonov, and J Goree. Transverse waves in a two-dimensional screened-coulomb crystal (dusty plasma). *Physical review letters*, 84(22):5141, 2000.

[37] A Homann, A Melzer, S Peters, R Madani, and A Piel. Laser-excited dust lattice waves in plasma crystals. *Physics Letters A*, 242(3):173–180, 1998.

[38] Bin Liu, J Goree, and Yan Feng. Mode coupling for phonons in a single-layer dusty plasma crystal. *Physical review letters*, 105(8):085004, 2010.

[39] Hubertus M Thomas and Gregor E Morfill. Melting dynamics of a plasma crystal. *Nature*, 379(6568):806–809, 1996.

[40] VA Schweigert, IV Schweigert, A Melzer, A Homann, and A Piel. Plasma crystal melting: A nonequilibrium phase transition. *Physical review letters*, 80(24):5345, 1998.

[41] Srimanta Maity, Amita Das, Sandeep Kumar, and Sanat Kumar Tiwari. Interplay of single particle and collective response in molecular dynamics simulation of dusty plasma system. *Physics of Plasmas*, 25(4):043705, 2018.

[42] Srimanta Maity and Amita Das. Molecular dynamics study of crystal formation and structural phase transition in yukawa system for dusty plasma medium. *arXiv preprint arXiv:1810.10216*, 2018.

[43] V Nosenko, J Goree, ZW Ma, and A Piel. Observation of shear-wave mach cones in a 2d dusty-plasma crystal. *Physical review letters*, 88(13):135001, 2002.

[44] D Samsonov, J Goree, HM Thomas, and GE Morfill. Mach cone shocks in a two-dimensional yukawa solid using a complex plasma. *Physical Review E*, 61(5):5557, 2000.

[45] Wojciech J Miloch. Wake effects and mach cones behind objects. *Plasma Physics and Controlled Fusion*, 52(12):124004, 2010.

[46] WJ Miloch, J Trulsen, and HL Pécseli. Numerical studies of ion focusing behind macroscopic obstacles in a supersonic plasma flow. *Physical Review E*, 77(5):056408, 2008.

[47] M Bonitz, C Henning, and D Block. Complex plasmas: a laboratory for strong correlations. *Reports on Progress in Physics*, 73(6):066501, 2010.

[48] Yasuaki Hayashi and Kunihide Tachibana. Observation of coulomb-crystal formation from carbon particles grown. *Jpn. J. Appl. Phys*, 33(6A Pt 2), 1994.

[49] Gregor E Morfill and Alexei V Ivlev. Complex plasmas: An interdisciplinary research field. *Reviews of modern physics*, 81(4):1353, 2009.

[50] Lewi Tonks and Irving Langmuir. Oscillations in ionized gases. *Phys. Rev.*, 33:195–210, Feb 1929.

[51] Francis F Chen. *Introduction to plasma physics and controlled fusion*, volume 1. Springer, 1984.

[52] Gregor E Morfill and Manfred Scholer. *Physical processes in interstellar clouds*, volume 210. Springer Science & Business Media, 2012.

[53] JT Wasson, RH Hewins, RH Jones, and ERD Scott. Chondrules and the protoplanetary disk. 1996.

[54] E Thomas Jr, RL Merlino, and M Rosenberg. Magnetized dusty plasmas: the next frontier for complex plasma research. *Plasma Physics and Controlled Fusion*, 54(12):124034, 2012.

[55] Edward Thomas Jr, Uwe Konopka, Robert L Merlino, and Marlene Rosenberg. Initial measurements of two-and three-dimensional ordering, waves, and plasma filamentation in the magnetized dusty plasma experiment. *Physics of Plasmas*, 23(5):055701, 2016.

[56] Edward Thomas, Robert L Merlino, and Marlene Rosenberg. Design criteria for the magnetized dusty plasma experiment. *IEEE Transactions on Plasma Science*, 41(4):811–815, 2013.

[57] Edward Thomas Jr, Brian Lynch, Uwe Konopka, Robert L Merlino, and Marlene Rosenberg. Observations of imposed ordered structures in a dusty plasma at high magnetic field. *Physics of Plasmas*, 22(3):030701, 2015.

[58] VN Tsytovich and U De Angelis. Kinetic theory of dusty plasmas. i. general approach. *Physics of plasmas*, 6(4):1093–1106, 1999.

[59] VN Tsytovich and U De Angelis. Kinetic theory of dusty plasmas ii. dust–plasma particle collision integrals. *Physics of Plasmas*, 7(2):554–563, 2000.

[60] VN Tsytovich and U De Angelis. Kinetic theory of dusty plasmas. iii. dust–dust collision integrals. *Physics of Plasmas*, 8(4):1141–1153, 2001.

[61] VN Tsytovich and U De Angelis. Kinetic theory of dusty plasmas. iv. distribution and fluctuations of dust charges. *Physics of Plasmas*, 9(6):2497–2506, 2002.

[62] G Kalman and KI Golden. Response function and plasmon dispersion for strongly coupled coulomb liquids. *Physical Review A*, 41(10):5516, 1990.

[63] Kenneth I Golden, G Kalman, and Philippe Wyns. Response function and plasmon dispersion for strongly coupled coulomb liquids: Two-dimensional electron liquid. *Physical Review A*, 41(12):6940, 1990.

[64] GJ Kalman, KI Golden, Z Donko, and P Hartmann. The quasilocalized charge approximation. In *Journal of Physics: Conference Series*, volume 11, page 254. IOP Publishing, 2005.

[65] Kenneth I Golden and Gabor J Kalman. Quasilocalized charge approximation in strongly coupled plasma physics. *Physics of Plasmas*, 7(1):14–32, 2000.

[66] M Rosenberg and G Kalman. Dust acoustic waves in strongly coupled dusty plasmas. *Physical Review E*, 56(6):7166, 1997.

[67] M Rosenberg, GJ Kalman, P Hartmann, and J Goree. Effect of strong coupling on the dust acoustic instability. *Physical Review E*, 89(1):013103, 2014.

[68] G Kalman, M Rosenberg, and HE DeWitt. Collective modes in strongly correlated yukawa liquids: Waves in dusty plasmas. *Physical review letters*, 84(26):6030, 2000.

[69] Amita Das, Vikram Dharodi, and Sanat Tiwari. Collective dynamics in strongly coupled dusty plasma medium. *Journal of Plasma Physics*, 80(6):855–861, 2014.

[70] Abdourahmane Diaw and Michael Sean Murillo. Generalized hydrodynamics model for strongly coupled plasmas. *Physical Review E*, 92(1):013107, 2015.

[71] Patrick Ludwig, Wojciech J Miloch, Hanno Kählert, and Michael Bonitz. On the wake structure in streaming complex plasmas. *New Journal of Physics*, 14(5):053016, 2012.

[72] Dietmar Block, Jan Carstensen, Patrick Ludwig, Wojciech J Miloch, Franko Greiner, Alexander Piel, Michael Bonitz, and Andre Melzer. Wake formation and wake field effects in complex plasmas. *Contributions to Plasma Physics*, 52(10):804–812, 2012.

[73] Patrick Ludwig, Hanno Kählert, and Michael Bonitz. Ion-streaming induced order transition in three-dimensional dust clusters. *Plasma Physics and Controlled Fusion*, 54(4):045011, 2012.

[74] Sita Sundar, Hanno Kählert, Jan-Philip Joost, Patrick Ludwig, and Michael Bonitz. Impact of collisions on the dust wake potential with maxwellian and non-maxwellian ions. *Physics of Plasmas*, 24(10):102130, 2017.

[75] Sita Sundar. Wake effects of a stationary charged grain in streaming magnetized ions. *Physical Review E*, 98(2):023206, 2018.

[76] H Ohta and S Hamaguchi. Molecular dynamics evaluation of self-diffusion in yukawa systems. *Physics of Plasmas*, 7(11):4506–4514, 2000.

[77] Bin Liu and J Goree. Superdiffusion in two-dimensional yukawa liquids. *Physical Review E*, 75(1):016405, 2007.

[78] Bin Liu, J Goree, and OS Vaulina. Test of the stokes-einstein relation in a two-dimensional yukawa liquid. *Physical review letters*, 96(1):015005, 2006.

[79] Z Donkó and B Nyıri. Molecular dynamics calculation of the thermal conductivity and shear viscosity of the classical one-component plasma. *Physics of Plasmas*, 7(1):45–50, 2000.

[80] T Saigo and S Hamaguchi. Shear viscosity of strongly coupled yukawa systems. *Physics of Plasmas*, 9(4):1210–1216, 2002.

[81] V Nosenko and J Goree. Shear flows and shear viscosity in a two-dimensional yukawa system (dusty plasma). *Physical review letters*, 93(15):155004, 2004.

[82] Z Donkó, J Goree, and P Hartmann. Viscoelastic response of yukawa liquids. *Physical Review E*, 81(5):056404, 2010.

[83] FF Munarin, K Nelissen, WP Ferreira, GA Farias, and FM Peeters. Hysteresis and reentrant melting of a self-organized system of classical particles confined in a parabolic trap. *Physical Review E*, 77(3):031608, 2008.

[84] Pter Hartmann, Zoltn Donko, Pradip M Bakshi, Gabor J Kalman, and Stamatios Kyrkos. Molecular dynamics studies of solid–liquid phase transition in 2-d yukawa systems. *IEEE transactions on plasma science*, 35(2):332–336, 2007.

[85] Srimanta Maity and Amita Das. Molecular dynamics study of crystal formation and structural phase transition in yukawa system for dusty plasma medium. *Physics of Plasmas*, 26(2):023703, 2019.

[86] WL Slattery, GD Doolen, and HE DeWitt. Improved equation of state for the classical one-component plasma. *Physical Review A*, 21(6):2087, 1980.

[87] Setsuo Ichimaru. Strongly coupled plasmas: high-density classical plasmas and degenerate electron liquids. *Reviews of Modern Physics*, 54(4):1017, 1982.

[88] Hiroyuki Ikezi. Coulomb solid of small particles in plasmas. *The Physics of fluids*, 29(6):1764–1766, 1986.

[89] PK Shukla and VP Silin. Dust ion-acoustic wave. *Physica Scripta*, 45:508, 1992.

[90] A Barkan, Robert L Merlino, and N DâĂŹangelo. Laboratory observation of the dust-acoustic wave mode. *Physics of Plasmas*, 2(10):3563–3565, 1995.

[91] Frank Verheest. Nonlinear dust-acoustic waves in multispecies dusty plasmas. *Planetary and space science*, 40(1):1–6, 1992.

[92] AV Ivlev and G Morfill. Dust acoustic solitons with variable particle charge: Role of the ion distribution. *Physical Review E*, 63(2):026412, 2001.

[93] P Bandyopadhyay, G Prasad, A Sen, and PK Kaw. Experimental study of nonlinear dust acoustic solitary waves in a dusty plasma. *Physical review letters*, 101(6):065006, 2008.

[94] R Bharuthram and PK Shukla. Large amplitude ion-acoustic solitons in a dusty plasma. *Planetary and space science*, 40(7):973–977, 1992.

[95] SI Popel and MY Yu. Ion acoustic solitons in impurity-containing plasmas. *Contributions to Plasma Physics*, 35(2):103–108, 1995.

[96] Y Nakamura and A Sarma. Observation of ion-acoustic solitary waves in a dusty plasma. *Physics of Plasmas*, 8(9):3921–3926, 2001.

[97] Y Nakamura, H Bailung, and PK Shukla. Observation of ion-acoustic shocks in a dusty plasma. *Physical review letters*, 83(8):1602, 1999.

[98] Q-Z Luo, N DâĂŹAngelo, and RL Merlino. Experimental study of shock formation in a dusty plasma. *Physics of Plasmas*, 6(9):3455–3458, 1999.

[99] Padma K Shukla and AA Mamun. Dust-acoustic shocks in a strongly coupled dusty plasma. *IEEE transactions on plasma science*, 29(2):221–225, 2001.

[100] F Li and O Havnes. Shock waves in a dusty plasma. *Physical Review E*, 64(6):066407, 2001.

[101] M Rosenberg. Ion-and dust-acoustic instabilities in dusty plasmas. *Planetary and space science*, 41(3):229–233, 1993.

[102] RL Merlino, A Barkan, C Thompson, and N DâĂŹangelo. Laboratory studies of waves and instabilities in dusty plasmas. *Physics of Plasmas*, 5(5):1607–1614, 1998.

[103] Amita Das and Predhiman Kaw. Suppression of rayleigh taylor instability in strongly coupled plasmas. *Physics of Plasmas*, 21(6):062102, 2014.

[104] Mathieu Marciante and Michael Sean Murillo. Thermodynamic and kinetic properties of shocks in two-dimensional yukawa systems. *Physical review letters*, 118(2):025001, 2017.

[105] J Pramanik, G Prasad, A Sen, and PK Kaw. Experimental observations of transverse shear waves in strongly coupled dusty plasmas. *Physical review letters*, 88(17):175001, 2002.

[106] Yan Feng, J Goree, and Bin Liu. Frequency-dependent shear viscosity of a liquid two-dimensional dusty plasma. *Physical Review E*, 85(6):066402, 2012.

[107] Vikram Singh Dharodi, Sanat Kumar Tiwari, and Amita Das. Visco-elastic fluid simulations of coherent structures in strongly coupled dusty plasma medium. *Physics of Plasmas*, 21(7):073705, 2014.

[108] A Melzer, S Nunomura, D Samsonov, ZW Ma, and J Goree. Laser-excited mach cones in a dusty plasma crystal. *Physical Review E*, 62(3):4162, 2000.

[109] André Melzer. Laser manipulation of particles in dusty plasmas. *Plasma Sources Science and Technology*, 10(2):303, 2001.

[110] V Nosenko, J Goree, ZW Ma, DHE Dubin, and A Piel. Compressional and shear wakes in a two-dimensional dusty plasma crystal. *Physical Review E*, 68(5):056409, 2003.

[111] ZW Ma and A Bhattacharjee. Molecular dynamics simulations of mach cones in two-dimensional yukawa crystals. *Physics of Plasmas*, 9(8):3349–3354, 2002.

[112] Sanat Kumar Tiwari and Abhijit Sen. Fore-wake excitations from moving charged objects in a complex plasma. *Physics of Plasmas*, 23(10):100705, 2016.

[113] Surabhi Jaiswal, P Bandyopadhyay, and A Sen. Experimental observation of precursor solitons in a flowing complex plasma. *Physical Review E*, 93(4):041201, 2016.

[114] A Melzer, A Homann, and A Piel. Experimental investigation of the melting transition of the plasma crystal. *Physical Review E*, 53(3):2757, 1996.

[115] D Samsonov, SK Zhdanov, RA Quinn, SI Popel, and GE Morfill. Shock melting of a two-dimensional complex (dusty) plasma. *Physical review letters*, 92(25):255004, 2004.

[116] IV Schweigert, VA Schweigert, A Melzer, and A Piel. Melting of dust plasma crystals with defects. *Physical Review E*, 62(1):1238, 2000.

[117] Liu Bin, Liu Yan-Hong, Chen Yan-Ping, Yang Si-Ze, and Wang Long. Structure and phase transition of a two-dimensional dusty plasma. *Chinese Physics*, 12(7):765, 2003.

[118] André Schella, Tobias Miksch, André Melzer, Jan Schablinski, Dietmar Block, Alexander Piel, Hauke Thomsen, Patrick Ludwig, and Michael Bonitz. Melting scenarios for three-dimensional dusty plasma clusters. *Physical Review E*, 84(5):056402, 2011.

[119] A Melzer, VA Schweigert, IV Schweigert, A Homann, S Peters, and A Piel. Structure and stability of the plasma crystal. *Physical Review E*, 54(1):R46, 1996.

[120] JB Pieper, J Goree, and RA Quinn. Three-dimensional structure in a crystallized dusty plasma. *Physical Review E*, 54(5):5636, 1996.

[121] Yasuaki Hayashi. Structure of a three-dimensional coulomb crystal in a fine-particle plasma. *Physical Review Letters*, 83(23):4764, 1999.

[122] Hiroo Totsuji, Tokunari Kishimoto, and Chieko Totsuji. Structure of dusty plasma in external fields: Simulation and theory. *Japanese journal of applied physics*, 36(7S):4980, 1997.

[123] Sandeep Kumar and Amita Das. Spiral waves in driven strongly coupled yukawa systems. *Physical Review E*, 97(6):063202, 2018.

[124] Sandeep Kumar, Bhavesh Patel, and Amita Das. Spiral waves in driven dusty plasma medium: Generalized hydrodynamic fluid description. *Physics of Plasmas*, 25(4):043701, 2018.

[125] Steve Plimpton. Fast parallel algorithms for short-range molecular dynamics. *Journal of computational physics*, 117(1):1–19, 1995.

[126] Shūichi Nosé. A molecular dynamics method for simulations in the canonical ensemble. *Molecular physics*, 52(2):255–268, 1984.

[127] William G Hoover. Canonical dynamics: Equilibrium phase-space distributions. *Physical review A*, 31(3):1695, 1985.

[128] O Havnes, T Aslaksen, TW Hartquist, F Li, F Melandsø, GE Morfill, and T Nitter. Probing the properties of planetary ring dust by the observation of mach cones. *Journal of Geophysical Research: Space Physics*, 100(A2):1731–1734, 1995.

[129] O Havnes, F Li, F Melandso/, T Aslaksen, TW Hartquist, GE Morfill, T Nitter, and V Tsytovich. Diagnostic of dusty plasma conditions by the observa-

tion of mach cones caused by dust acoustic waves. *Journal of Vacuum Science & Technology A: Vacuum, Surfaces, and Films*, 14(2):525–528, 1996.

[130] Gordon David Crapper. Introduction to water waves. 1985.

[131] Sanat Kumar Tiwari and Abhijit Sen. Wakes and precursor soliton excitations by a moving charged object in a plasma. *Physics of Plasmas*, 23(2):022301, 2016.

[132] André Melzer, Thomas Trottenberg, and Alexander Piel. Experimental determination of the charge on dust particles forming coulomb lattices. *Physics Letters A*, 191(3-4):301–308, 1994.

[133] Vladimir E Fortov, Anatoli P Nefedov, Vladimir M Torchinsky, Vladimir I Molotkov, Oleg F Petrov, Alex A Samarian, Andrew M Lipaev, and Alexei G Khrapak. Crystalline structures of strongly coupled dusty plasmas in dc glow discharge strata. *Physics Letters A*, 229(5):317–322, 1997.

[134] Daniel HE Dubin. Theory of structural phase transitions in a trapped coulomb crystal. *Physical review letters*, 71(17):2753, 1993.

[135] K Qiao and TW Hyde. Structural phase transitions and out-of-plane dust lattice instabilities in vertically confined plasma crystals. *Physical Review E*, 71(2):026406, 2005.

[136] Ke Qiao and Truell W Hyde. Structural phase transitions and vertical mode spectra in 2-d finite plasma crystals. *IEEE transactions on plasma science*, 36(5):2753–2758, 2008.

[137] VA Schweigert, IV Schweigert, A Melzer, A Homann, and A Piel. Alignment and instability of dust crystals in plasmas. *Physical Review E*, 54(4):4155, 1996.

[138] Peter Hartmann, Zolán Donkó, Gabor J Kalman, Stamatios Kyrkos, Kenneth I Golden, and Marlene Rosenberg. Collective dynamics of complex plasma bilayers. *Physical review letters*, 103(24):245002, 2009.